MSc Mamata Sumant Savanagouder

Furthering the understanding of mechanism and function of HCMV IE1 chromatin association

PhD thesis was undertaken in

Department of Reproductive Immunology & Pathology

Institute of Animal Reproduction and Food Research

Polish Academy of Sciences in Olsztyn

under the supervision of

dr hab. Magdalena Weidner-Glunde

Olsztyn 2023

Work was supported by the Polish National Science Centre grant no. 2017/26/E/NZ6/01124

Dedicated in the loving memory of appa….

Not a day goes by where you don’t creep into my thoughts….

If not for you, I would not have set out on this journey of PhD….

ACKNOWLEDGEMENTS

Firstly, and the most important of all, I would like to thank my supervisor dr hab. Magdalena Weidner-Glunde for her continued guidance over the past 5 years, without which this work would not have been possible. She has kept me on track, pushed me to keep working even when our hypothesis did not yield the results we expected, and provided key ideas, which were instrumental in developing the project to its current state. I have truly enjoyed our scientific discussions during lab meetings, her excitement to discuss science is very contagious! She has been extremely generous with her time helping me understand key concepts in herpesvirus biology and the importance of proper experimental set up. Given the challenges we faced as a new lab in an institute with no experience in working with viruses, I have never seen her give up even at the lowest of lows (and we've had several!). I have only seen her get tougher as the going gets tough. Her level of dedication to science surpasses that of any scientist I have worked with till date, and I would be very happy if I could inculcate even a fraction of her dedication. Being her first PhD student has given me the opportunity to learn and understand the complexity of setting up a smoothly functioning lab. This experience is invaluable; I would not have had this opportunity anywhere else, and I would like to thank her for that. Although, the past 5 years have been extremely challenging with more lows than ups, her mentorship has helped me develop as a scientist and become a stronger individual. I would like to especially thank her for organizing thesis committee meeting even though it was not part of the doctoral program. This gave me an opportunity to discuss our results with well-known herpes virologists and get helpful feedback that has shaped the development of this project.

I would like to thank my thesis committee members – Dr. Martin Messerle, Dr. Ravit Boger, Dr. Paul Lieberman, and Dr. Thomas Schulz for taking time out of their busy schedules and their valuable suggestions. I would also like to thank Dr. Eva Borst and Karen Wagner for teaching me how to produce HCMV in large quantities (anyone who has done this knows how challenging it is!), equipping me with one of the most important and basic tool to study HCMV biology.

I sincerely thank the director of our Institute, prof. dr hab. Mariusz Piskuła for providing the infrastructure and a great working environment to carry out my PhD work. I would like to thank the head of the doctoral school – prof. dr hab. Aneta Andronowska for finding an English doctoral program in Poland, that I could enroll in and her help in finding me an Institute that would accept English as a foreign language is invaluable. Without her help throughout the whole process, my PhD would not have been possible. I would also like to thank the past and current head(s) of the doctoral program at the Institute of genetics and animal biotechnology of the polish academy of sciences – prof. dr hab. Paweł Lipiński, prof. dr hab. n. farm Agnieszka Białek, and prof. dr hab. Anna Piliszek

for organizing our classes, which could not have been easy with students from different cities and countries.

I am grateful for all the help I received from present and past lab members - dr Ewa Kruminis-Kaszkiel, Agnieszka Bacławska, and Divya Das for their help in ordering reagents on time and in performing experiments. Our lab could not have functioned well if not for them and this piece of work would not have been possible. I especially thank Divya Das, whose company and conversations have kept me going over the past two years.

I would like to thank prof. dr hab. Dariusz Skarżyński and the members of the department of reproductive immunology & pathology, for having such a great working environment. Being a foreigner in a new place with different culture and mannerisms can be very intimidating, but everyone in the department has been so welcoming that I have never felt like an outsider since the day I joined the department. I sincerely thank you all for this feeling of belonging in what would've otherwise been an extremely lonely journey. I would like to especially mention Karolina Łukasik, who has been a source of information for all things Polish and has never hesitated to offer her help. Since my first day in Poland, she has helped me understand the Polish culture and integrate into the society. I'm happy to have found a great friend in you. I also want to mention Dr. Beenu Moza Jalali, who has been the voice of reason over the past few years. Her objective and unbiased advice has helped me understand and analyze situations from different perspectives and has made me a better person. I thank you for giving me a shoulder to cry on and all the hugs when I needed it the most! I will truly miss it.

My friends have been the best support system I could ever ask for, I could not have completed this PhD journey if not for them. Marcelina and Marcin, you have been my crutches in Poland, without you navigating life in Poland would've been practically impossible. Thank you for all the laughs and keeping me grounded over the past five years. Hari, you have been an unending source of comfort especially the past year. You have helped me see the light at the end of the tunnel and kept me focused on what I needed to get done. Thank you for all the late-night pep talks, my life would've been hard without them. Manish, thank you for always making time to answer my calls and giving me advice when I needed it the most. I always look forward to and enjoy our lengthy conversations on life and science. I would also like to thank Mano, who has been become a close friend over the past two years. Thank you for your support and keeping me company on days when I had to work late and even feeding me when I had no motivation to cook. It has been amazing to be able to talk to someone in kannada (our local indian language) on a daily basis. It is very rare to find a mentor and a friend in one person and I have been one of the lucky few to have found both in Raghu. Thank you for all the times you've listened to me cry and offered me comfort and sound advice. The joy you find in the

success of your students is a quality I truly appreciate in you and hope you are proud of the work I have done.

I thank my dad for encouraging and motivating me to set out on this journey of getting a PhD. He had always hoped he could do a PhD but unfortunately due to certain circumstances he could not and hoped that one of his children would be able to. I hope he would've been proud of me had he been here today. I want to especially thank my mum, who has listened to me complain for hours about things she doesn't understand but has still offered me comfort and advice to the best of her ability. It must not have been easy for her to live alone and so far away from her kids, I thank her for her sacrifices and unending support in pursuing my professional goals. I would be remiss if I did not mention my brothers, Prashant anna and Duby anna, who have silently supported my professional goals and let me figure my way through life and become my own person. I thank you for all your support and encouragement throughout my life. I really couldn't have asked for better brothers.

Last but not the least, I want to thank my cat – Hissy, who has been a great source of comfort on very difficult days. Your purring is the best medicine I could ever ask for. It has been nice to go back home to you at the end of the day rather than to an empty house.

Table of Contents

LIST OF FIGURES

LIST OF TABLES

LIST OF ABBREVIATIONS

AD	acidic domain
BAC	bacterial artificial chromosome
BPV1	bovine papillomavirus type 1
BS	binding sites
CAS	chromosome-associated spots
CBR	chromosome-binding region
cCMV	congenital CMV
CD	core domain
cDNA	complementary deoxyribonucleic acid
CHX	cycloheximide
CMC	carboxymethylcellulose
CMV	cytomegalovirus
CTD	chromatin tethering domain
DBD	DNA binding domain
DNA	deoxyribonucleic acid
DS	dyad symmetry
E-L	early-late
EBNA1	EBV nuclear antigen 1
EBV	Epstein-Barr virus
EDTA	ethylenediaminetetraacetic acid
EGFP	enhanced green fluorescent protein
EMT	epithelial to mesenchymal transition
EV	empty vector
FL	full length
FP	forward primer
FR	family of repeats
GBM	glioblastoma multiforme
GFP	green fluorescent protein
GR	glycine-arginine-rich
HCMV	human cytomegalovirus
HFF	human foreskin fibroblasts
HHV	human herpesvirus
HPF	human placental fibroblasts
HPV	human papillomavirus

HSV	herpes simplex virus
IE	immediate early
IE1FL	IE1 full length
IFA	immunofluorescence assay
IL-6	interleukin 6
iPSC	induced pluripotent stem cells
KSHV	Kaposi's sarcoma associated herpesvirus
LANA	latency-associated nuclear antigen
LB	Luria-Bertani
LBS	LANA binding site
LUNA	latent unique nuclear antigen
MAPPs	mitotic accumulation of PML protein
MEF	mouse embryonic fibroblasts
MEM	Minimal Essential Media
mEGFP	monomeric EGFP
MIE	major immediate early
MIEP	major immediate early promoter
MOI	multiplicity of infection
MP	maintenance protein
mRNA	messenger ribonucleic acid
MW	molecular weight
NBM	nucleosome binding motif
NLS	nuclear localization signal
NSC	neural stem cells
NT	non-transfected
NTD	N-terminal domain
ORF	open reading frame
PBS	phosphate buffered saline
PCR	polymerase chain reaction
PFA	paraformaldehyde
PML	promyelocytic leukemia
PV	papillomavirus
qRT-PCR	quantitative reverse transcriptase PCR
rDNA	ribosomal DNA
RNA	ribonucleic acid
RP	reverse primer

RT	room temperature
SDS	sodium dodecyl sulfate
TAE	tris acetate EDTA
TC	temporal class
TP	temporal profile
TR	terminal repeats
UL	Unique Long
US	Unique Short
VZV	varicella zoster virus
WT	wild type

1. ABSTRACT

Human cytomegalovirus (HCMV), like all herpesviruses, establishes lifelong latent infections in its host. However, the molecular mechanisms involved in HCMV latency establishment remain largely unknown. In gammaherpesviruses (eg. Kaposi's sarcoma-associated herpesvirus - KSHV), whose latency has been extensively studied, the viral genome is maintained as an episome tethered to host chromatin via a maintenance protein (MP) – for KSHV the Latency-associated nuclear antigen (LANA). MP simultaneously binds to the viral genome and host chromatin thereby tethering the viral genome to the host chromatin. While it has been shown that HCMV genomes persist in latently infected cells cells, very little is known about the mechanism of tethering and genome maintenance. The immediate early 1 (IE1) protein encoded by HCMV is known to localize to metaphase chromosomes in a pattern described as "painting of the chromosomes". The chromatin tethering domain (CTD) of IE1 was shown to mediate this localization through binding to histones, H2A and H2B. However, the functional significance of this association has not been uncovered yet. An isoform of IE1, IE1x4 protein was proposed to be the MP of HCMV and to function in a manner analogous to KSHV LANA. Additionally, HCMV genomes were shown to be tethered to host chromosomes during lytic infection and IE1 was observed to be involved in this process. The work presented in my thesis demonstrates that IE1x4 binds to mitotic chromosomes, however, the localization pattern of IE1x4 does not change in the presence of the TR region of the HCMV genome (the presumed latent origin of replication) in transfected cells as has been observed eg. for KSHV LANA. Further, IE1x4 protein was not detected during latency in infected T98G and KASUMI-3 cells, two known latency systems. Moreover, I show that in addition to the previously known painting localization pattern, IE1 also localizes as double spots (referred to as CAS – chromosome-associated spots) on mitotic chromosomes. The IE1 CAS can be observed only in some tumor cell types. The CAS formation is dependent on the IE1 core domain and is therefore independent of the CTD. The IE1 localizes to spots at the pericentromeric regions of mitotic chromosomes and recruits PML to these spots. The percentage of cells with IE1 CAS localization pattern increases in infected T98G cells, as the infection progresses from lytic to the latent phase, suggesting a role for IE1 CAS in latency or latency establishment. The IE1 CAS are reminiscent of the localization pattern of HPV8 and HPV5 E2 proteins, which function as viral maintenance proteins, therefore I hypothesize that IE1 CAS could mediate HCMV genome tethering in T98G cells.

STRESZCZENIE

Ludzki wirus cytomegalii (human cytomegalovirus - HCMV), podobnie jak wszystkie herpeswirusy, ustanawia długotrwałą utajoną (latentną) infekcję w komórkach gospodarza. Jednak mechanizmy molekularne zaangażowane w ustanawianie latencji HCMV pozostają w dużej mierze nieznane. W przypadku gamma-herpeswirusów (np. Kaposi's sarcoma-associated herpesvirus - KSHV), których latencja jest szeroko zbadana, genom wirusowy jest utrzymywany jako episom, kolista cząsteczka DNA, związany z chromatyną gospodarza poprzez maintenance protein (MP), „białko utrzymujące" - w przypadku KSHV jest nim antygen jądrowy związany z latencją (latency-associated nuclear antygen - LANA). MP jednocześnie wiąże się z genomem wirusowym i chromatyną gospodarza, tym samym przyczepiając genom wirusowy do genomu komórkowego. Chociaż wykazano, że DNA HCMV utrzymuje się w komórkach zawierających latentny wirus, bardzo niewiele wiadomo na temat mechanizmu wiązania i długoterminowego utrzymywania się genomu w komórce. Wiadomo, że immediate early protein 1 (IE1) kodowane przez HCMV w metafazie pokrywa równomiernie („maluje") chromosomy. Wykazano, że domena wiążąca chromatynę (chromatin tethering domain - CTD) białka IE1 jest odpowiedzialna za tę lokalizację poprzez oddziaływanie z histonami H2A i H2B. Jednak funkcjonalne znaczenie tej lokalizacji nie zostało jeszcze odkryte. Zaproponowano, że białko IE1x4, izoforma białka IE1, jest MP wirusa HCMV i funkcjonuje w sposób analogiczny do białka LANA. Ponadto wykazano, że genomy HCMV wiążą się do chromosomów gospodarza podczas infekcji litycznej, a białko IE1 jest zaangażowane w ten proces. Wyniki badań przedstawione w mojej pracy doktorskiej pokazują, że IE1x4 wiąże się z chromosomami mitotycznymi, jednak wzór lokalizacji IE1x4 nie zmienia się w obecności regionu TR genomu HCMV (domniemane miejsce inicjacji latentnej replikacji), co zaobserwowano np. w przypadku KSHV LANA. Co więcej, białko IE1x4 nie zostało wykryte podczas latencji w zakażonych komórkach T98G i KASUMI-3, dwóch znanych systemach latentnych. Ponadto, wykazałam, że oprócz wcześniej znanego wzoru lokalizacji „malowania chromosomów", IE1 lokalizuje również w formie podwójnych punktów (określane jako CAS - chromosome-associated spots) na chromosomach mitotycznych. CAS IE1 można zaobserwować tylko w niektórych typach komórek nowotworowych. Tworzenie CAS jest zależne od domeny głównej (core domain) białka IE1 i co za tym idzie jest niezależne od CTD. IE1 lokalizuje w punktach w regionach otaczających centromery chromosomów mitotycznych i rekrutuje PML do tych miejsc. Procent zakażonych komórek T98G wykazujących lokalizację IE1 w postaci CAS wzrasta, gdy infekcja przechodzi z fazy litycznej do fazy utajonej, co sugeruje rolę IE1 CAS w latencji lub ustanawianiu latencji. Lokalizacja IE1 w formie CAS przypomina rozmieszczenie na chromosomach białek E2 HPV8 i HPV5, pełniących funkcje białek zapewniających utrzymanie genomu wirusowego w komórce, w związku z czym stawiam hipotezę, że IE1 CAS mogą pośredniczyć w wiązaniu genomu HCMV do chromatyny w komórkach T98G.

2. INTRODUCTION

2.1 HERPESVIRUSES

Herpesviridae is an ancient family of viruses that have co-evolved with their hosts, developing elaborate mechanisms for evading host immune response resulting in life-long persistence, known as latency. Herpesviruses are ubiquitously present throughout the animal kingdom; there are more than 200 herpesviruses currently known and likely many more that are yet to be discovered. Many classes of animals, among others mammals, birds, amphibians, and mollusks, have at least one associated herpesvirus. There are nine known herpesviruses that afflict humans: herpes simplex virus 1 [HSV-1, also known as human herpesvirus 1 (HHV-1)], herpes simplex virus 2 (HSV-2, also known as HHV-2), varicella-zoster virus (VZV, also known as HHV-3), Epstein-Barr virus (EBV, also known as HHV-4), human cytomegalovirus (HCMV, also known as HHV-5), human herpesviruses 6A, 6B, and 7 (HHV-6A, HHV-6B, HHV-7), and Kaposi's sarcoma–associated herpesvirus (KSHV, also known as HHV-8) [1].

Herpesviruses are enveloped viruses characterized by a large (124–295 kb) linear double-stranded deoxyribonucleic acid (DNA) genome and their ability to establish latent infection in an animal host. Latency is defined as the maintenance of the viral genome in an infected host cell with restricted viral gene expression and no production of infectious viral particles. In response to certain stimuli, the virus can reactivate to lytic replication, which is defined by complete viral gene expression and production of infectious virus particles. The Herpesviridae family can be divided into three subfamilies: Alphaherpesvirinae, Betaherpesvirinae, and Gammaherpesvirinae, based on DNA sequence similarity and similarities in genome sequence arrangement [1]. Members of Alphaherpesvirinae (HSV-1 and 2 and VZV) exhibit broad host and cell tropism, have a short replication cycle (hours) and spread fast in culture. Latency is established in sensory neurons; however, the virus can also infect and replicate in fibroblasts, epithelial cells, and neurons [2, 3]. The Betaherpesvirinae (HCMV, HHV-6A and B, and HHV-7) exhibit species-specific tropism and a longer (days) replication cycle [4]. They spread slower in culture and in the case of HCMV, infection results in characteristic cell enlargement [5]. Members of this subfamily infect epithelial cells, endothelial cells, smooth muscle cells, monocytes, T lymphocytes, and fibroblasts, whereas latency is observed in CD34+ hematopoietic stem cells and CD14+ monocytes or T lymphocytes [5-7]. The Gammaherpesvirinae (EBV and KSHV) exhibit a very narrow and species-specific tropism. They primarily infect lymphocytes, epithelial and endothelial cells, and establish latency in B lymphocytes [8]. The characteristics of the Herpesviridae family is summarized in table 1.

Table 1. Summary of characteristics of Herpesviridae subfamilies.

Characteristics	Alphaherpesvirinae	Betaherpesvirinae	Gammaherpesvirinae
Host Range	variable, often broad	restricted	species-specific
Reproductive cycle	short (hours)	long (days)	long (days)
human herpesvirus representatives	HSV-1, HSV-2, and VZV	HCMV, HHV-6A, HHV-6B, and HHV-7	KSHV and EBV
Primary infection	epithelial cells	HCMV – fibroblasts, epithelial cells, endothelial cells, hepatocytes, myeloid cells, and neural cells HHV-6/7 – T-cells	KSHV – endothelial cells EBV – epithelial cells
Latency	neurons	HCMV – CD34+ haematopoetic cells, CD14+ monocytes, NSC HHV-6/7 – T-cells	B-cells

All herpesviruses share a common subset of 43 core genes [5]. Most of the core genes are required for the propagation of the virus in culture and perform vital functions including, DNA replication, virion packaging, and virion entry/egress. After infection, gene expression occurs in a temporal fashion and viral proteins are classified by the timing of expression: immediate early (IE), early (E), and late (L) proteins. IE genes encode the very first viral proteins expressed after virus entry into the host cell. Expression of early proteins requires the previous expression of IE genes, which are transactivators of early gene expression. Late proteins are expressed only after the initiation of viral DNA replication and are mainly necessary for DNA packaging and the formation and egress of the virions. Each class of viral proteins, except for IE proteins, is dependent upon the expression of the previous class [1].

2.2 HUMAN CYTOMEGALOVIRUS

2.2.1 EPIDEMIOLOGY

HCMV infection is globally ubiquitous; a seroprevalence of 60% in developed countries and more than 90% in many developing countries was reported in 2019 [9]. A more recent study has shown

that seroprevalence ranged from 39.3% to 48.0% among adult men and 24.6% to 95.7% among women of reproductive age in developed countries globally [10]. In Poland, a high seroprevalence of 81.9% among women of childbearing age has been observed [11]. The average annual incidence of congenital CMV (cCMV) is 48 per 100,000 live births in Poland [12].

2.2.2 HCMV-ASSOCIATED DISEASE

A primary HCMV infection typically occurs at an early age and is generally asymptomatic. Infection spreads naturally via bodily fluids including saliva, breast milk, and genital secretions [13-16].

HCMV is an opportunistic pathogen with the ability to reactivate from latency in individuals with a compromised immune system. HCMV is the cause of life-threatening disease and disorders in solid organ and bone marrow transplant patients, cancer patients, and AIDS patients. HCMV is linked to a higher risk of graft rejection, as well as an increased morbidity and mortality [17]. Patients can suffer from HCMV pneumonia, gastrointestinal disease, central nervous system disease, hepatitis, retinitis, in addition to CMV syndrome, which is characterized by fever and malaise as well as leukopenia, thrombocytopenia, elevated liver enzymes such as alanine aminotransferases and aspartate transaminase [18-20].

Vertical transmission from mother to fetus may cause congenital CMV (cCMV) disease; symptoms include intrauterine growth retardation, jaundice, microcephaly, developmental delay, sensorineural hearing loss (most common neurodevelopmental impairment in this setting) and significant subsequent mortality rates [21, 22]. HCMV infection occurs in approximately 0.5% of live births, and around 10% of infections are symptomatic [21].

In addition to CMV disease, asymptomatic HCMV infection in healthy individuals has also been linked to an increased incidence of atherosclerosis, arterial hypertension, glioblastoma and Guillain-Barré syndrome, and such conditions reduce overall life expectancy in these seropositive individuals [23-27].

2.2.3 VIRUS STRUCTURE

HCMV is the largest virus of the herpesviruses, with the virus particle having a diameter of approximately 230 nm, characterized by a linear double-stranded DNA genome of 240 kb. The HCMV virion particle is composed of a lipid bilayer envelope surrounding the tegument and capsid. The icosahedral capsid is embedded within the tegument and contains the linear viral genome, which is packaged as naked, non-chromatinized DNA. The tegument is a compact, dense layer composed of viral and cellular proteins and is a unique feature of herpesviruses [28]. In addition to proteins, several species of both viral and cellular RNAs are present in the tegument including non-coding and coding RNA [29, 30]. The tegument is responsible for 40% of the virion mass, the majority of which consists of five viral proteins: UL47, UL48, UL32, UL82, AND UL83 [28]. The virion envelope is

richly coated with several viral glycoproteins such as gB, gM/N, gH, gL, and gO, which mediate entry of the virion via cell receptor-mediated endocytosis [31].

2.2.4 HCMV LIFE CYCLE

HCMV can establish lytic infection in a wide range of cell types during primary infection in vivo, including fibroblasts, epithelial cells, endothelial cells, hepatocytes, myeloid cells, and neural cells [5, 6, 32].

In contrast to lytic infection, the virus appears to establish latent infection in a more restricted range of cells. One site of latency is in cells of the early myeloid lineage, which includes CD34+ progenitor cells and CD14+ monocytes [33-36]. In vitro studies suggest that aortic endothelial cells, but not brain microvascular endothelial cells support latent HCMV infection [37]. Recently it has been shown that latency can be established in neural stem cells [32].

HCMV entry occurs in three phases: first, the virion glycoprotein B (gB), along with the glycoprotein M/glycoprotein N complex (gM/gN), tethers the virus to the cell surface via heparan sulphate glycosaminoglycans [38-40] Next, the virion binds to cellular receptors - integrins (αVβ3, α6β1, and α2β1) and the epidermal growth factor receptors (EGFRs), both of which bind gB [41-43]. Lastly, fusion of the viral and cellular membranes is mediated by gB and the trimeric complex of glycoprotein H, glycoprotein L and glycoprotein O (gH/gL/gO) in fibroblasts through its interactions with platelet-derived growth factor-α (PDGFR-α); while a pentameric complex of glycoproteins gH/gL, Unique Long (UL)128, UL130 and UL131 mediate fusion by interaction with PDGFR-α in epithelial and endothelial cells [44-51]. After membrane fusion, the viral capsid loses its tegument layer. The released tegument proteins facilitate the transactivation of viral gene expression, transport of the viral capsid towards the nucleus using motor proteins and microtubules. Following capsid delivery to the nuclear membrane, the viral genome is released and enters the nucleus through nuclear pore complex. Once inside the nucleus, the genomes are occupied with histones and chromatinized. The viral genomes can either initiate a productive lytic replication cycle or establish a quiescent, latent state [52-55].

The viral DNA circularizes when it is released from the capsid into the nucleus. It is replicated using a rolling circle mechanism with head to tail concatemer formation followed by cleavage into genome length fragments and packaging into the viral capsid [56, 57]. Replication starts at the origin of lytic replication, OriLyt, located in the UL region of the genome. OriLyt contains multiple functional elements including repetitive sequences, AT-rich regions, an oligopyrimidine stretch known as y-block, transcription factor binding sites, and an RNA-DNA hybrid region with an ability to form stem-loop structure [57-62]. Transient replication assays revealed that 11 viral genes: UL36-38, UL44 (pol accessory protein), UL54 (DNA polymerase), UL57 (single-stranded DNA binding protein),

UL70 (primase), UL102 (primase-associated factor), UL105 (helicase), UL112/113 (early proteins), IRS1/TRS1 (immediate early RNA-binding), IE1/2 (transactivator) and UL84 are required for efficient DNA replication. 6 of these (UL44, UL54, UL57, UL70, UL102, UL105) are common to all herpesviruses and are known as the "core replication proteins" and form the HCMV replisome [63, 64]. pUL44 is responsible for recruiting the components of the replisome complex to the OriLyt and UL112-UL113 may also play a role in this process [65, 66]. UL84 together with IE2, bind to the oriLyt and facilitate viral DNA replication initiation [59, 67].

DNA synthesis is carried out by the viral polymerase UL54, which interacts with the polymerase accessory factor UL44 [68, 69]. The helicase-primase complex, consisting of UL105, UL70 and UL102, plays a key role in unwinding the existing viral DNA template and providing a primer for UL54 to initiate DNA replication [70, 71].

Capsids are assembled in the nucleus out of proteins encoded by UL86, UL46, UL85, and UL48A. Viral DNA is encapsidated by the terminase complex (UL89, UL56, UL51) through a channel formed by pUL104 [72, 73]. The capsids are then released from the nucleus via an envelopment/de-envelopment process. Primary envelopment requires pUL50 and pUL53, and results in an enveloped capsid within the perinuclear space [74-77]. This intermediate then buds out of the outer nuclear membrane, shedding its envelope and resulting in cytoplasmic capsids. Tegument proteins such as pp150, pp65 and pp28 are then incorporated by binding to the capsids [78-80]. Tegumented capsids then bud into cytoplasmic vesicles studded with viral glycoproteins to acquire a double-layered membrane in a pp28-dependent manner. They are then trafficked out of the cell, fusing with the plasma membrane to release infectious particles with a single membrane [81].

2.2.5 HCMV GENE EXPRESSION

2.2.5.1 LYTIC PHASE

During productive infection, HCMV gene expression occurs in a sequential manner and is classically divided into immediate-early (IE), early (E), early-late (E-L), and late (L) genes. IE genes are primarily responsible for activating the transcription of early genes. Early genes encode functions necessary to initiate viral DNA replication, these genes are initially transcribed at low levels and upregulated after the onset of viral DNA replication. Early-late genes are initially transcribed at low levels and its expression is independent of DNA replication. Late genes are expressed only after DNA replication is complete and include proteins required for the assembly and morphogenesis of HCMV virions [4]. The classical IE/E/E-L/L cascade was functionally defined using metabolic inhibitors: cycloheximide (CHX) and phosphonoformate (PFA). IE transcripts accumulate in the presence of CHX, a protein synthesis inhibitor. PFA, a viral DNA replication inhibitor, leads to partial inhibition of E genes and complete inhibition of L genes [82].

Recent proteomic and transcriptomic studies have revealed a more complex expression profile than the classical IE/E/L pattern [83, 84]. Proteomic analysis using a "quantitative temporal viromics" approach classified the viral proteins based on their temporal profiles (TPs) into TP 1 to 5. TP1 proteins are expressed with a similar pattern to IE proteins and high levels of expression are observed from 6 hours post infection (hpi) with decrease in expression observed from 24 hpi upto 96 hpi (last tested timepoint). TP2 and TP3 correlate with early and early-late expression pattern. TP2 proteins accumulate rapidly at early time points and constant expression is observed through infection. TP3 proteins accumulate slower with maximum expression observed at 48 hpi. TP4 proteins have a distinct expression profile, with maximum expression observed at 48 hpi and lower expression at all other time points. TP5 proteins correlate with late proteins; their expression peaks between 72 and 96 hpi with minimal expression at 24 and 48 hpi [83]. Single cell transcriptomic analysis correlates well with the TP1 to TP5 protein classification reported by the Weekes group, however the transcripts were classified into seven temporal classes (TCs) to better demonstrate the complexity of viral gene expression [83, 84]. These TCs are: TC1- immediate-early; TC2 - early; TC3 - delayed early; TC4 - early-late; TC5 - late-replication-independent; TC6 - late-translation-independent; and TC7 - late viral gene expression [84]. TC1 genes were highly expressed at 4 hpi, TC2 and TC3 have early and delayed early kinetics and contain many genes classically defined as early. The late clusters (TC5–TC7) contain many known late genes with peak expression between 48 and 72 hpi [84].

2.2.5.2 LATENCY

Classically defined, latent genes are those that are expressed throughout the infection, both in the lytic cycle as well as in latency, in contrast to lytic genes described as those expressed only in the lytic cycle. Viral gene expression during latent infection has been extremely hard to characterize and is still a matter of controversy [35, 85, 86]. Studies of primary cells infected in vitro, as well as the detection of viral transcripts in cells derived from seropositive individuals, suggest that limited viral gene expression occurs in latency [87, 88]. Several studies have shown that gene expression from the viral genome is repressed during latency, especially the major immediate early promoter (MIEP) and this is considered to be the major mechanism maintaining latency [89-92].

Recently, the use of more sensitive assays revealed that HCMV latency exhibits a broader expression of several IE and early genes than so far known, but it is not clear how these genes contribute to the establishment and/or maintenance of latency [87, 88, 93-95]. Single cell transcriptomic analysis of latent cells revealed low level expression of transcripts of all kinetic classes, resembling a late-lytic transcription profile and this study did not find evidence for a latency-specific transcriptional profile [84, 96, 97]. These findings have complicated defining distinct latent and lytic patterns of gene expression or using the absence of IE gene expression alone as an indicator of latency establishment.

To define latency, several studies now use the ratio of relative levels of immediate early or replicative genes (e.g., IE1-86kDa, IE2-72kDa, UL135) to latency genes (e.g., UL138, LUNA) [84, 96, 98-100].

So far, studies using experimental models for latent HCMV infection have identified a few genes that are expressed during latency: US28, latent unique nuclear antigen (LUNA), UL111A (viral IL-10), UL138, UL144, and a smaller variant of the UL123-encoded IE1 protein (IE1x4) [101-108]. Long noncoding RNAs, including lncRNAs 4.9 and 2.7, have also been detected during HCMV latency [93]. Of the 26 miRNAs encoded by HCMV, at least 12 are expressed in latently infected cells [109].

Thus, the current understanding of HCMV gene expression and regulation during lytic phase and latency deviates from the classical definitions and is more complex than originally assumed.

2.3 IMMEDIATE EARLY 1 PROTEIN

The 72-kDa immediate early (IE) 1 protein (called IE1-72kDa, IE72, or IE1) is a nuclear phosphoprotein of 491 amino acids. Expression of the IE1 protein in cell nuclei is detected as early as 2 h after HCMV infection. It originates from the open reading frame UL123 located in the MIE region, which also encodes the IE2 protein (UL122). Both proteins are expressed from a single gene consisting of five exons (exons 1-5). The IE1 mRNA contains exons 1–4, while IE2 is expressed from exons 1–3 and 5 [110, 111]. The two major IE proteins share a common N-terminal region of 85 amino acids (exons 2 and 3). Due to alternative splicing and an additional promoter within this gene, several smaller gene products are also expressed at different stages of infection as shown in figure 1 [112-115]. IE1 is required for viral early gene expression and replication in human fibroblasts at low multiplicities of infection [116, 117]. However, in the clinical strain TB40E, IE1 is required for replication also at high multiplicities of infection, suggesting that IE1 plays an even more important role in clinical isolates then in the laboratory adapted HCMV strains [118].

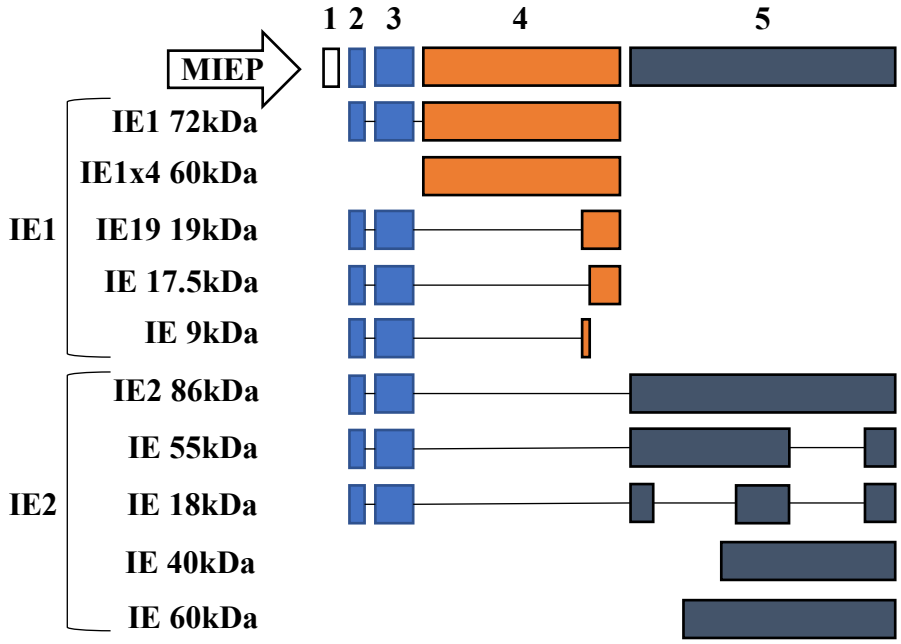

Figure A.1. Schematic of exons of the major immediate early (MIE) gene locus of HCMV. *The MIE locus contains exons 1 to 5, denoted by numbers on top of the schematic and the arrow represents the major immediate early promoter (MIEP). The protein products are loosely divided into IE1 (containing exon 4 sequences) and IE2 (containing exon 5 sequences).*

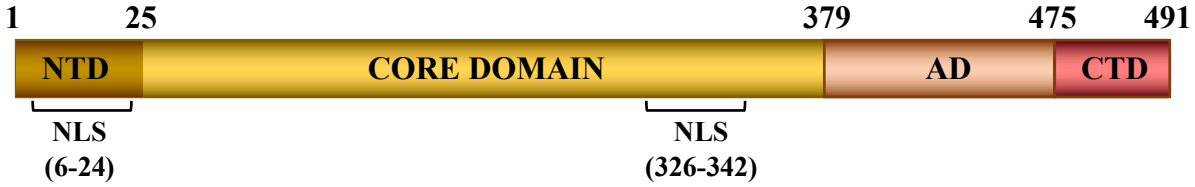

Figure A.2. Schematic of IE1 protein domains. *The IE1 protein (491 amino acids) consists of the N-terminal domain (NTD), core domain, acidic domain (AD), and chromatin tethering domain (CTD). Amino acid residue numbers are denoted on top of the schematic. The residues corresponding to nuclear localization signals (NLS) are marked below.*

The IE1 protein sequence can be divided into four distinct regions: N-terminal domain (NTD), core domain (CD), acidic domain (AD), and a short 16-amino-acid chromatin tethering domain (CTD) at the C-terminus as depicted in figure 2 [119-122]. The NTD is comprised of 24 residues, encoded by exon 2 and is shared with IE2 and most IE protein variants with exception of IE40kDa and IE60kDa. It contains a nuclear localization signal (NLS) that has been shown to be required and sufficient to mediate nuclear import of IE1 [119, 122]. Residues encoded by exon 3 (residues 25–85) and exon 4 (residues 86–382) form the CD of IE1, which is involved in several protein interactions. Deletions in the CD have been shown to abrogate the transactivation function of IE1 in reporter assays [123-125].

The CD of IE1 is essential and sufficient to target the promyelocytic leukemia (PML) protein and to overcome the PML-mediated intrinsic immune defense, which was observed in transfection and infection experiments [125, 126]. Two binding sites (BS) for the cell-cycle regulator p107, corresponding to residues 45–52 (in exon 3) and 312–318 (in exon 4), are also found in the CD [127-129]. Several reports have shown that the CD is highly sensitive to mutations resulting in loss of structural stability, decreased protein expression and loss of protein interactions [124, 126, 130]. The CD is structurally conserved among primate and rodent CMV IE1 proteins and mediates dimerization of IE1 [131, 132]. A second NLS, in addition to the one found in NTD, has been reported in the CD (residues 326 and 342) [133]. The AD as the name suggests, is rich in acidic residues and is highly disordered. It mediates interaction with STAT1, STAT2, and STAT3, thereby compromising STAT-mediated interferon (IFN) signaling [134-136]. The C-terminal 16-residue CTD is responsible for the association of IE1 with chromosomes and will be discussed in detail in the next section [121, 137, 138].

2.4 IE1 AND CHROMATIN ASSOCIATION

The association of IE1 with mitotic chromosomes was first observed over 30 years ago; this association can be observed both during HCMV infection and ectopic expression of IE1 [119, 121, 126, 136, 137, 139-141]. Domain responsible for chromosome association was first mapped to MIE exon 4 sequences and, subsequently, to residues 421 to 486 [119, 137]. Eventually, the amino acids 476 to 491 were determined to be required and sufficient for mitotic chromatin interaction and this region was termed the chromatin tethering domain (CTD) [121]. Subsequently, the nucleosome binding motif (NBM) – residues 479 to 488 - was identified. Four amino acids of the NBM are essential for binding to histones H2A and H2B, namely: H481, M483, T485 and R486 [138]. The crystal structure of the CTD bound to nucleosomes confirmed the interaction of IE1 with the acidic patch of H2A-H2B [142]. The IE1 CTD forms a hairpin loop and occupies similar regions in the acidic patch of the nucleosome as the KSHV latency-associated nuclear antigen [138, 142]. Following these studies, many publications have suggested that IE1 may play a role in genome tethering of HCMV [101, 137, 138, 140, 143].

2.5 VIRAL MAINTENANCE PROTEINS (MP)

During latency, viruses such as EBV, KSHV, and papillomaviruses (PV) maintain their genome as a circular extrachromosomal plasmid in the nucleus of proliferating cells. These viruses encode a maintenance protein (MP) that tethers the viral genome to host cell chromatin to ensure its partitioning to daughter cells. Viral tethering proteins are detected on mitotic chromosomes in complex with their

respective viral genome. Tethering is best understood for EBV nuclear antigen 1 (EBNA1), latency-associated nuclear antigen (LANA) of KSHV, and E2 of PVs [144, 145].

2.5.1 EBV NUCLEAR ANTIGEN 1 (EBNA1)

EBNA1 is the maintenance protein of EBV. EBNA1 protein contains two major domains: the N-terminal domain and the C-terminal DNA binding domain. The N-terminal domain (NTD) contains the glycine-arginine-rich (GR) regions – GR1 and GR2, which mediate binding to cellular chromatin [146]. The NTD also contains the UR1 domain said to be important for transcription activation and episome maintenance [147, 148]. A nuclear localization signal is also present in the NTD [149, 150]. The C-terminal domain contains the DNA binding domain, which mediates binding to the viral genome, and a dimerization domain [151-153].

EBNA1 is diffusely distributed on mitotic chromosomes in the absence of EBV genome, whereas it forms double spots in the pericentromeric regions on several chromosomes, in the presence of the EBV genome and colocalizes with the viral genomes [146, 154-156].

Binding to viral genome: EBNA1 binds to the EBV genome in a sequence-specific manner through the DNA binding domain (DBD) located at the C-terminus of the protein, which forms a dimeric eight-stranded beta-barrel structure [152, 153]. The DBD binds to the EBNA1 binding sites in the oriP, the viral latent origin of replication of EBV. The oriP contains two functional elements: family of repeats (FR) and dyad symmetry (DS); the FR contains 20 EBNA1 binding sites and the DS contains 4 EBNA1 binding sites [157, 158]. Binding of EBNA1 to the DS is required for initiation of EBV genome replication, whereas binding to the FR is required for transcriptional activation and latent genome maintenance [159-166]. Additionally, EBNA1 interacts with Brd4 and localizes to the FR element of oriP [167].

Binding to cellular chromatin: EBNA1 mediates interactions with host cell chromatin by two modes: by direct binding to specific DNA sequences and by interaction with cellular chromosome-binding proteins. EBNA1 binding to host chromosomes is mediated by two glycine-arginine-rich (GR) regions in its N-terminal - domains A and B (also known as linking regions 1 and 2) [146, 151]. GR-rich regions function as AT-hooks that bind to AT-rich regions of the host DNA [151, 154, 168]. Inhibiting the binding of the AT-hooks has been shown to reduce EBV genome maintenance during latency [169]. EBNA1 interacts with the cellular chromosome-associated EBNA1-binding protein 2 (EBP2) via domain B [151]. EBNA1 also interacts with regulator of chromosome condensation 1 (RCC1), a protein shown to directly bind to cellular histones; inhibition of this interaction disrupts EBNA1 chromatin association [170].

2.5.2 LATENCY ASSOCIATED NUCLEAR ANTIGEN (LANA) OF LANA

LANA is the maintenance protein of KSHV. LANA has three distinct regions: a small N-terminal domain, a large central region containing multiple interspersed repeat sequences, and a C-terminal DNA binding/dimerization domain. The N-terminal domain contains the chromosome-binding region (CBR), which mediates binding to cellular chromatin and is required for LANA-mediated transactivation [171, 172]. The N-terminal domain also contains a nuclear localization signal [171, 173]. The C-terminal DNA binding/dimerization domain mediates association with the viral genome as well as dimerization [174]. LANA is diffusely distributed on chromosomes in the absence of KSHV genome, whereas in the presence of the KSHV genome it colocalizes with the viral genomes and is found in multiple spots on both arms of all the chromosomes [171, 173, 175].

Binding to viral genome: The C-terminal DNA binding/dimerization domain (DBD) of LANA binds to the TR region (the latent origin of replication) of the KSHV episome. Each KSHV genome contains 35-40 TR repeats on an average, each of which contains three 18–20bp LANA binding site (LBS) motifs [174-177]. The LANA DBD structure is formed by two molecules of LANA, which come together to form the beta-barrel core. On one side of the beta-barrel is the DNA binding region which mediates binding to viral genome and opposite to this region is the basic patch, which mediates binding to chromatin. The surface alpha helices on the beta barrel structure contact residues in the LBS motifs within the TR regions [176, 178, 179]. The KSHV TR element is both necessary and sufficient for the initiation of DNA synthesis and genome maintenance [177, 180, 181].

Binding to cellular chromatin: The N-terminal LANA CBR forms a hairpin structure that associates with the H2A/H2B interface of nucleosomes and mediates LANA's association with mitotic chromosomes [171, 172, 182, 183]. A truncated form of LANA consisting of the C-terminal region (residues 996-1139) localizes to pericentromeric and peri-telomeric regions of the chromosomes [184, 185]. LANA has been shown to interact with other chromatin associated proteins: the N-terminal region interacts also with MeCP2 and HP1 while C-terminal region interacts with chromosomal methyl-CpG-binding protein 2 (MeCP2), DEK, and nuclear mitotic apparatus (NuMa) [184, 186-192].

2.5.3 E2 OF PAPILLOMAVIRUSES

The PV E2 protein (E2) contains two conserved domains linked by a flexible hinge. The N-terminal transcriptional activation domain interacts with multiple cellular proteins that influence replication, transcription, and tethering of E2 to host chromatin. It is important for transcriptional regulation and interaction with E1. The C-terminal domain contains the DNA binding and dimerization domain (DBD) [193-195]. The hinge region contains sites for post-translational modifications that are

conserved within each genus and regulate E2 half-life, nuclear location, protein-protein interactions, and tethering to host chromatin [196].

Binding to viral genome: The DBD of E2 binds specifically to 12-bp E2 BS motifs in the viral genome [193-195]. The DBD when bound to its target DNA, forms a dimeric, eight-stranded, anti-parallel beta-barrel structure. Two alpha helices on the surface of the barrel forms the DNA recognition surface and specific amino acids are involved in base recognition [197]. The DBD structure is well conserved in E2 proteins across all PV genera and has substantial similarity to the DBDs of LANA and EBNA1, although there is low amino acid sequence similarity among the three proteins [152, 176, 197].

Binding to cellular chromatin: Among the papillomaviruses, bovine papillomavirus type 1 (BPV1) E2 protein is best studied. BPV1 E2 protein and viral genomes colocalize on mitotic chromosomes as small speckles on the arms of all chromosomes, in complex with Brd4 [198-202]. Although the E2 proteins are well conserved across the PV genera, each E2 protein binds to distinct regions of mitotic chromosomes. The HPV8 and HPV5 E2 protein localizes to pericentromeric region of chromosomes as double speckles and was found colocalizing with HPV genomes [203-205]. On human host chromosomes, HPV8 E2 localizes to the ribosomal DNA (rDNA) loci between the β-satellite DNA and centromeric DNA on the short arms of the acrocentric chromosomes – 13, 21, 14, 22, and 15 [204]. HPV8 E2 was found to colocalize with rDNA transcription factor UBF on mitotic chromosomes [204]. HPV8 E2 requires the C-terminal DNA binding and dimerization domain and the hinge region for mitotic chromosome association [198, 201, 204, 206].

2.6 IE1 AND VIRAL GENOME TETHERING

As in most herpesviruses, latent HCMV genomes are thought to be maintained as extrachromosomal, covalently closed circular episomes within cell nuclei [207]. It has been suggested that IE1 may perform functions analogous to KSHV LANA as a maintenance protein (MP) in HCMV latency [101, 138]. The CTD of IE1 shares several similarities with the N-terminal LANA CBR: they form a hairpin-like structure that “pokes” into the acidic patch of the nucleosome, occupy the same regions of the acidic patch of the nucleosome, engage the same sets of histone residues, and compete for binding with nucleosomes [138, 142]. However, the genome tethering mechanism in cells latently infected with HCMV remains elusive.

A smaller variant of IE1, the IE1x4 protein (~60kDa) was proposed to be the HCMV MP and was found to be expressed exclusively during latency in CD34+ hematopoietic cells, but not in CD14+ monocytes [93]. It was shown to be required for the maintenance and replication of a plasmid containing the HCMV latent origin – the terminal repeats (TR) region [101]. The authors proposed

that the IE1 CTD interacts with H2A–H2B on the nucleosome surface to bind to the host chromosomes, whereas the AD tethers the viral genome indirectly via the cellular transcription factor Sp1, which binds to the TR [101]. This is a plausible mechanism for tethering by IE1 or IE1x4 as IE1 is not known to directly bind to DNA as other viral MPs, and the dimerization of IE1 may facilitate simultaneous binding to the viral genome and host chromosomes.

Another variant of IE1, the IE19 protein (19kDa) was shown to play a role in genome maintenance in dividing cells during lytic infection. Tethering by IE19 prevents the loss of genomes in mitosis following infection in the S-phase [208]. However, IE19 protein is yet to be detected in infected cells; only mRNA expression has been observed thus far.

Recently, HCMV genomes were demonstrated to associate with host chromosomes at perichromatin regions during lytic phase [209]. IE1 was observed to play a supporting role in the tethering process during lytic phase. These results suggest that proteins other than IE1 are also involved in the process [209]. Surprisingly, it appears that genome tethering via IE1 occurs by both CTD dependent and independent mechanisms, suggesting that IE1 may associate with host chromatin by mechanisms independent of the CTD [209].

Therefore, further studies need to be carried out to understand the explicit role of IE1 in viral genome tethering, as the mechanism appears to be more complex than has been observed for other viral MPs.

2.7 HCMV AND GLIOBLASTOMA

Glioblastoma is the most common primary brain tumor. It is highly malignant and associated with very poor prognosis [210, 211]. After surgery and combined radio- and chemotherapy, the expected 5-year survival rate is less than 5%. An annual incidence of 2–3 new cases per 100,000 individuals has been reported, with a median survival of 15 months [212]. In 2002, HCMV was first reported to be present in glioblastoma samples and was not detected in the surrounding healthy brain tissue [213]. Since then, there has been high inconsistency in the detection of HCMV in glioblastoma samples, making the role of HCMV in glioblastoma controversial [214-217]. In 2011, a group of oncologists and virologists published a consensus statement regarding major questions in the association of HCMV with glioblastoma. They concluded that HCMV sequences and viral gene expression exist in many high-grade gliomas and that in vitro studies suggest that HCMV can upregulate key signaling cellular pathways involved in promoting tumor phenotype in glioblastomas [218]. Recently, a systematic review of published data revealed that HCMV is highly prevalent in glioblastomas, but optimized immunohistochemistry techniques are required to detect it, which could explain previous inconsistent results. HCMV DNA was often detected with in situ hybridization (ISH) probes, whereas it was not reliably detected by PCR based techniques and NGS sequencing, stressing the importance

of employing the appropriate detection method and optimized conditions [27]. The involvement of HCMV in glioblastoma multiforme (GBM) is supported by the observation that treatment against HCMV improves the patient´s response to cancer therapy, and thereby improves the prognosis [219-222].

Currently, HCMV is not considered to be a classic oncogenic virus but is thought to be oncomodulatory [218, 223-225]. Few studies have shown that HCMV can induce transformation of human embryonic lung fibroblasts and human mammary epithelial cells [226, 227]. Recently it was shown that HCMV can also transform human astrocytes to glioblastoma cells [228]. It is important to note that, in these studies, transformation potential was observed only with HCMV-DB and BL clinical strains (the high-risk oncogenic strains) [227, 228]. HCMV was shown to increase cellular proliferation in infected GBM cells by interfering with the regulation of key cellular factors such as p53, Rb, PI3K/Akt, GFAP, and TSP-1, which are known to be involved in cell cycle control, cellular differentiation, and proliferation [229-233]. Increased proliferation was also induced by HCMV through upregulating endocan (a proteoglycan), which has been shown to be involved in several cellular processes, including angiogenesis [234]. Immortalization may be promoted by increased hTERT expression and thereby increased telomerase activity observed in various HCMV infected cancer cell lines including glioblastoma [235]. Interleukin 6 (IL-6) and TNF-α expression was increased following HCMV infection in GBM cell line (U87MG) [234]. Another study showed that IL-6 treatment significantly upregulated HCMV gene expression in infected glioma cultures [236]. Taken together, this suggests that pro-inflammatory cytokines in the tumor environment further augment HCMV gene expression and consequently tumor progression driven by virus induced cellular signaling. Infected GBM cells exhibit epithelial to mesenchymal transition (EMT) when treated with TGF-β, resulting in decreased expression of E-cadherin and increased expression of vimentin and MMP-2. Consequently, HCMV infection may enhance invasion and migration of tumor cells through EMT [237]. Depletion of Rho GTPases in infected GBM cells led to a reduction in proliferation rate and invasion, suggesting an important role for Rho GTPases in tumor progression in the context of HCMV infection [238]. Stem cell markers such as CD133, Notch1, Sox2, Oct4, Nestin, and stem cell regulators such as STAT3 and BMX are upregulated in HCMV infected glioma cultures, thereby increasing the stemness properties of these cells [236, 239, 240]. These results further stress the need for an anti-HCMV therapy along with chemo- and radio- therapy in the treatment of GBM. Recently, it was demonstrated that HCMV manipulates the tumor microenvironment, potentially leading to cancer progression by metabolic reprogramming of infected glioblastoma cells and manipulation of key metabolic pathways of neighboring cells in a paracrine manner independent of viral transmission [241]. HCMV infection has been shown to trigger host-cell replication stress, resulting in genome instability through enhanced 53BP1 foci formation,

accumulation of single-stranded DNA, asymmetric host DNA replication forks, enhanced frequency of aberrant chromosomal mitotic figures and micronuclei in various cancer cell lines including, glioblastoma [242]. These studies are consistent with HCMV playing an oncomodulatory role in glioblastoma progression by enhancing cellular proliferation, survival, immunosuppression, angiogenesis, invasion, and by creating a pro-inflammatory environment.

Amongst the HCMV gene products detected in GBM samples, IE1, pp71, glycoprotein B, and US28 have previously been shown to be involved in tumor induction and progression. Overexpression of HCMV pp71 induces a pro-inflammatory response via the activation of NF-κB signaling in adult neural precursor cells [243]. HCMV glycoprotein B was shown to mediate viral entry into host cell via the receptor tyrosine kinase PDGFR-alpha, resulting in activation of the PI3-K/AKT signaling pathway thereby promoting cell proliferation [230, 232]. US28 was shown to regulate several cellular pathways including STAT3, VEGF, and e-NOS signaling, which promote GBM pathogenesis by regulating angiogenesis, invasion, and immune evasion respectively [233, 244]. US28 has also been demonstrated to increase hypoxia inducible factor-1 (HIF-1)-dependent proliferation of GBM cell line U251 through upregulation of glycolysis [245]. The role of IE1 in glioblastoma is further discussed below.

2.8 IE1 AND GLIOBLASTOMA

IE1 is the most frequently detected HCMV protein in glioblastoma samples, with some studies reporting 100% prevalence in glioblastoma and 82% in low-grade glioma [246]. Significant association of IE1 expression level with tumor grade and prognosis has been reported and IE1 might have onco-modulatory effects that vary with tumor grade. In GBM, IE1 localizes to the cytoplasm as well as the nucleus in contrast to the exclusive nuclear localization observed in other cells. This suggests that IE1 may have additional roles in GBM [213].

IE1 promotes the tumor phenotype by promoting tumorsphere formation, regulating key cellular factors such as p53, Rb, PI3K/Akt, increasing the stemness properties, proliferation, migration, and survival of these cells [229, 247, 248]. Increased telomerase activity correlated with the expression of IE1 alone in GBM cell lines and IE1 was found to co-localize with hTERT protein in gliomas. In addition, high expression of Sp1 was observed in these cells and was found bound to the hTERT promoter [235]. IE1 is a known interactor of Sp1, it is tempting to speculate that IE1 may exert its effect on hTERT via Sp1. IE1 was shown to induce host-cell replication stress and genome instability in HCMV-infected cancer lines including GBM [242]. Interestingly, it was observed that the HCMV-induced cell cycle arrest seen in infected fibroblasts is overcome in GBM cells (U373MG & T98G) [143].

3. AIMS OF THE THESIS

The goal of the thesis was to study the mechanism of association of HCMV IE1 protein with the cellular chromatin. The first part of the study concentrated on investigating the role of IE1x4 in HCMV genome tethering during latency, since this isoform of IE1 was so far most studied in the context of chromosome binding and the functional consequences of this association. The IE1x4 protein has been shown to bind to the TR region and be required for viral genome maintenance and replication [101]. It was proposed that the IE1x4 protein tethers the HCMV genome to the cellular chromatin, in a manner analogous to KSHV LANA, the gammaherpesvirus latency protein, and that IE1x4 may be its functional homologue [101]. In the case of gammaherpesviral maintenance proteins (EBNA1 and LANA1) the presence of the viral genome (or even just the latent origin of replication) leads to relocalization of the viral protein from painting of the chromosomes to spots [171, 173, 175, 249]. To test whether the same phenomenon can be observed for the HCMV IE1x4 protein and the HCMV TR region (suggested to be the latent origin of replication), I analyzed the localization pattern of IE1x4 in the presence of HCMV TR region. In addition, I have also checked for the expression of IE1x4 during latency in T98G and KASUMI-3 cells, used as latency models for HCMV.

While performing the above experiments, I observed that in T98G cells IE1 in addition to painting chromosomes also forms chromosome associated spots (CAS) pattern and this discovery formed the bases for the study in the second part of my thesis. To understand the reason for unique localization of IE1 in glioblastoma cells, I selected cell types with features overlapping the characteristics of T98G cells i.e., glioblastoma cells, cells of neural origin, cells able to support HCMV latency and analyzed the localization pattern of IE1 in these cells following transfection with IE1 or HCMV infection. The IE1 CTD was shown to be responsible for the painting pattern on the mitotic chromosomes observed for this protein [138, 142]. To understand whether the same or different domain is responsible for the CAS localization, I have mapped the domain responsible for this localization pattern. In an attempt to determine more precisely the region of the chromosome the IE1 CAS localize to, I co-stained with the centromeres. Finally, since it was shown before that IE1 localized in the painting pattern re-localizes PML protein to the chromosomes, I tested if it is also the case for the IE1 present in the form of CAS. Since I have observed the painting and CAS localization during the same phase of the cell cycle i.e., metaphase, I tried to understand what determines the two different patterns and checked first if IE1 protein expression levels influence the localization pattern. In addition to this, I have performed live imaging of IE1 to understand what happens to IE1 CAS as the cell undergoes cell division – if the switch from CAS to painting or vice versa occurs during or after the cell division.

4. MATERIALS AND METHODS

4.1 Bacterial strain

Escherichia coli TG2 strain was grown in Luria-Bertani (LB) media at 37°C with agitation at 200 rpm and was used for all cloning purposes. The following antibiotics were added when required - ampicillin (100 mg/ml, A & A Biotechnology #2017-25) and kanamycin (50 mg/ml, A & A Biotechnology #2016-5). LB broth (#X968.1) and LB agar (#X969.1) were purchased from Carl Roth and prepared according to manufacturer's instructions. Briefly, 10 g of LB agar was added to 250 ml of water and autoclaved at 121°C for 15 min. To prepare LB broth 6.25 g of LB broth was added to 250 ml of water and autoclaved at 121°C for 15 min.

4.2 Preparation of competent E.coli TG2

Competent E.coli TG2 were prepared using the rubidium chloride method. An overnight culture of TG2 was diluted 1:100 in LB medium and grown at 37°C with shaking at 200 rpm to an OD600 of 0.5. Cells were kept on ice for 15 min and centrifuged at 1000 × g for 10 min at 4°C. The pellet was gently resuspended in 20 ml of RF1 buffer per 50 ml of starting culture. Cells were incubated on ice again for 15 min and centrifuged at 1000 × g for 10 min at 4°C. The pellet was resuspended in 2 ml RF2 buffer per 50 ml of starting culture. Cells were incubated on ice for 15 min, pipetted into 200 µl aliquots and snap frozen in liquid nitrogen. Competent cells were used immediately or stored at -80°C.

RF1 buffer:

100 mM $RbCl_2$ (Carl Roth #4471.4)

30 mM K-acetate (Chempur #117443303)

10 mM $CaCl_2$ (Acros Organics #323525000)

50 mM $MnCl_2$ (Chempur #116159604)

15% (v/v) glycerol (Chempur #114433204)

pH 5.8 adjusted with acetic acid (Poch #568760114)

RF2 buffer:

10 mM MOPS (Sigma #M9381)

75 mM $CaCl_2$ (Acros Organics #323525000)

10 mM $RbCl_2$ (Carl Roth #4471.4)

15% (v/v) glycerol (Chempur #114433204)

pH 6.5 adjusted with KOH (Poch #746800420)

4.3 Transformation of E.coli TG2

For transformation, 20 µl of the ligation mixture or 50 ng of the DNA was mixed with 200 µl of competent cells and kept on ice for 1 hour. The mixture was heat-shocked for 45 sec at 42°C and incubated on ice for 5 min. 800 µl of prewarmed LB broth was added and bacteria were incubated at 37°C with shaking at 200 rpm for 1 h. 100 µl and 900 µl of the transformed E.coli TG2 were plated separately on two LB agar plates with appropriate antibiotic and plates were incubated at 37°C overnight.

4.4 Polymerase chain reaction (PCR)

Standard PCR reactions were carried out in a final volume of 50 µl using Q5 High-Fidelity DNA Polymerase as per the manufacturer's instructions. Briefly, the reaction was set up using 50 ng of template DNA, two gene-specific primers (0.5 µM each), 200 µM dNTPs (EURx #E0503-01), 1 x polymerase buffer, 1U Q5 High-Fidelity DNA polymerase (New England Biolabs #M0491S), and nuclease free water (Invitrogen # AM9939) in a 0.2 ml PCR tube. DNA fragments were amplified with the appropriate oligonucleotide primers (listed in table 1) in an Eppendorf thermocycler. The incubation time for denaturation was used as per manufacturer's instructions (refer to table 1). Annealing temperature was calculated based on the primer melting temperatures (Tm) and extension time calculated based on the length of the amplified PCR product. The PCR products were run on 1% agarose gel in 1x TAE buffer at 100 V for 1 h, along with 1 kb DNA ladder (Sigma #D0428). Bands corresponding to the expected size were excised and purified using the QIAquick gel extraction kit (Qiagen #28706) according to the manufacturer's instructions and eluted in 30 µl of elution buffer to be used in further cloning reactions. The program in table 2 was used for all PCR reactions.

<u>50x TAE buffer (1L)</u>

242 g Tris (Sigma #T1503)

57.1 ml glacial acetic acid (Poch #568760114)

100 ml 0.5 M EDTA pH 8 (Sigma #E5134)

To make 1x TAE buffer, 20 ml of 50x TAE buffer was added to 980 ml of water.

Table 2. Primers used for cloning

#	Primer name	Primer sequence (5' to 3')	[Tm]
1	IE1 FL HindIII for - corrected !	GATCAAGCTTGCATGGAAAGCAGCGCCAAG	80.7
2	IE1 FL BamHI rev - corrected !	GATCGGATCCCTACTGGTCGGCCTTGGATCT	79.9
3	IE1x4 C-terminal myc FP HindIII	GATCAAGCTTCGAGTGGACATGGTCCGACACCGGATCAAAGAACACATGCTGAAGAAG	73.8
4	IE1x4 C-terminal myc RP BamHI	GATCGGATCCCTACAGATCCTCTTCAGAGATGAGTTTCTGCTCCATCTGGTCGGCCTTGGATCT	75.5
5	IE1x4 C-terminal GFP FP HindIII	GACTAAGCTTCGAGTGGACATGGTCCGACACC	78.6
6	IE1x4 C-terminal GFP RP BamHI	GACTGGATCCACTGGTCGGCCTTGGATCT	79.1
7	IE1/IE1x4 M483A FP	GCACACACCCCGCCGTCACAAGATCC	81.4
8	IE1/IE1x4 M483A RP	GGATCTTGTGACGGCGGGGTGTGTGC	81.4
9	IE1/IE1x4 H481A FP	CAAGAGCACAGCCCCCGCCGTCA	69.5
10	IE1/IE1x4 H481A RP	TGACGGCGGGGGCTGTGCTCTTG	69.5
11	IE1/IE1x4 T485A + R486A FP	CCCGCCGTCGCTGCATCCAAGGCC	75.0
12	IE1/IE1x4 T485A + R486A RP	GGCCTTGGATGCAGCGACGGCGGG	75.0
13	IE1 Δexon 2 FP	GATCAAGCTTATGGAGCAGAAACTCATCTCTGAAGAGGATCTGCCTGAAACACCCGTG	87.4
14	IE1_CD_BamHI_STOP_RP	GATCGGATCCCTAGGACTCTTCGGCAATGGCTCTCA	82.8

15	IE1_AD_HindIII_myc_FP	GATCAAGCTTATGGAGCAGAAACTCATCTCTGAAGAGGATCTGGACGAGG AAGAT	85.8
16	IE1_AD_BamHI_STOP_RP	GATCGGATCCCTAGCTTGTTGTAGGTTCCTCAGCGC	81.0
17	IE1_CTD_HindIII_myc_FP	GATCAAGCTTATGGAGCAGAAACTCATCTCTGAAGAGGATCTGGGCGGCA AGAGCACA	89.0
18	IE1_ΔEX2+EX3_HindIII_myc_FP	GATCAAGCTTATGGAGCAGAAACTCATCTCTGAAGAGGATCTGGTCAAGCA GATCAAAG	85.0
19	IE1_CD_HindIII_FP	GATCAAGCTTGCCCTGAAACACCCGTGACC	80.2
20	IE1_AD_HindIII_FP	GATCAAGCTTGCGACGAGGAAGATGCTATCGC	79.5
21	IE1_CTD_HindIII_FP	GATCAAGCTTGCGGCGGCAAGAGCACACAC	83.3
22	IE1_ΔEX2+EX3_HindIII _FP	GATCAAGCTTGCGTCAAGCAGATCAAAGTGCGC	81.4
23	TR1_FP	CTTGGGGCGGTGGGTCCGAGCTGCGGTATGGGTCACGGCG	88.3
24	TR2_FP	CCCGGACGTAGCAAAAAAGCTAACTGCCCGTGCGGCTCGC	84.2
25	TR_RP	GACGTTAATAAAGAGTAGCGGCGGTTGTGATAGGGCGACCGC	81.9
26	cc41-43	CAGACCATGCTGGCGGCAGCAGTGAACAGCCAG	80.3
27	cc41-43	CTGGCTGTTCACTGCTGCCGCCAGCATGGTCTG	80.3
28	cc78-80	CAACGAGAACCCCGCGGCAGCTGTGCTGGCCGAG	83.9
29	cc78-80	CTCGGCCAGCACAGCTGCCGCGGGGTTCTCGTTG	83.9
30	cc196-199	CAAGGCCAGAGCCGCGGCGGCCGCGCTGAAGCGCAAG	87.9
31	cc196-199	CTTGCGCTTCAGCGCGGCCGCCGCGGCTCTGGCCTTG	87.9

32	cc210-217	CTACATGTGCTACGCGAACATCGCGTTCTTCACCGCGAACAGCGCCTTTC	85.5
33	cc210-217	GAAAGGCGCTGTTCGCGGTGAAGAACGCGATGTTCGCGTAGCACATGTAG	85.5
34	cc244-245	CAGTGCAGCCCCGCCGCGATCATGGCCTAC	80.3
35	cc244-245	GTAGGCCATGATCGCGGCGGGGCTGCACTG	80.3
36	cc326-327	GTGATGCTGGCCGCGGCGCCCCTGATCACC	81.5
37	cc326-327	GGTGATCAGGGGCGCCGCGGCCAGCATCAC	81.5
38	cc332-334	CCCCTGATCACCGCGCCTGCAGTGATCAACGTG	80.3
39	cc332-334	CACGTTGATCACTGCAGGCGCGGTGATCAGGGG	80.3
40	cc3359-362	CATTCTGGGCGCCGCTCCTCTGGCAGTGTGCAGCCC	84.4
41	cc3359-362	GGGCTGCACACTGCCAGAGGAGCGGCGCCCAGAATG	84.4

Table 3. PCR amplification program

Steps	**Initial denaturation**	**Denaturation**	**Annealing**	**Extension**	**Final Extension**
Temperature	95°C	95°C	refer to table 3	72°C	72°C
Duration	10 min	15 s	60 s	1-2 min (1kb/sec)	10 min
No. of Cycles	1 cycle	30 cycles			1 cycle

4.5 Constructs

4.5.1 Cloning - DNA manipulations

T4 DNA ligase (#M0202S) and restriction enzymes – BamHI (#R3136S), HindIII (#R3104S), and DpnI (#R0176S) were purchased from New England Biolabs. DNA fragments used in cloning reactions were purified using the QIAquick gel extraction kit (Qiagen #28706) according to the manufacturer's instructions and eluted in 30 µl of elution buffer. Plasmid DNA isolations were performed using the Qiagen plasmid midi kit (Qiagen #12143) according to the manufacturer's instructions and eluted in 100 µl of elution buffer. The plasmid was diluted to 0.5 µg/µl in elution buffer for further use in experiments. Briefly, 2 µg of plasmid DNA or 30 µl of purified PCR amplified product was digested using restriction enzymes (20 U each) BamH1 and HindIII (for all IE1 cloning) in a 50 µl reaction mixture at 37^{o}C for 1 h. The digested PCR product and plasmid were run on 1% agarose gel in 1xTAE buffer (refer to section 4) at 100 V for 1 h, along with 5 µl of 1kb DNA ladder (Sigma #D0428) to obtain pure digested products. Bands corresponding to the expected size were excised and purified using the QIAquick gel extraction kit (Qiagen #28706) according to the manufacturer's instructions and eluted in 30 µl of elution buffer. The ligation reaction mixture (20 µl total volume) was set up at a 1:5 vector to insert ratio (where 100 ng of vector was used for all ligation reactions and the amount of insert was calculated based on the number of base pairs). The T4 DNA ligase (400U) was used, and the reaction was incubated at room temperature (RT) for 1 h. After which 10 µl of the reaction mixture was transformed into competent TG2 E. coli and incubated overnight at 37°C. All the clones generated were sequenced to ensure the sequences were devoid of unintended mutations and only then used in further experiments.

4.5.2 Cloning of IE1, and IE1x4

The oligonucleotide primers used for this study were purchased from Sigma (>85% purity, HPLC grade) and are listed in table 1. Synthetic codon optimized HCMV IE1 gene with an N-terminal myc tag containing 5' HindIII and 3' BamHI restriction sites was purchased from Invitrogen. The IE1 gene was dropped out from a delivered cloning vector by digesting with HindIII and BamHI restriction enzymes and was cloned into HindIII and BamHI digested pcDNA 3.1 (+) [a kind gift from prof. Thomas Schulz] to generate myc-IE1 plasmid. HCMV IE1 gene with N-terminal EGFP tag was cloned by PCR amplification (refer to section 4) of the IE1 gene cloned in the pcDNA3.1 plasmid using primers #1 & #2 (the primers were designed to include two additional nucleotides before the 5' HindIII site, to ensure that IE1

gene is in the correct frame with the EGFP protein) containing 5' HindIII and 3' BamHI restriction sites. The PCR reaction was run on an agarose gel and the PCR product was purified using QIAquick gel extraction kit (Qiagen #28706). The purified PCR product was digested with HindIII and BamHI restriction enzymes and was cloned into HindIII and BamHI digested pEGFP-C1 [a kind gift from prof. Thomas Schulz] to generate EGFP-IE1 plasmid. In general, for cloning the target gene was amplified using the program in table 1 and appropriate primers listed in table 1 and 3. The respective PCR products were digested with HindIII and BamHI restriction enzymes and cloned into HindIII and BamHI digested plasmids to generate the respective plasmids as mentioned in table 3.

Table 4. Expression plasmids used in the study and the primers used for cloning

	Expression Plasmid	**Plasmid backbone**	**Tag**	**Tag position**	**Template**	**Primers**	**Annealing temperature**
1	EGFP-IE1	pEGFP-C1	EGFP	N terminal	myc-IE1	#1 and #2	60°C
2	IE1x4-myc	pcDNA3.1 (+)	myc	C terminal	myc-IE1	#3 and #4	60°C
4	IE1x4-EGFP	pEGFP-N2	EGFP	C terminal	myc-IE1	#5 and #6	60°C
5	myc-IE1 ΔNTD	pcDNA3.1 (+)	myc	N terminal	myc-IE1	#13 and #2	60°C
6	myc-IE1_CD	pcDNA3.1 (+)	myc	N terminal	myc-IE1	#13 and #14	60°C
7	myc-IE1_AD	pcDNA3.1 (+)	myc	N terminal	myc-IE1	#15 and #16	60°C
8	myc-IE1_CTD	pcDNA3.1 (+)	myc	N terminal	myc-IE1	#17 and #2	60°C
9	myc-IE1_AD+CTD	pcDNA3.1 (+)	myc	N terminal	myc-IE1	#15 and #2	60°C
10	myc-IE1 Δex2+ex3	pcDNA3.1 (+)	myc	N terminal	myc-IE1	#22 and #2	60°C
11	EGFP-IE1_CD	pEGFP-C1	EGFP	N terminal	myc-IE1	#19 and #14	60°C
12	EGFP-IE1_AD	pEGFP-C1	EGFP	N terminal	myc-IE1	#20 and #16	60°C
13	EGFP-IE1_CTD	pEGFP-C1	EGFP	N terminal	myc-IE1	#21 and #2	60°C
14	EGFP IE1_AD+CTD	pEGFP-C1	EGFP	N terminal	myc-IE1	#20 and #2	60°C

15	EGFP-IE1 Δex2+ex3	pEGFP-C1	EGFP	N terminal	myc-IE1	#22 and #2	60°C
16	myc-IE1 M483A	pcDNA3.1 (+)	myc	N terminal	myc-IE1	#7 and #8	55°C
17	myc-IE1 NBM	pcDNA3.1 (+)	myc	N terminal	myc-IE1 M883A	#9 and #10 #11 and #12	55°C
18	myc-IE1 cc41-43	pcDNA3.1 (+)	myc	N terminal	myc-IE1	#26 and #27	55°C
19	myc-IE1 cc78-80	pcDNA3.1 (+)	myc	N terminal	myc-IE1	#28 and #29	55°C
20	myc-IE1 cc196-199	pcDNA3.1 (+)	myc	N terminal	myc-IE1	#30 and #31	55°C
21	myc-IE1 cc210-217	pcDNA3.1 (+)	myc	N terminal	myc-IE1	# 32 and #33	55°C
22	myc-IE1 cc244-245	pcDNA3.1 (+)	myc	N terminal	myc-IE1	#34 and #35	55°C
23	myc-IE1 cc326-328	pcDNA3.1 (+)	myc	N terminal	myc-IE1	#36 and #37	55°C
24	myc-IE1 cc332-334	pcDNA3.1 (+)	myc	N terminal	myc-IE1	#38 and #39	55°C
25	myc-IE1 cc359-362	pcDNA3.1 (+)	myc	N terminal	myc-IE1	#40 and #41	55°C

4.5.3 Cloning of HCMV TR

For cloning the HCMV terminal repeat (TR) regions i.e., TR1 and TR2, the red recombinase system in GS1783 was taken advantage of (Tischer BK, 2010). Using pcDNA 3.1 (+) vector as the template and homing primers #23 and #25 (for TR1) and #24 and #25 (for TR2), pcDNA 3.1 (+) vector backbones were generated containing sequences homologous to the HCMV TR flanking the 3' HindIII and 5' BamHI restriction sites. The obtained PCR products were electroporated (voltage: 2.5 kV, capacitance: 25 μF, resistance: 200 Ω) into GS1783 E. coli containing TB40-BAC4. Resulting colonies were picked and assessed for the presence of the TR gene sequences. TR1 and TR2 were further subcloned into pEGFP-C1 to generate plasmids GFP-TR1 and GFP-TR2.

4.5.4 Cloning of deletion mutants of IE1

Domains of IE1 i.e., core domain (CD; aa 25-378), acidic domain (AD; aa 379-475), chromatin tethering domain (CTD; aa 476-491), and a construct containing AD and CTD (AD + CTD; aa 379-491) were also cloned into pcDNA 3.1 (+) and pEGFP-C1 as described in section 6 using primers listed in table 4. Briefly, primers #13 and #2 were used to generate myc-IE1 ΔNTD,

#13 and #14 for myc-IE1 CD, #15 and #16 for myc-IE1 AD, #17 and #2 for myc-IE1 CTD, #15 and #2 for myc-IE1 AD+CTD, #22 and #2 for myc-IE1 Δex2+ex3, #19 and #14 for EGFP-IE1 CD, #20 and #16 for EGFP-IE1 AD, #21 and #2 for EGFP-IE1 CTD, #20 and #2 for EGFP-IE1 AD+CTD, and #22 and #2 for EGFP- IE1 Δex2+ex3.

4.5.5 Cloning of point and clustered charge mutants of IE1

Point mutants of IE1 i.e., M483A and M483A_H481A_T485A_R486A were generated in a sequential manner by site-directed mutagenesis using the following amplification protocol, which has been described previously [250]. Using myc-IE1 plasmid as the template, two PCR reactions were set up in parallel with the forward and the reverse primers in separate tubes. The PCR reaction was carried out as mentioned in table 4. After PCR, the two PCR products were combined and heated to 95°C and then slowly cooled to 37°C to promote reannealing of denatured plasmid templates and PCR products. The generated PCR products were digested with DpnI (NEB) for 1 h at 37oC and transformed into TG2 bacteria. Using primers #7 and #8 and myc-IE1 plasmid as the template, myc-IE1_M483A was generated first. Using primers #9 and #10 and myc-IE1_M483A plasmid as the template, myc-IE1_M483A_H481A was generated next. Using primers #11 and #12 and myc-IE1_M483A_H481A plasmid as the template, myc-IE1_M483A_H481A_T485A_R486A (called myc-IE1_NBM henceforth) was finally generated.

Clustered charge mutants of IE1 were generated using myc-IE1 as the template as described above. Primers listed in table 4 were used to generate the following mutants: cc41-43 (#26 & #27), cc78-80 (#28 & #29), cc196-199 (#30 & #31), cc210-217 (#32 & #33), cc244-245 (#34 & #35), cc326-327 (#36 & #37), cc332-334 (#38 & #39), and cc359-362 (#40 & #41).

Table 5. PCR amplification program for site directed mutagenesis

Steps	Initial denaturation	Denaturation	Annealing	Extension	Final Extension
Temperature	94°C	94°C	55°C	72°C	72°C
Duration	2 min	40 s	40 s	4 min (1kb/sec)	10 min

4.5.6 KSHV LANA and LANA+TR

pGTR4 – plasmid expressing the terminal repeat region of KSHV, pGTR4:73 – plasmid expressing the terminal repeat region of KSHV along with KSHV ORF73, and H-LANA-pcDNA3 – plasmid expressing KSHV LANA (ORF73) were a kind gift from prof. Thomas Schulz.

4.6 Cells

T98G (Sigma #92090213) was cultured in modified Eagle's media (Cytogen #04-08500) supplemented with 10% heat-inactivated fetal bovine serum (Sigma #F9665), 1x non-essential amino acids (Gibco #11140050), 1x sodium pyruvate (Gibco #11360070), and 1x penicillin-streptomycin (Gibco # 15140122) at 37°C with 5% CO_2.

HeLa [a kind gift from prof. Thomas Schulz], human foreskin fibroblasts (HFF) [a kind gift from prof. Martin Messerle] and human placental fibroblasts (HPF) [isolated in our lab – for the isolation procedure please refer to section 7] were cultured in Dulbecco's modified Eagle's with high glucose GlutaMAX™ medium (Gibco #31966-021) supplemented with 10% heat-inactivated fetal bovine serum (Sigma #F9665) and 1x penicillin-streptomycin (Gibco # 15140122) at 37°C with 5% CO_2.

MRC-5 [a kind gift from prof. Thomas Schulz] and U87MG (ATCC #ATCC-HTB-14) were cultured in modified Eagle's media (Cytogen #04-08500) supplemented with 10% heat-inactivated fetal bovine serum (Sigma #F9665), 1x non-essential amino acids (Gibco #11140050), 1x sodium pyruvate (Gibco #11360070), and 1x penicillin-streptomycin (Gibco # 15140122) at 37°C with 5% CO_2.

THP1 [a kind gift from prof. Marek Zygmut] was cultured in RPMI media (Gibco #11875093) supplemented with 10% heat-inactivated fetal bovine serum (Sigma #F9665), and 1x penicillin-streptomycin (Gibco # 15140122) at 37°C with 5% CO_2.

HT-29 was cultured in McCoy’s 5A media (Gibco #16600082) supplemented with 10% heat-inactivated fetal bovine serum (Sigma #F9665), and 1x penicillin-streptomycin (Gibco # 15140122) at 37°C with 5% CO_2.

4.7 Isolation of human placental fibroblasts

Human placental fibroblasts (HPF) were isolated from term placenta as previously described [251]. Briefly, the placental tissue was cut into fragments and the membrane was teased off to obtain placental villi. The villi were collected into 50 ml of M199 medium (Sigma #M5017),

treated with collagenase type IA (6.25 mg/ml, Sigma #C2674) for 6 min and centrifuged at 200 × g for 10 min at 4°C. The pellet was treated with 1.5 ml trypsin-EDTA (0.25%, Sigma #T4049) in 50 ml of M199 medium for 20 min at 37°C and centrifuged at 200 × g for 10 min at 4°C. Trypsin digestion was repeated twice. The pellet was then treated with collagenase type IA (6.25 mg/ml, Sigma #C2674) in 50 ml of M199 medium for 3 min and centrifuged at 200 × g for 10 min at 4°C. Following enzyme treatment, the pellet was treated with 5 ml red blood cell lysing buffer (Sigma #R7757) for 10 min. The cells were then filtered through 100 µm filter (Falcon #352360) and centrifuged at 200 × g for 10 min at 4°C. The pellet was resuspended in Dulbecco's modified Eagle's with high glucose GlutaMAX™ medium (Gibco #31966-021) supplemented with 10% heat-inactivated fetal bovine serum (Sigma #F9665) and 1x antibiotic antimycotic solution (Sigma # A5955), placed in a T75 flask and incubated at 37°C with 5% CO_2 until confluent and then frozen for use in further experiments.

4.8 Generation of induced pluripotent stem cells (iPSC)

iPSCs were generated from HPF using the CytoTune™-iPS 2.0 Sendai Reprogramming Kit (ThermoFisher Scientific #A16517) as per manufacturer's instructions. Briefly, human placental fibroblasts were seeded at 4×10^4 cells per well of a 6 well plate. After 2 days they were infected with Sendai virus encoding individual Yamanaka factors (hKOS: MOI 5, hc-Myc: MOI 5, and hKlf4: MOI 3). 7 days post infection, the reprogrammed placental fibroblasts were plated on irradiated mouse embryonic fibroblasts (MEF, Gibco #A34181). After 2 days, the medium was changed to iPSC medium. The cells were stained for Sendai virus (anti-SeV, MBL #PD029) to confirm the presence of the virus in the reprogrammed placental fibroblasts. The iPSC colonies were then selected for expansion by live staining with anti-TRA-1-60 (Gibco #A25618). For this, bright field images of the cell culture plate with colonies circled and numbered at the bottom of the plate were correlated with fluorescence images of the cell culture plate to pick colonies of interest based on TRA-1 staining. Several colonies were selected that were fully positive for TRA1-60 as well as some colonies that had higher expression of TRA1-60, but not in all the cells. After removing the media from the well, using a stereomicroscope (SteREO Discovery, Carl Zeiss), the colony of interest was trypsinized with 10 µl of trypsin (Sigma #T4049) and seeded into one well of a 24 well plate. Each colony was seeded into an individual well on MEF, grown until confluency and then frozen.

After thawing, iPSCs were maintained on Lam-521 (0.5 μg/cm^2, BioLamina #LN521) coated plates in Essential 8 medium (Gibco #A1517001) by passaging them at 1 × 10^6 per 10 cm^2 dish or 1 × 10^5 per 6 well plate every 4 days.

iPSC medium

39 ml DMEM/F12, GlutaMAX supplement (Gibco #10565018)

10 ml KnockOut Serum Replacement (Gibco #10828028)

0.5 ml Minimal Essential Media (MEM) Non-Essential Amino Acids Solution (Sigma #M7145)

0.5 ml Penicilin/Streptomycin (Gibco #15140122)

50 μl β-mercaptoethanol (Sigma #M3148)

20 μl bFGF (10 μg/ml, Invitrogen #13256029)

4.9 Differentiation of iPSC to neural stem cells (NSC)

Differentiation was initiated by seeding iPSC onto Lam-111 (1μg/cm^2, Biolamina #LN111) coated cell culture plates at density of 1.5 × 10^5 cells per well of a 6-well plate in differentiation medium 1. From day 0 to 3, 10 μM Rock inhibitor (Sigma #SCM075) was added to the cells. On day 4, the medium was changed to differentiation medium 2. From day 4 onwards, the cells were cultured in differentiation medium 2 to maintain them as neural stem cells stage to be used in further experiments.

Differentiation medium 1

DMEM/F12 :Neurobasal 1:1 (Gibco #11320033; Gibco #21103049),

1% N2 supplement (Gibco #17502001)

2% B27 supplement 1:50 (Gibco #12587001)

10 μM SB431542 (Sigma #616464)

100 ng/ml rhNoggin (Gibco #PHC1506)

300 ng/ml rhSHH-C24II (Sigma #PMC8031)

0.8μM CHIR99021 (Sigma #SML1046)

Differentiation medium 2

DMEM/F12: Neurobasal 1:1 (Gibco #21103049)

0.5% N2 supplement (Gibco #17502001)

1% B27 supplement (Gibco #12587001)

10μM SB431542 (Sigma #616464)

100 ng/ml rhNoggin (Gibco #PHC1506)
300 ng/ml rhSHH-C24II (Sigma #PMC8031)
0.8µM CHIR99021 (Sigma #SML1046)

4.10 Transfection

T98G cells were seeded [for IFA on glass coverslips (thickness no. 1, Carl Roth #P234.1)] at 3×10^5 cells per well of a 6 well plate and transfected with the respective plasmid (1 µg) using Lipofectamine 3000 [Lipofectamine 3000 reagent – 7.5 µl and P3000™ reagent – 5 µl, (Invitrogen #L3000015)] per well. After 48 h, cells were harvested and processed for immunoblotting (refer to section 4.15), immunofluorescence (refer to section 4.16), or chromosome spread (refer to section 4.17).

HeLa cells were seeded (for IFA on coverslips) at 1×10^5 cells per well in a 6 well plate and transfected with the respective plasmid (1 µg/well) using Fugene 6 (Promega #E2691) at 3:1 ratio of Fugene 6 to DNA. After 36 h, cells were harvested and processed for immunoblotting (refer to section 4.15), immunofluorescence (refer to section 4.16), or chromosome spread (refer to section 4.17).

4.11 Virus

The HCMV mutant generated in this study is based on the recently described TB40R-Cre backbone, a TB40-BAC4-based bacterial artificial chromosome (BAC) containing the genome of the HCMV strain TB40/E. TB40R-Cre harbors a re-insertion of the previously deleted US2-US6 genes, as well as two loxP sites flanking both the BAC vector and Cre recombinase sequences, thereby resulting in excision of BAC and Cre sequences upon virus reconstitution in cell culture [252]. To replace the RL13 open reading frame (ORF) of TB40R-Cre by sequences encoding the monomeric EGFP (mGFP) under control of the MCMV major immediate early promoter via “en passant” mutagenesis [253], plasmid pMCMV-mGFP-in was constructed by Gibson assembly following the manufacturer’s instructions (Gibson assembly master mix, New England BioLabs #E2611S). The mGFP ORF comprising an internal KnR cassette (plus elements required for “en passant” mutagenesis) was PCR-amplified from pEP-mGFP-in [254] using primers mGFP-in.for
(5’- CGCTGCAGCCCGGGTATGGTGAGCAAGGGCGAG -3’)
and mGFP-in.rev
(5’-ACGTCGACGGATCCTTTACTTGTACAGCTCGTCCATGC-3’)

and cloned into plasmid pMCMV3 [255] cut with XbaI. A PCR fragment was then produced from pMCMV-mGFP-in using primers TB40-RL13-MIEP.for
(5'-
ACAACATCCGAAGAAACATCAATGCCCATTAACCGAAATCCAACAACGTTTAAA
CGGTACTTTCCCATAGCTG-3') and TB40R-RL13-mGFP.rev
(5'-
GAAACATATTATTGGCTAAAAAGAAAAGCAAAAGTTTATTGGTGTGCATGTTACT
TGTACAGCTCGTCCAT-3') and recombined with the TB40R-Cre BAC genome followed by excision of the KnR marker, giving rise to TB40R-RL13-mGFP.
TB40R-RL13-mGFP was grown in HFF/HPF as described previously [256]. Briefly, HFFs were plated in T75 flasks at a density of 3×10^6 per flask. The next day, cells were infected at MOI 0.02 and incubated at 37°C with 5% CO_2. After 5 h, the media was replaced with fresh media. Once 80-90% of the cells are infected (about 12 days), the supernatants were harvested and centrifuged at 3,500 × g for 1 h at 4°C. The supernatant was harvested and purified by ultracentrifugation at 103,282 × g for 1 h at 4°C in SW40Ti rotor using Beckman Optima L-100 XP ultracentrifuge. The supernatant was discarded, and the pellet was resuspended in 300 µl viral stock buffer and stored at -80°C in 30 µl aliquots. Titers were determined by standard plaque assay on HFF cells. HFF were plated in 48-well plates and infected with serial dilutions (10^{-1} to 10^{-8}) of the purified virus and overlaid with carboxymethylcellulose (CMC)-DMEM medium. Plaque formation was monitored, and plaques were counted 14 days post infection following Giemsa staining. Briefly, the cells were fixed with 4% paraformaldehyde (PFA) for 20 min at RT and stained with 25% Giemsa (Carlroth, # T862.2) in phosphate buffered saline (PBS) for 20 min and washed with dd water. Titers were expressed as PFU/ml of the stock and used to calculate the multiplicity of infection (MOI) for infection experiments.

Viral stock buffer

50 mM Tris pH 7.8 (Sigma #T1503)
12 mM KCl (Poch #739740114)
5 mM EDTA (Sigma #E5134)
20% heat-inactivated fetal bovine serum (Sigma #F9665)

CMC-DMEM medium (1L)

Prepare 10x DMEM using 1 bottle of DMEM medium powder (Sigma #D5523) dissolved in 100 ml of H_2O. Filter sterilize the solution using 0.22 µm filter (TPP #99505) and store at 4°C for further use.

10 ml 10x DMEM

11.64 g CMC (Sigma #C4888)

5% heat-inactivated fetal bovine serum (Sigma #F9665)

2 mM Glutamine (Gibco #25030081)

1% Penicillin-Streptomycin (Gibco #15140122)

0.37% $NaHCO_3$ (Gibco #25080-094)

0.351% D-(+)-glucose (Sigma #G8644)

4.12 Infections

T98G infection was carried out as described previously [257]. Briefly, serum starved (78 h) T98G cells were plated at 5×10^5 cells per 10 cm^2 dish (on coverslips for IFA), allowed to attach for 2 h and then infected (no centrifugal enhancement) with TB40R-RL13-mGFP virus at MOI 10 (virus titered on HFF). Infected T98G cells were passaged every 7 days and plated at density of 5×10^5 cells per 10 cm^2 dish for 5 passages to allow HCMV latency establishment. Infected cells were harvested at indicated times post-infection for immunoblotting (refer to section 4.15), immunofluorescence (refer to section 4.16), chromosome spread (refer to section 4.17), and qRT-PCR (refer to section 4.20) analysis.

NSC were infected on day 3 of differentiation with TB40R-RL13-mGFP virus at MOI 3. Centrifugal enhancement at 950 × g for 30 min at 20°C was performed to increase infection efficiency. Cell culture medium was changed 6 h post-infection. Infected cells were harvested at indicated times post-infection for chromosome spread (refer to section 4.17).

U87MG cells were plated at 2×10^5 cells per well in a 12 well plate. The next day, cells were infected at MOI 2 and incubated for 5 h, following which the medium was replaced with fresh medium. On day 2 post infection the cells were harvested for chromosome spreads (refer to section 4.17).

HT-29 cells were plated at 1×10^5 cells per well in a 12 well plate. Cells were infected at MOI 1 and incubated for 5h, following which the medium was replaced with fresh medium. On day 2 post infection the cells were harvested for chromosome spreads (refer to section 4.17).

1.5×10^6 THP1 cells were plated at a density of 0.5×10^6 per ml in a 6 well plate and infected at MOI 2. Centrifugal enhancement at 400 × g for 30 min at 20°C was performed to increase

infection efficiency. The cells were incubated for 5 h at 37°C with 5% CO_2, following which the medium was replaced with fresh medium. On day 2 post infection the cells were harvested for chromosome spreads (refer to section 4.17).

4.13 Infectivity assay

HFFs were plated at a cell density of 5 x 10^5 per well of a 6 well plate on a glass coverslip. The next day supernatant from infected T98G cells was harvested and centrifuged at 200 × g for 5 min. The supernatant was collected, and 5 ml was added to the confluent HFFs and incubated for 5 h at 37°C with 5% CO_2, following which the medium was replaced with fresh medium. The cells were incubated up to 14 days and was replaced with fresh medium every 3 days. After 14 days, the coverslips were harvested and stained with anti-IE1 antibody (refer to section 16).

4.14 Monitoring the ratio of IE1 CAS to painting pattern

4.14.1 T98G infection

T98G cells were infected as described in section 16. Cells were treated with colcemid and harvested to make chromosome spreads on 1-, 4-, 7-, 10- and 14-days post infection (dpi) (refer to section 4.17). The remaining attached cells were harvested in lysis buffer with protease inhibitors, phosphatase inhibitors, and desumoylating enzyme inhibitor for immunoblotting (refer to section 4.15).

4.14.2 T98G transfection

T98G cells were transfected (as described in section 14) with 0.25, 0.5, 1.0 and 1.5 µg of myc-IE1 plasmid and filled up with pcDNA3.1(+) empty vector to a total plasmid DNA concentration of 1.5 µg per sample. For e.g., for sample containing 0.25 µg of myc-IE1 plasmid, 1.25 µg of pcDNA3.1(+) empty vector was added for a total concentration of 1.5 µg. After 48 h, cells were harvested in lysis buffer with protease inhibitors, phosphatase inhibitors, and desumoylating enzyme inhibitor for immunoblotting (refer to section 4.17) or were treated with colcemid and processed for chromosome spread (refer to section 4.15).

4.15 Immunoblotting

Cell lysates for immunoblotting assays were prepared from 3 × 10^5 T98G cells transfected using Lipofectamine 3000 and harvested 48h after transfection. Cells were suspended in 300 µl of lysis buffer with protease inhibitors, phosphatase inhibitors, and desumoylating enzyme

inhibitor. The lysates were sonicated with 10 pulses at 60 kHz on ice, cell debris was pelleted for 15 min at 4°C at 21,000 × g. The supernatant was harvested, and total protein concentration was determined using Quick Start™ Bradford Protein Assay Kit 1 (Bio-Rad #5000201). Samples were prepared in SDS loading buffer, boiled at 95°C for 10 min, cooled on ice for 5 min, loaded on an SDS-polyacrylamide gel (8% or 10%) for separation. The proteins were separated in 1x electrophoresis buffer at 20 mA per gel for 1 h 30 min and transferred to a nitrocellulose membrane in transfer buffer at 350 mA for 1 h at 4°C. Proteins were detected using primary antibodies described in table 8 and secondary antibodies mentioned in section 4.19. SuperSignal™ West Pico PLUS Chemiluminescent Substrate (Thermo Fisher Scientific #34577) was prepared by mixing equal parts of the substrate and stable peroxide solutions and used to develop the blot (1 ml per blot). The ChemiDoc Touch Imaging System (Bio-Rad) chemiluminescence was used to acquire the signal.

Lysis buffer

50 mM Tris pH 7.6 (Sigma #T1503)
100 mM NaCl (Poch #794121116)
0.5 mM EDTA (Sigma #E5134)
1% glycerol (Chempur #114433204)
0.2% IGEPAL (Sigma #I8896)

Protease inhibitors

1.5 µM aprotinin (Applichem, #A2132,0010)
10 µM leupeptin (Applichem, #A2183,0010)
100 µM phenylmethylsulfonyl fluoride (Applichem #A0999,0005)
1 µM benzamidine (Sigma #434760)
1.46 µM pepstatin A (Applichem #A2205,0010)

Phosphatase inhibitors

1 mM sodium fluoride (Sigma #201154)
1 mM sodium orthovanadate (Sigma #CAS13721-39-6)

Desumoylating enzyme inhibitor

250 µM N-ethylmaleimide (Sigma #E1271)

5x SDS loading buffer

50 mM Tris pH 6.8 (Sigma #T1503)

45% glycerol (Chempur #114433204)

5% SDS (Sigma #L3771)

0.1% pyronin Y (Chem Cruz #sc203755A)

3.5% β-mercaptoethanol (Sigma #M3148)

10x electrophoresis buffer stock (1L)

30 g Tris (Sigma #T1503)

144.2 g glycine (Poch #527560117)

1x electrophoresis buffer (1L)

100 ml 10x electrophoresis buffer

10 ml 10% SDS (Sigma #L3771)

890 ml H_2O

Transfer buffer (1L)

100 ml 10x electrophoresis buffer

200 ml Methanol (Poch #621990110)

700 ml H2O

4.16 Immunofluorescence assay

Cells grown on coverslips for transfection or infection experiments were washed with PBS and the samples were fixed with paraformaldehyde (PFA) for most experiments. In some experiments methanol and ethanol were also used for fixation.

For fixation using PFA, 4% PFA in PBS was added to the coverslips and incubated for 20 min at room temperature. PFA was quenched with 125 mM glycine for 10min at room temperature and the coverslips were washed 3 times for 5 min with PBS.

For fixation using methanol, ice-cold methanol was added to coverslips and incubated at -20°C for 10 min. The coverslips were then washed with PBS three times.

For fixation using ethanol, 100% ethanol was added to coverslips and incubated at -20°C for 10 min. The coverslips were then washed with PBS three times.

Following fixation cells were permeabilized in 0.2% Triton X-100 in PBS for 10 min at room temperature. The samples were then blocked for 30 min at 37ºC in a humidifying chamber with blocking buffer. Next, coverslips were incubated with 50 □l drop of primary antibody (refer to table 5) in blocking buffer on a parafilm for 1 h at 37°C in a humidifying chamber and were subsequently washed 3 times for 5 min with PBS in a 6 well plate. Incubation with secondary antibody (refer to section 20) and DAPI (4′, 6-diamino-2phenylindol; 1:100, Sigma #D9564) in blocking buffer was performed as for the primary antibody – in a drop on parafilm – for 1 h at 37°C in a humidifying chamber. Coverslips were washed 3 times for 5 min with PBS and mounted with Mowiol containing a tip of spatula of DABCO (Sigma #D27802) and dried overnight on a flat surface in the dark. Images were acquired using Carl Zeiss LSM800 microscope with a 63x objective and processed using FIJI image analysis software [258]. The images acquired by the microscope in .czi format were converted to .tif format. The color images were then converted to monochromatic format for each channel. The images were cropped to the desired size and scale bar was introduced. Brightness and contrast were increased (as indicated in the figure legends) for better visualization. The raw intensity values were not changed.

Blocking buffer

5% bovine serum albumin (Sigma, #A7906)
0.2% Triton X-100 (Sigma #T8787)
in PBS

Mowiol

2.4 g Mowiol (Sigma #324590)
12 ml Tris (20 mM, pH 8.5, Sigma #T1503)
6 g glycerol (Chempur #114433204)
6 ml H_2O

4% PFA

4 g paraformaldehyde (Sigma #)
10 ml 10x PBS
1 ml 1N NaOH (Poch #)
Adjust pH with HCl and then adjust final volume to 100 ml.
Aliquots were stored in -20°C until further use

Table 6. List of primary antibodies used in the studies

Antibody	Host	Company	Catalog number	Dilution of the antibody used	
				WB	IFA
anti-myc	rabbit	Cell signaling technology	#2278	1:1000	1:25
anti-GFP	mouse	Takara	#632380	1:2000	-
anti-IE1/2	mouse	Abcam	#ab53495	1:1000	1:100
anti-IE1x4	mouse	Santa Cruz	#sc-69834	1:100	1:10
anti-IE1	mouse	Merck Millipore	#MAB810R	1:1000	1:100
anti-UL44	mouse	Virusys	#CA006-100	1:1000	1:100
anti-gB	mouse	Abcam	#ab54023	1:1000	1:100
anti-CENP-A	rabbit	Cell signaling technology	#2186	-	1:100
anti-PML	mouse	Santa Cruz	#sc-966	-	1:100
anti-LANA	rat	A kind gift from prof. Thomas Schulz	-	-	1:100

4.17 Chromosome spreads

Cells were treated with colcemid (Gibco #15210040) under conditions specific for particular cells, as summarized in table 6. Following the appropriate incubation time with colcemid the plate was gently tapped to detach the mitotic cells and the supernatant was collected and centrifuged at 200 × g for 10 min. The pellet was resuspended in 200 µl of prewarmed 75 mM KCl and subjected to swelling for 5 min at 37°C. During this incubation, the slides were prepared by placing them in the cytospin adaptor, followed by the 9 mm cut out filter card, then the cytospin funnel and finally fastening the set up securely using the “ears” provided. After the incubation, the swollen cells (200 µl) were added into the funnel and cytospun (MPW 350R centrifuge with #12452 rotor) for 10 min at 250 × g onto Superfrost/Plus slides (Epredia #J1800AMNZ) at 25°C. The area with cells was marked using a hydrophobic marker and fixed with 4% PFA in PBS for 20 min at room temperature. PFA was quenched with 125 mM glycine for 10 min at room temperature and the slides were washed 3 times for 5 min with PBS. Subsequently, cells were permeabilized in KCM solution for 10 min at room temperature. Primary antibodies (refer to table 5) diluted in KCM solution were added to the samples and

incubated for 1 h at 37°C in a humidifying chamber. Slides were washed 3 times for 5 min with PBS after the incubation. Incubation with secondary antibody (refer to section 20) and DAPI (4′, 6-diamino-2phenylindol; 1:100, Sigma #D9564) in KCM solution was performed for 1 h at 37°C in a humidifying chamber. The slides were washed 3 times for 5 min with PBS and mounted with Mowiol (refer to section 16) containing a tip of spatula of DABCO (Sigma #D27802) and dried overnight on a flat surface in the dark. Images were acquired using Carl Zeiss LSM800 microscope 63x objective at 2x digital zoom. The images were processed using FIJI Image analysis software [258]. The images acquired by the microscope in .czi format were converted to .tif format. The color images were then converted to monochromatic format for each channel. The images were cropped to the desired size and scale bar was introduced. Brightness and contrast were increased (as indicated in the figure legends) for better visualization. The raw intensity values were not changed.

KCM solution

120 mM KCl (Poch #739740114)

20 mM NaCl (Poch #794121116)

10 mM Tris pH 7.7 (Sigma #T1503)

0.1% Triton X-100 (Sigma #T8787)

Table 7. Colcemid treatment conditions

Cells	Colcemid concentration	Treatment period
T98G	0.2 µg/ml	6h
U87	0.05 µg/ml	24h
HeLa	0.1 µg/ml	12h
HPF	0.5 µg/ml	24h
HT-29	0.1 µg/ml	12h
NSC	0.05 µg/ml	6h
THP1	0.3 µg/ml	6h

4.18 Live Imaging

T98G cells were plated at a density of 1×10^5 cells per well of a 4 well chambered coverglass (Thermo scientific #155383). The next day cells were transfected with 0.25 µg of GFP-IE1

plasmid. 24 h post transfection, cells were treated with 2 µl/ml of NucSpot live 650 DNA stain (Biotium #40082) and incubated for 1 h at 37°C with 5% CO_2. Following this incubation, the cells were set up for live imaging using Carl Zeiss LSM800 microscope with the settings mentioned below for 48h.

Channels: AF488 and AF647

Objective: 40x, 0.5x zoom

Pin hole size: 50 µm

Voltage: 725 V (AF488) and 750 V (AF647)

Laser power: 0.25% (AF488) and 0.5% (AF647)

Scan speed: 6

Acquisition: every 30 mins

Images were processed using FIJI image analysis software [258]. The images acquired by the microscope in .czi format were converted to .tif format. The color images were then converted to monochromatic format for each channel. The images were cropped to the desired size and scale bar was introduced. Brightness and contrast were increased (as indicated in the figure legends) for better visualization. The raw intensity values were not changed.

4.19 Antibodies

Primary antibodies used in this study are listed in the table 5.

The following secondary antibodies were used for immunoblotting:

- horseradish peroxidase (HRP)-conjugated goat anti-mouse immunoglobulin G (IgG) (1:2000, Dako #P0260),
- HRP-conjugated goat anti-rabbit IgG (1:2000, Dako #P0448).

The following secondary antibodies were used for immunofluorescence:

- Alexa Fluor 488-conjugated goat anti-rabbit IgG (1:200, Life Technologies #A11034)
- Alexa Fluor 594-conjugated AffiniPure donkey anti-mouse IgG (1:400, Jackson Immunolabs #715-585-150)
- Alexa Fluor 594-conjugated AffiniPure donkey anti-rabbit IgG (1:200, Jackson Immunolabs #711-585-152)
- Alexa Fluor 647-conjugated AffiniPure donkey anti-mouse IgG (1:400, Jackson Immunolabs #715-605-151)
- Alexa Fluor 594-conjugated goat anti-rat IgG (1:200, Invitrogen #A21209) [a kind gift from Dr. Antonio Galvao]

4.20 Real-time reverse transcriptase PCR (qRT-PCR)

Total RNA was isolated from cells (T98G - 100% confluent cells from 10 cm^2 dish) using RNeasy Mini Kit (Qiagen) in 30 µl of RNase free water, followed by removal of genomic DNA using DNA-free™ DNA Removal Kit (Invitrogen). For this a 50 µl reaction was set up using 30 µl of isolated RNA, 5 µl of 10x DNase buffer, 1 µl of beads containing rDNase, and 14 µl of RNase free water, and incubated at 37°C for 30 min. The DNase was inactivated by adding 5 µl of DNase inactivation reagent and incubating at room temperature for 2 min. The supernatant was removed after centrifugation at 10,000 × g for 5 min and RNA concentration was quantified using NanoDrop microvolume spectrophotometer (ThermoFisher Scientific). cDNA was synthesized from 1 µg of total RNA using SuperScript™ VILO™ cDNA Synthesis Kit (Invitrogen #11754050) in a 20 µl reaction of 4 µl 5x VILO reaction mixture, 2 µl 10x Superscript enzyme mix, and 1 µg RNA as the template. The resulting cDNA (1 µl per reaction) was then used along with Power SYBR™ Green PCR Master Mix (Applied Biosystems #4368577) and gene specific primers in ViiA 7 Real-Time PCR System (Applied Biosystems) using the program described in table 7. Primers used for detection of specific genes are shown in table 8.

Relative expression levels were calculated using the ΔΔCT method [259], which measured relative differences between the mock infected and infected samples at indicated time points. Samples were normalized to GAPDH.

Table 8. PCR program for qRT-PCR

Steps	Initial denaturation	Denaturation	Annealing/Extension
Temperature (°C)	95	95	60
Duration	10 min	15 s	60 s
No. of Cycles	1 cycle	40 cycles	

Table 9. Primers used in qRT-PCR

Gene		Primer sequence (5' to 3")	[Tm]	References
IE1x4	Forward	GCCTTCCCTAAGACCACCAAT	61.2	Self-designed
	Reverse	ATTTTCTGGGCATAAGCCATAATC	60.3	
IE1 exon 3-4	Forward	TTCCCAGAATTGGCCGAAGAA	59.5	[101]
	Reverse	CGCACCATGTCCACTCGAAC	62.5	
IE2 exon 5	Forward	ATGGTTTTGCAGGCTTTGATG	57.5	Self-designed
	Reverse	ACCTGCCCTTCACGATTCC	59.5	
UL44	Forward	CAGCTGCACGTTGATACGCATGTT	65.2	[93]
	Reverse	TCCGCCGGCCATCAAGTTCATCCT	68.5	
gB	Forward	GAGGACAACGAAATCCTGTTGGGCA	67.4	[260]
	Reverse	GTCGACGGTGGAGATACTGCTGAGG	70.7	
UL138	Forward	TCCACGTCGCTAACCAGAGAAACA	65.2	[93]
	Reverse	AATGTACCATGGCTACGGTGGTGA	65.2	
GAPDH	Forward	GCACAGTCAAGGCCGAGAAT	60.5	[261]
	Reverse	GCCTTCTCCATGGTGGTGAA	60.5	

4.21 Statistical Analysis

All statistical analyses were performed using the GraphPad Prism 10 software. Unpaired t-test was performed to compare percentages of CAS in T98G cells transfected with myc-IE1 or EGFP-IE1. Ordinary one-way ANOVA was performed to compare percentages of CAS for the following groups: day 4 infected cells with cells transfected with myc-IE or EGFP-IE1, across different concentrations of transfected myc-IE1 (0.25, 0.5, 1.0, and 1.5 μg), and different timepoints in HCMV infected T98G cells (1, 4, 7, 10, and 14 dpi). This was followed by Tukey's multiple comparison test. Pearson correlation coefficient (r) was determined for percentages of cells with CAS localization pattern vs IE1 band intensity in a western blot for the following: across different concentrations of transfected myc-IE1 (0.25, 0.5, 1.0, and 1.5 μg) and across different timepoints in infected cells (1, 4, 7, 10, and 14 dpi). Spearman's correlation coefficient (r) was also determined for percentages of cells with CAS localization pattern vs point in time after infection. For all parametric analyzes homogeneity of variance

was confirmed using the Brown-Forsythe test and normality was confirmed using Shapiro-Wilk test.

5. RESULTS

5.1 CHAPTER I - HCMV IE1x4 and viral genome tethering during latency

5.1.1 Cloned IE1x4 is expressed in transfected cells

I have cloned the HCMV IE1x4 gene into vectors with myc and EGFP tags in each case both as N-terminal and C-terminal fusions. The C-terminal fusions of IE1x4 (myc and EGFP) were well expressed in transfected HeLa cells and migrated with the apparent molecular weight (MW) of ~60kD and ~80kD for myc and EGFP fusions respectively (Fig. I.1A). The predicted MW of IE1x4 protein is 44.5kDa, however the protein was reported to migrate at ~60kD [101]. The N-terminal fusion of IE1x4 with myc tag was expressed only in the presence of proteasome inhibitor (MG132) and the EGFP-IE1x4 migrated higher than the IE1x4 protein tagged with EGFP at the C-terminus, suggesting that fusing tags at the N-terminus of the IE1x4 protein either disrupts the structure or prevents proper folding of this protein. Consequently, IE1x4 constructs with C-terminal fusion of myc or EGFP tags were used in further experiments.

I have observed that addition of deSUMOylating enzyme inhibitor (NEM) to the lysates prevented disappearance of an additional band migrating at a higher molecular weight (Fig. I.1A IE1x4-myc lane 13 and Fig. I.1B IE1x4- EGFP lane 13) suggesting presence of the SUMO modification previously reported for IE1 [262]. I observed increased level of IE1x4 expression in samples treated with proteasomal inhibitor (MG132) (Fig. I.1A IE1x4-myc lane 14 and Fig. I.1B IE1x4-EGFP lane 14), suggesting that IE1x4 might undergo proteasomal degradation. Efficient expression of the control IE1 protein with N-terminal myc or EGFP tag (Fig. I.1A and I.1B, IE1 lanes 1-4) was observed under all treatment conditions. IE1 or IE1x4 were not detected in non-transfected (NT) and empty vector (EV) control samples (Fig. I.1A and I.1B, lanes NT and EV). GAPDH was used as a loading control.

Expression of both IE1 and IE1x4 was also detected in transfected T98G cells (Fig. I.1C). Expression of IE1 or IE1x4 was not observed in non-transfected and empty vector control samples (Fig. I.1, lanes NT and EV). GAPDH was used as a loading control.

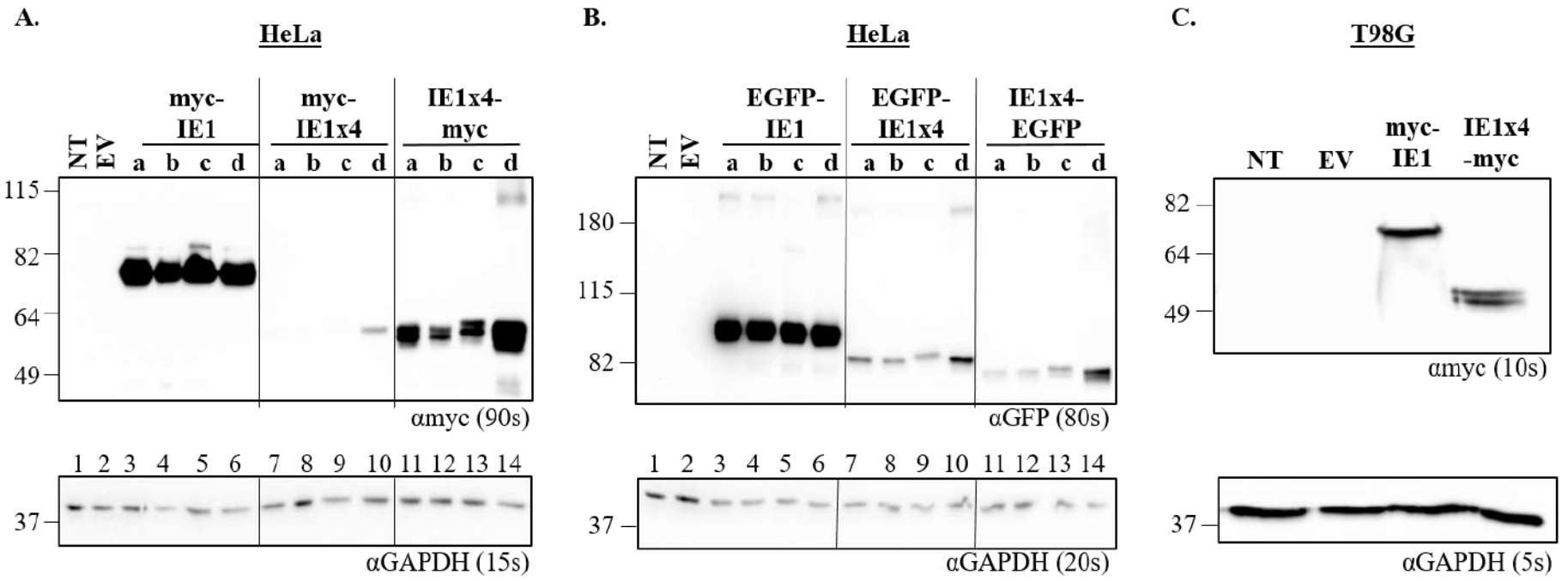

Figure I.1. Expression of IE1 and IE1x4 in HeLa and T98G cells. Transfected myc-tagged (A and C) or EGFP-tagged (B) IE1 and IE1x4 were detected in lysates of HeLa (A and B) and T98G cells (C). The inhibitors used for particular sample are indicated above the lane: a) protease and phosphatase, b) phosphatase, c) protease, phosphatase, and de-sumoylation, d) protease, phosphatase. Additionally, samples in lane d (i.e, lane 6, 10, and 14) were treated with MG132 for 12 h before harvest. Protease, phosphatase, and desumoylation inhibitors were used in all the cell lysates from T98G cells. Antibodies used to detect the proteins are indicated below the blot, the exposure time is indicated in the brackets. The numbers (1 to 14) above the GAPDH blots indicate the lane numbers and are applicable to the blot above it as well. EV - empty vector, NT - non transfected

5.1.2 IE1x4 localizes to the nucleus during interphase and to the chromosomes during mitosis

In transfected HeLa cells in interphase C-terminal fusions of IE1x4 (myc and EGFP) localized mostly in a diffuse nuclear pattern with additional weak cytoplasmic signal (Fig. I.2A and I.2B). However, for the N-terminal fusions of IE1x4 (myc and EGFP), I observed two distinct localization patterns: diffuse nuclear with weak cytoplasmic staining and exclusive cytoplasmic staining (Fig. I.2A and I.2B). This further fortified our decision to use C-terminal fusions of IE1x4 (myc and EGFP) in subsequent experiments. Localization pattern of IE1x4 in interphase in T98G cells was the same as in the HeLa cells, mostly diffuse nuclear with weak cytoplasmic staining (Fig. I.2C).

IE1 protein during interphase localized to the nucleus in three distinct patterns: diffuse, spotty, and a mixture of diffuse and spotty in both HeLa and T98G cells (Fig. I.2A-C), as has previously been reported [137]. No signal was observed in the secondary antibody control samples (Fig. I.2A and I.2C). Diffuse localization in the whole cell was observed for transfected EGFP protein serving as control (Fig. I.2B).

IE1x4 was observed to "paint" the chromosomes in mitosis in transfected HeLa (Fig. I.3A and I.3B) and T98G (Fig. I.3C) cells. Chromosome "painting" was also observed for IE1 during mitosis in both HeLa and T98G (Fig. I.3A-C) cells as has previously been reported [137]. In mitotic T98G cells in addition to the chromosome painting pattern, IE1 localized as paired spots on some of the chromosomes (Fig. I.3C). This localization pattern has not been reported before for IE1 and is the basis for the study presented in Chapter 2 of my thesis. EGFP protein, used as a control, localized in an "off-chromosomes" pattern (Fig. I.3A-C). The EGFP control shows that my handling of the cells during the chromosome spread procedure is sufficiently gentle to prevent loss of signal for proteins not associated with the chromosomes. No signal was observed in the secondary antibody control sample (Fig. I.3A and I.3C).

5.1.3 The localization pattern of IE1x4 does not change in the presence of HCMV TR

The TR region was proposed as the HCMV latent origin of replication and shown to mediate viral genome persistence [93, 101]. As IE1x4 was proposed to mediate viral genome tethering in a manner similar to that of KSHV LANA [101], I wanted to test if IE1x4 also changes its

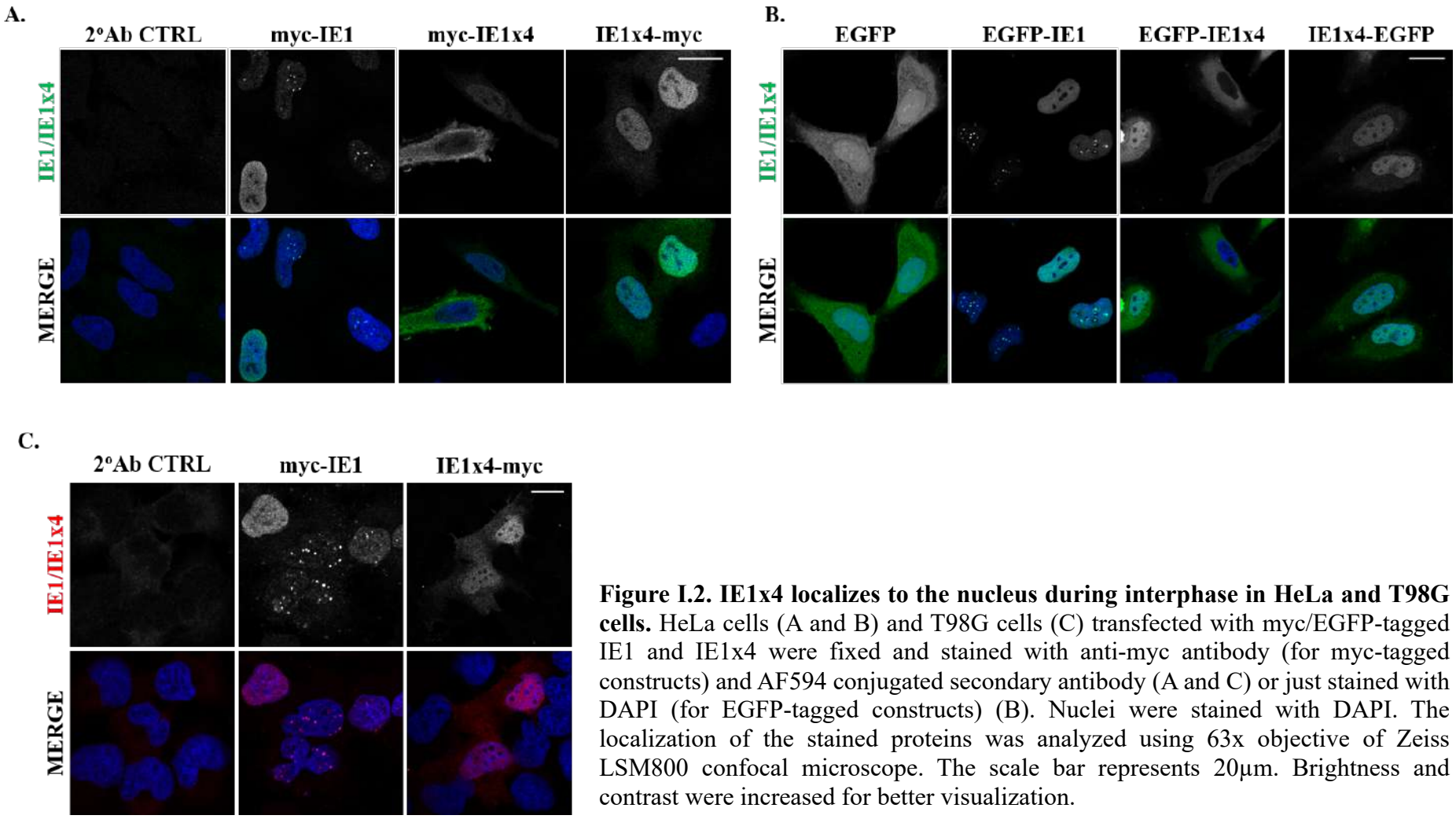

Figure I.2. IE1x4 localizes to the nucleus during interphase in HeLa and T98G cells. HeLa cells (A and B) and T98G cells (C) transfected with myc/EGFP-tagged IE1 and IE1x4 were fixed and stained with anti-myc antibody (for myc-tagged constructs) and AF594 conjugated secondary antibody (A and C) or just stained with DAPI (for EGFP-tagged constructs) (B). Nuclei were stained with DAPI. The localization of the stained proteins was analyzed using 63x objective of Zeiss LSM800 confocal microscope. The scale bar represents 20µm. Brightness and contrast were increased for better visualization.

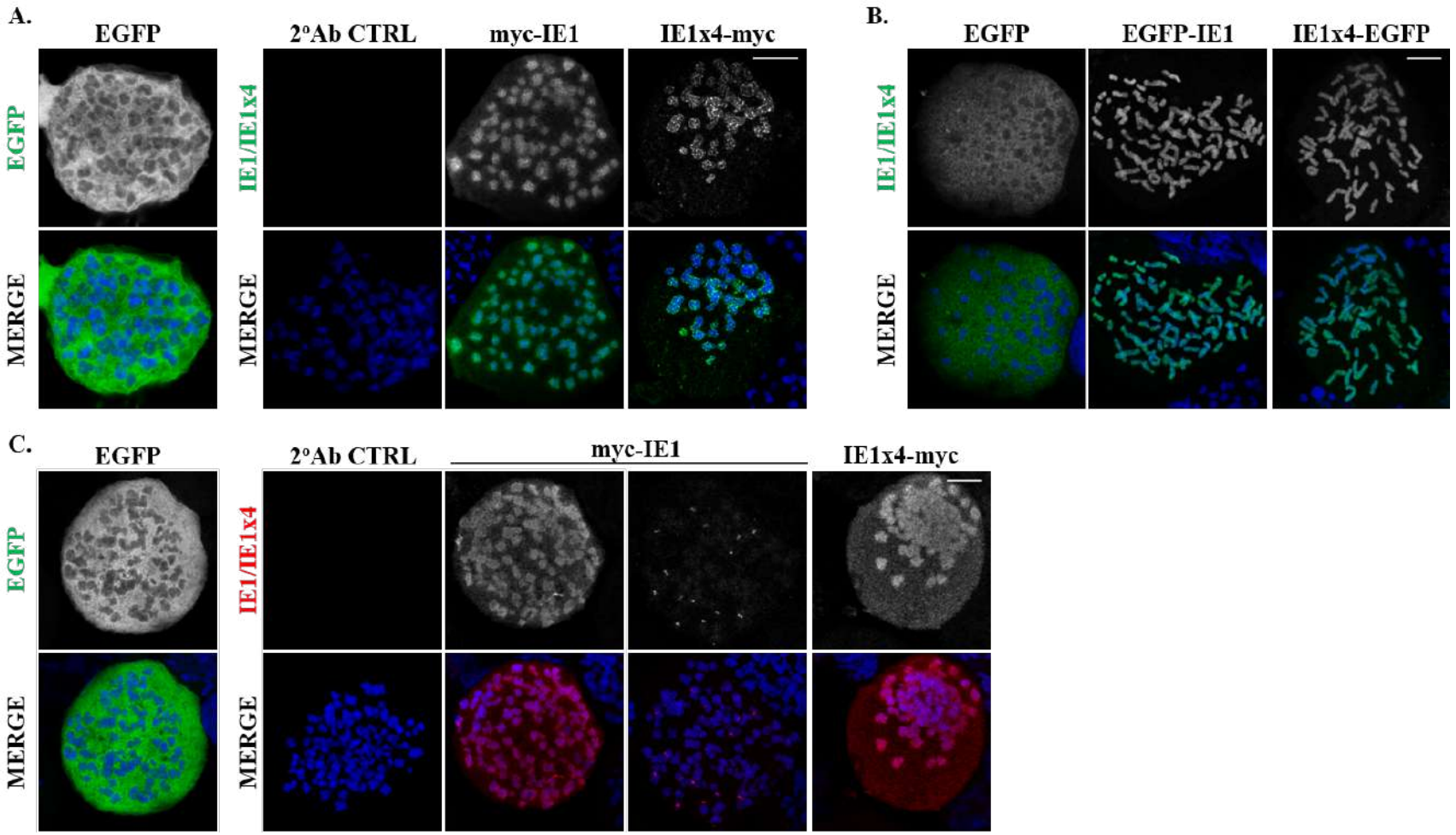

Figure I.3. IE1x4 localizes to the chromosomes during mitosis in HeLa cells. HeLa cells (A and B) and T98G cells (C) transfected with myc/EGFP-tagged IE1 and IE1x4 were arrested in metaphase to perform chromosome spreads. The cells were fixed and stained with anti-myc antibody (for myc-tagged constructs) and AF594 conjugated secondary antibody (A and C) or just stained with DAPI (for EGFP-tagged constructs) (B). Chromosomes were stained with DAPI. The localization of the stained proteins was analyzed using 63x objective of Zeiss LSM800 confocal microscope. The scale bar represents 10µm. Brightness and contrast were increased for better visualization.

localization pattern from painting of chromosomes to spots on chromosomes in the presence of the TR region as has been reported for KSHV LANA [249]. To test this, two versions of HCMV terminal repeat (TR) region were cloned, designated TR1 and TR2 (Fig. 1.4A). TR1 construct contains HCMV TR region including fragment of the sequence that encodes the TRS1 protein found at one of the ends of the TR sequence. The TRS1 protein was shown to have immunomodulatory functions during HCMV infection [263]. To control for the possible influence of the sequence encoding fragment of the TRS1 protein on the planned experiments, the TR2 construct was cloned excluding this sequence. Both versions of the TR region were cloned into a vector encoding EGFP protein, expression of which later served as a marker for presence of the vector carrying TR in the transfected cells.

In my hands in the interphase HeLa cells there was no change in localization pattern of IE1x4 neither in the presence of TR1 nor TR2, when equal amounts of TR1/2 and IE1x4 vectors were transfected (Fig. I.4B). The localization pattern was also analyzed after transfection with different ratios of IE1x4 to TR1/2 vectors i.e.: 7:3 and 3:7. I observed that the localization pattern of IE1x4 did not change even under these conditions (Fig. I.4B). Similarly, no change in localization pattern was observed for IE1 in the presence of TR1/2 under all the above conditions (Fig. I.4C). Since no obvious differences were observed in the localization pattern of IE1x4 in the presence of either TR1 or TR2 construct and transfection with TR2 resulted in higher cytotoxicity, only TR1 was used in remaining experiments. I have also analyzed the localization of IE1x4 in the presence of TR1 (transfecting equal ratio of vectors) in MRC-5 fibroblasts (Fig. I.5A), which in contrast to HeLa cells are permissive to HCMV lytic replication and T98G glioblastoma cells (Fig. I.5B), which support HCMV lytic and latent replication. Also, in those experiments no change in localization of IE1x4 was observed. Similarly, IE1 protein also did not change localization in the presence of TR1 in neither MRC-5 nor T98G cells. In all the above experiments no signal was observed for the secondary antibody controls (Fig. I.5A and I.5B).

Analogous to my results in interphase cells, I observed no change in localization pattern of IE1x4 or IE1 in the presence of HCMV TR1 (equal ratio of vectors transfected) in mitotic HeLa (Fig. I.6) and T98G (Fig. I.7) cells. No signal was observed for the secondary antibody controls in all the above experiments (Fig. I.6 and I.7). Off-chromosomes localization pattern was observed for EGFP protein control (Fig. I.6 and I.7).

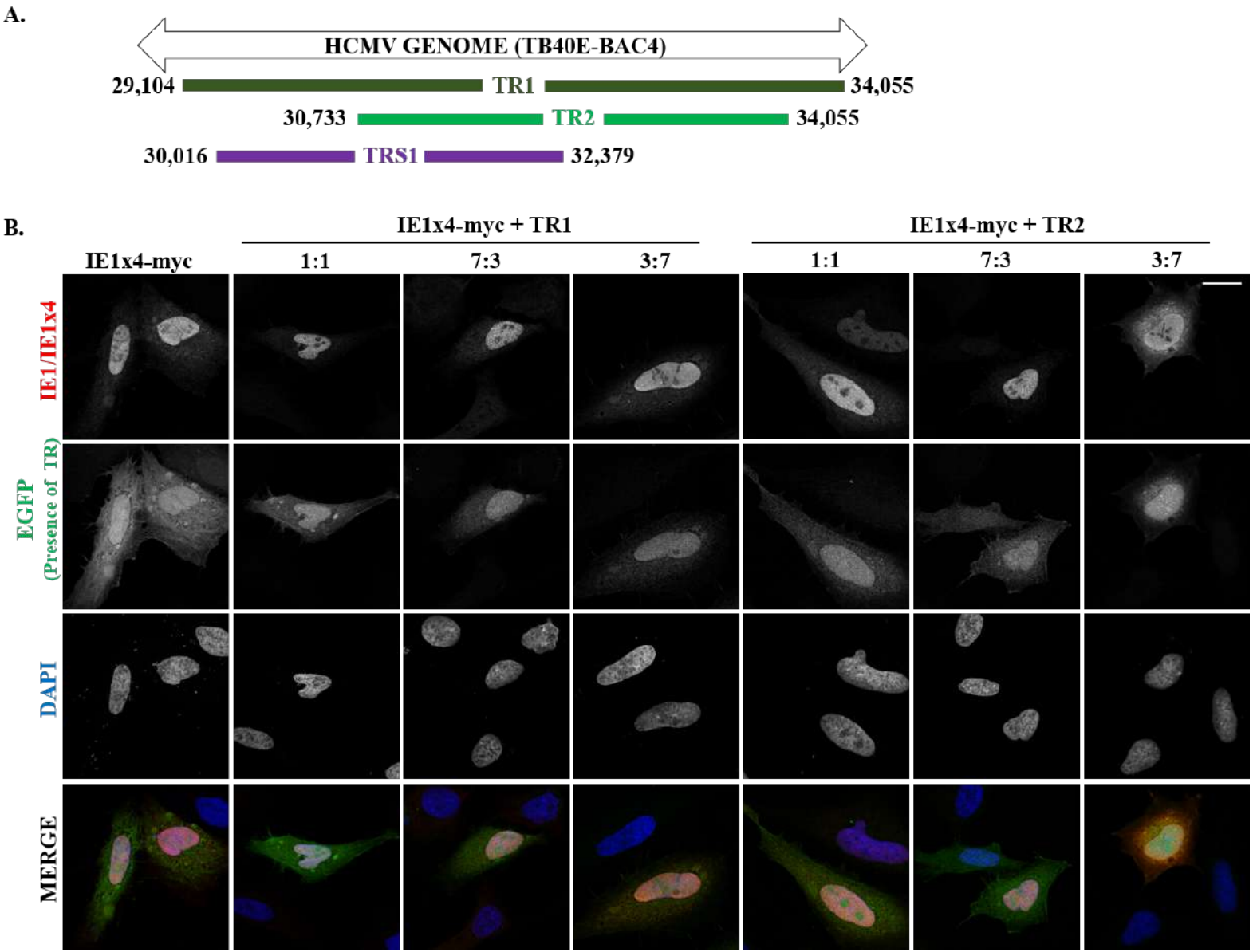
A.
HCMV GENOME (TB40E-BAC4)
29,104
TR1
34,055
30,733
TR2
34,055
30,016
TRS1
32,379
B.
IE1x4-myc
IE1x4-myc + TR1
1:1
7:3
3:7
IE1x4-myc + TR2
1:1
7:3
3:7
IE1/IE1x4
EGFP
(Presence of TR)
DAPI
MERGE

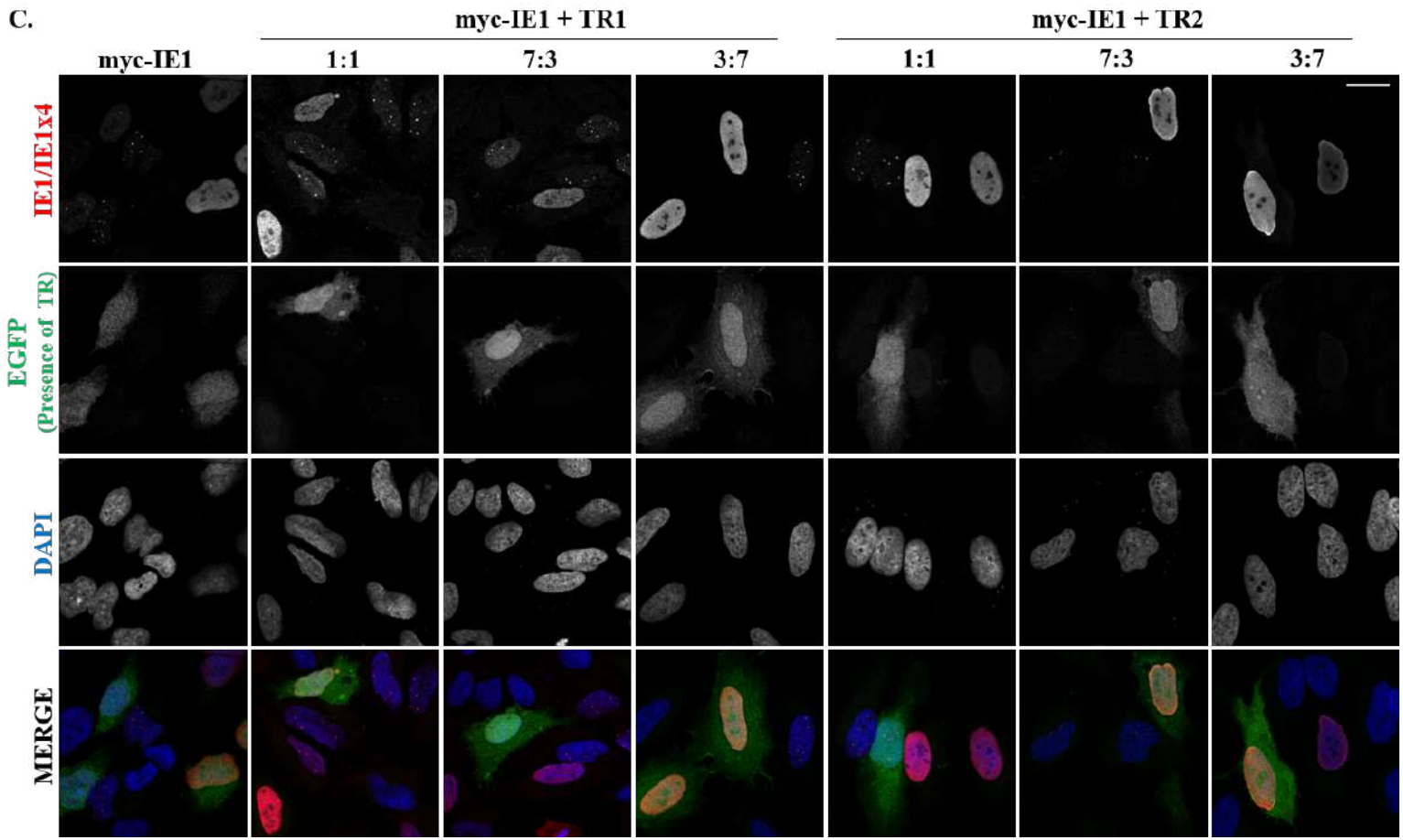

Figure I.4. Localization pattern of IE1x4 does not change in the presence of the HCMV TR region during interphase in HeLa cells. HeLa cells co-transfected with myc-tagged IE1/IE1x4 and a plasmid that contains the TR region of the HCMV genome and encodes the EGFP protein were fixed and stained with anti-myc antibody and AF594 conjugated secondary antibody. Nuclei were stained with DAPI. The localization of the stained proteins was analyzed using 63x objective of Zeiss LSM800 confocal microscope. The scale bar represents 20µm. Brightness and contrast were increased for better visualization. Graphical representation of the relative positions of TR1, TR2, and TRS1 in HCMV genome (A). Localization of IE1x4 in the presence of TR at ratios of 1:1, 7:3, and 3:7 (B). Localization of IE1 in the presence of TR at ratios of 1:1, 7:3, and 3:7 (C).

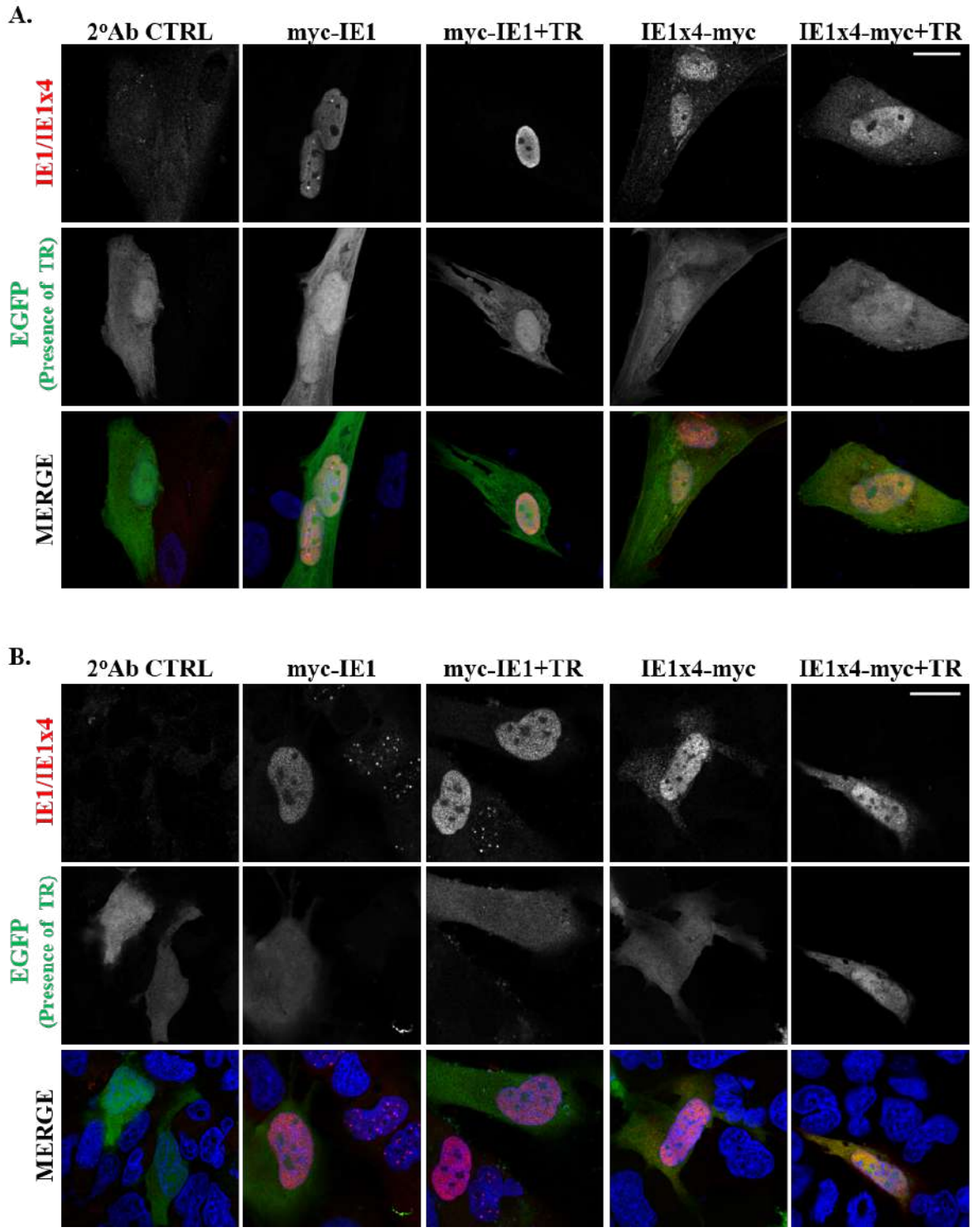

Figure I.5. Localization pattern of IE1x4 does not change in the presence of the HCMV TR region during interphase in MRC-5 and T98G cells. MRC-5 (A) and T98G (B) cells co-transfected at equal ratio (1:1) with myc-tagged IE1/IE1x4 and a plasmid that contains the TR region of the HCMV genome and encodes the EGFP protein. The cells were fixed and stained with anti-myc antibody and AF594 conjugated secondary antibody. Nuclei were stained with DAPI. The localization of the stained proteins was analyzed using 63x objective of Zeiss LSM800 confocal microscope. The scale bar represents 20µm. Brightness and contrast were increased for better visualization.

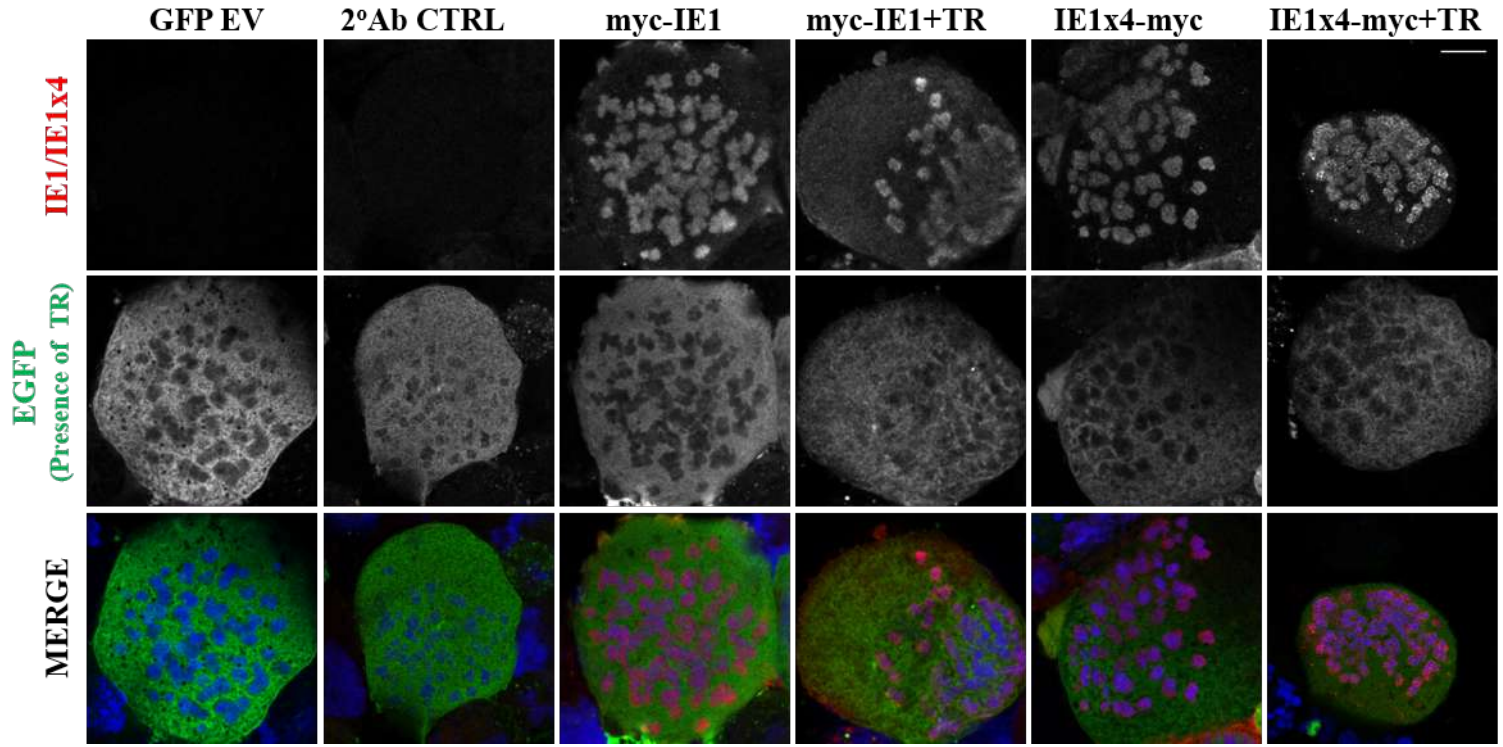

Figure I.6. Localization pattern of IE1x4 does not change in the presence of the TR region during mitosis in HeLa. HeLa cells co-transfected at equal ratio (1:1) with myc-tagged IE1/IE1x4 and a plasmid that contains the TR region of the HCMV genome and encodes the EGFP protein. The cells were fixed and stained with anti-myc antibody and AF594 conjugated secondary antibody. Nuclei were stained with DAPI. The localization of the stained proteins was analyzed using 63x objective of Zeiss LSM800 confocal microscope. The scale bar represents 10µm. Brightness and contrast were increased for better visualization.

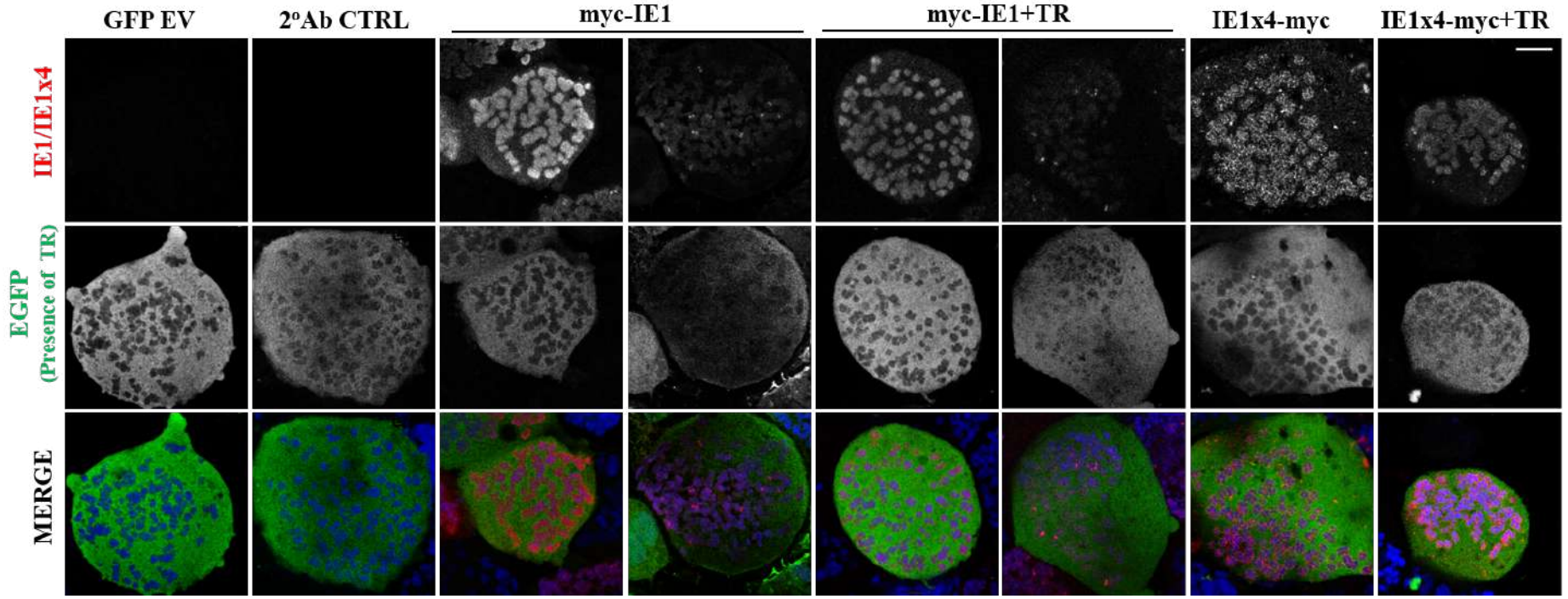

Figure I.7. Localization pattern of IE1x4 does not change in the presence of the TR region during mitosis in T98G. T98G cells co-transfected at equal ratio (1:1) with myc-tagged IE1/IE1x4 and a plasmid that contains the TR region of the HCMV genome and encodes the EGFP protein. The cells were fixed and stained with anti-myc antibody and AF594 conjugated secondary antibody. Nuclei were stained with DAPI. The localization of the stained proteins was analyzed using 63x objective of Zeiss LSM800 confocal microscope. The scale bar represents 10μm. Brightness and contrast were increased for better visualization.

Our results do not support the concept of IE1x4 as the protein tethering HCMV genome through the TR sequence in the cell types we tested, since the localization pattern of IE1x4 did not change in the presence of the HCMV TR.

5.1.4 Establishment of latency in T98G cells

Viral genome persistence is necessary for establishment of latency. Since I wanted to study HCMV latency I set out to establish latent HCMV infection in a T98G cell line, which has been published as a model for HCMV latency [264, 265]. To confirm efficient establishment of HCMV latency in T98G cells expression of viral genes from different replication stages were analyzed. Quantitative RT-PCR analysis showed that the immediate early transcripts IE1 and IE2 are detected up to 35dpi (the last timepoint of the experiment), a significant level of UL44 early viral transcript is not detected past 21dpi, and gB, a late transcript past 28dpi (Fig. I.8D).

I observed expression of the latent UL138 transcript throughout the 35 days, however the expression levels decreased significantly at 21dpi followed by a sustained low-level expression at the following time points 28dpi and 35dpi. These results together with significant drop in expression of lytic genes (UL44 and gB) at 28dpi and thereafter suggest that latency was established (Fig. I.8D) and the lytic replication ceased past 28dpi. Relative differences between mock infected and infected samples at indicated time points were calculated and all samples were normalized to GAPDH for the analysis of gene expression by qRT-PCR. The results are presented as fold change relative to mock infected control.

Using immunofluorescence staining I also checked the expression of viral proteins in T98G cells upon HCMV latency establishment. IE1 positive cells could be observed up to 35dpi (Fig. I.8A), however the number of positive cells decreased from 7dpi to 35dpi with very rare cells being positive at 28dpi and 35dpi. UL44 and gB positive cells could be detected at 7dpi, at 14dpi the number of positive cells decreased, and no positive cells could be detected from 21dpi to 35dpi (Fig. I.8A) indicating the cessation of lytic replication between 14dpi and 21dpi. No staining was observed in mock infected T98G cells stained with the respective antibodies as controls (Fig. I.8A).

Analysis of expression of viral proteins by western blotting showed that IE1 and UL44 are expressed at 7dpi, but not thereafter (Fig. I.8B). Immunofluorescence staining and immunoblotting.

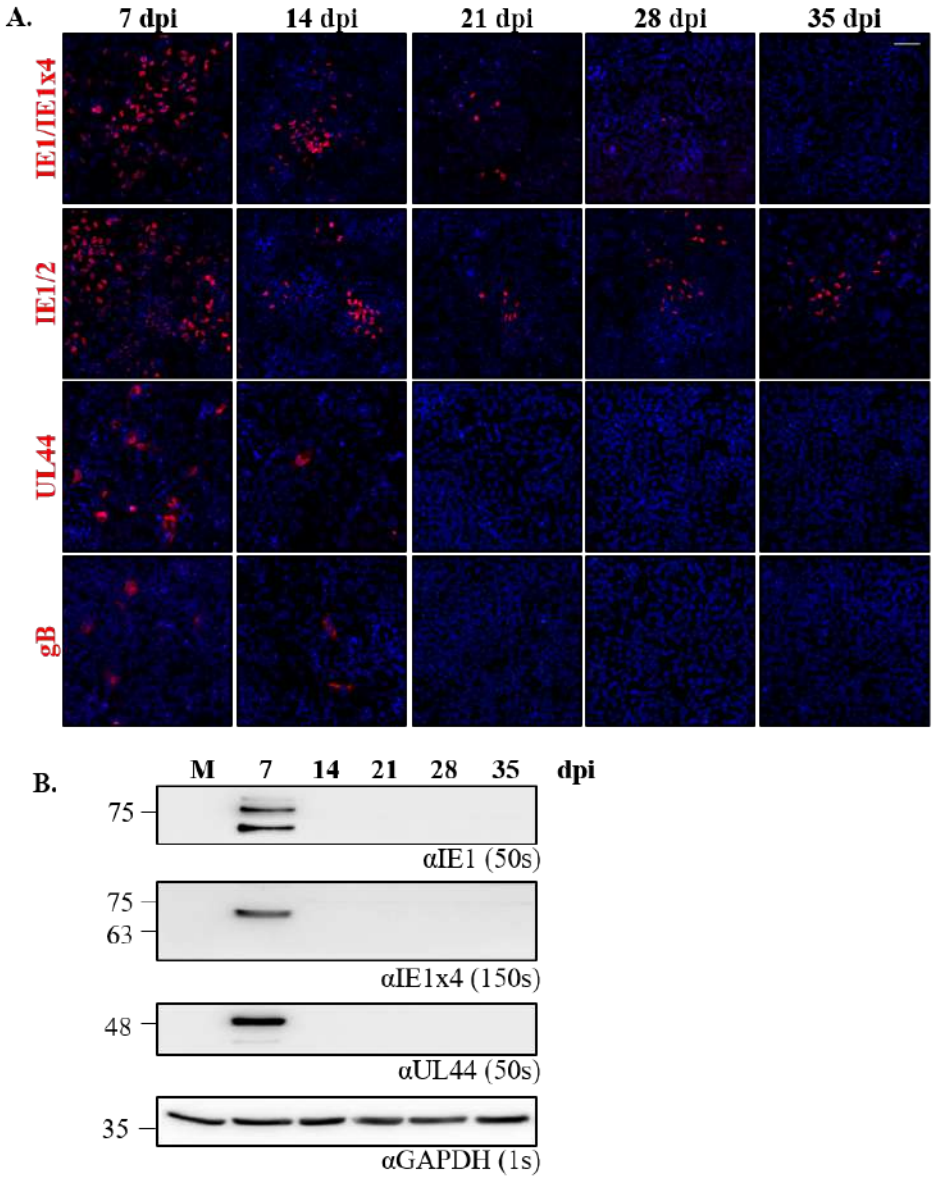
A.
7 dpi
14 dpi
21 dpi
28 dpi
35 dpi
IE1/IE1x4
IE1/2
UL44
gB
B.
M
7
14
21
28
35
dpi
75
αIE1 (50s)
75
63
αIE1x4 (150s)
48
αUL44 (50s)
35
αGAPDH (1s)

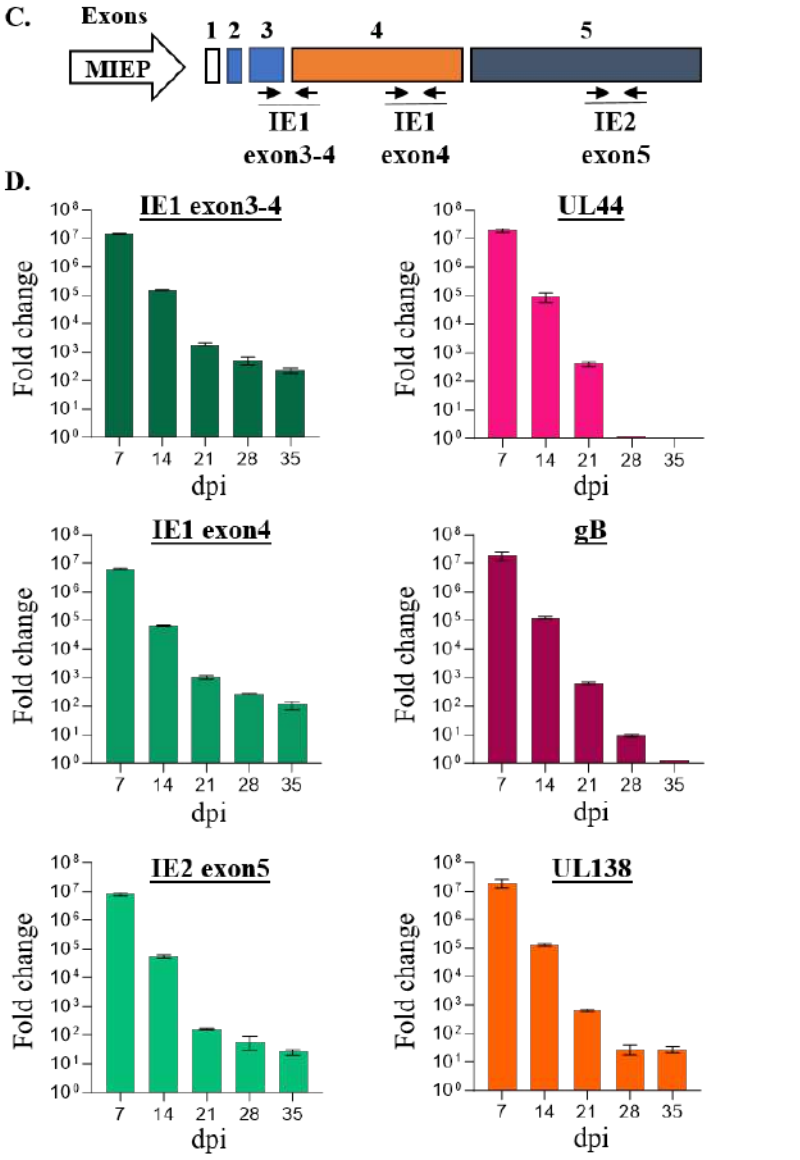
C.
Exons
MIEP
1 2 3
4
5
IE1
exon3-4
IE1
exon4
IE2
exon5
D.
IE1 exon3-4
UL44
IE1 exon4
gB
IE2 exon5
UL138
Fold change
dpi
7
14
21
28
35

E.

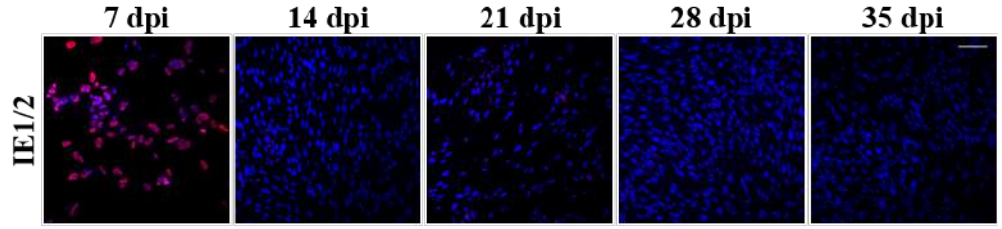

F.

dpi	qRT-PCR					IFA			Western blot		Production of viral particles
	IE1	IE2	UL44	gB	UL138	IE1	UL44	gB	IE1	UL44	
7	++	++	++	++	++	+	+	+	+	+	+
14	++	++	++	++	++	+	+	+	-	-	-
21	+	+	+	+	+	+	-	-	-	-	-
28	+	+	+/-	+	+	+	-	-	-	-	-
35	+	+	-	+/-	+	+/-	-	-	-	-	-

Figure I.8. IE1x4 protein is not expressed in latently infected T98G cells. T98G cells were infected with HCMV TB40E at MOI 10. Cells were continuously passaged every 7 days up to 35 dpi and harvested at indicated time points.
A. Expression of HCMV lytic proteins (IE1, IE1x4, UL44, and gB) analyzed by IFA. The cells were fixed and stained with rspective antibodies and AF594 conjugated secondary antibody. Nuclei were stained with DAPI. Images were taken using 10x objective of Zeiss LSM800 confocal microscope and the scale bar represents 100µm. Brightness and contrast were increased for better visualization.
B. Expression of HCMV lytic proteins analyzed by WB. Lysates of mock/infected cells harvested at different time post infection were separated on an SDS PAGE gel, transferred and the membranes were probed with antibodies indicated below the blot. The exposure times are indicated in brackets.
C. Schematic of major immediate early locus and exons 1 to 5, the large white arrow represents the major immediate early promoter (MIEP) of the HCMV. The arrows below the scheme indicate the qRT-PCR primers used to identify IE1FL, IE1x4, and IE2 transcripts
D. Expression of viral gene transcripts was examined by qRT-PCR. Controls included a mock infected sample and no RT samples. GAPDH was used as a house keeping control gene.
E. Infectivity assay to analyze the production of viral particles by infected T98G. Supernatant from infected T98G cells was harvested at different time points post infection and added to HFFs permissive to HCMV infection. The HFF cells were fixed and stained with anti-IE1 antibody and AF594 conjugated secondary antibody. Nuclei were stained with DAPI. Images were taken using 10x objective of Zeiss LSM800 confocal microscope and the scale bar represents 100µm. Brightness and contrast have been increased for better visualization.
F. Summary table showing the establishment of latency in T98G cells as analyzed by qRT-PCR, immunofluorescence, western blotting, and infectivity assay.

data taken together suggest that IE1 expression occurs only in a limited number of cells during latency in T98G cells. This expression in limited number of cells could be detected by immunofluorescence staining, but not by immunoblotting as the sensitivity of this assay is much lower (Fig. I.8A and I.8B). IE1 transcripts could also be detected up to 35dpi (Fig. I.8D). Therefore, immunofluorescence staining and immunoblotting data correlate with the results obtained in my qRT-PCR analysis of IE1, UL44, and gB gene expression patterns.

To test if the infected T98G cells produced viral particles (indicative of active lytic replication) I performed and infectivity assay. Confluent monolayers of HFF cells were incubated with supernatant from infected T98G and the infection efficiency was assessed by IE1 staining. I observed no viral particle production by infected T98G cells past 7dpi (Fig. I.8E). Taken together, these results confirm that latency was established in T98G cells (Fig. I.8F).

5.1.5 IE1x4 protein is not expressed in latent T98G cells

As my goal was to analyze the role of IE1x4 during HCMV latency, I set out to check the expression of this gene in latently/persistently infected T98G glioblastoma. To analyze the expression of IE1x4 and to differentiate it from IE1 full length (IE1FL) transcript, I used two primer sets. One of them allowed amplification of only the exon 4 region of the IE1 locus (common to both IE1x4 and IE1FL), and a second one amplified the region spanning exon 3 and 4 that is present in IE1FL, but not in IE1x4 (Fig. I.8C). I observed that in T98G cells both transcripts containing exon 4 and exon 3-4 junction could be detected up to 35dpi (final timepoint), which includes, as shown above, the period of established latency. Since IE1 exon 3-4 and exon 4 transcripts were both detected throughout our experiment at comparable levels, we conclude that it is IE1FL (containing both exons 3 and 4) that is expressed and not IE1x4 (Fig. I.8D). Previously it has been suggested that the IE1FL is expressed exclusively in the lytic cycle and in the latent CD34+ cells only the IEx4 transcript is detectable [101].

To analyze IE1x4 protein expression, an antibody recognizing an epitope encoded by the exon 4, common to IE1 and IE1x4 (designated: αIE1x4) and an antibody recognizing an epitope encoded by exons 2/3 common to IE1 and IE2 (designated: αIE1/2), but not present in IE1x4 were used. αIE1x4 antibody can detect both IE1 and IE1x4 proteins, whereas αIE1/2 antibody can detect IE1 and IE2, but not IE1x4. In my hands, IE1x4 (expected size ~60kD) could not be detected in cell lysates of infected T98G cells at any time point, whereas IE1FL (~72kD) could

be detected by immunoblotting only at 7dpi (Fig. I.8B). Immunofluorescence staining of infected T98G using αIE1x4 and αIE1/2 showed that specific staining could be observed up to 28dpi with αIE1x4 and up to 35dpi (end point) with αIE1/2 antibodies, however the number of positive cells reduced as infection progressed from 7dpi (lytic) to 35dpi (latency) (I.8A). Taken together, these data suggest that IE1FL is expressed at high levels during the lytic cycle, but also in a limited number of T98G cells during latency (Fig. I.8A-D)

5.1.6 IE1, but not IE1x4 is expressed in latent KASUMI-3 cells

As IE1x4 transcript and protein were reported to be expressed in latent CD34+, but not in CD14+ cells [93, 101] we checked the expression of IE1x4 protein in latently infected KASUMI-3 cells, a CD34+ myeloid progenitor cell line, which has been shown to support HCMV latency [266]. To this end, cell lysates from latently infected KASUMI-3 cells (a kind gift from laboratory of prof. J. Sinclair) separated on an SDS PAGE gel, were probed with αIE1x4 and αIE1/2 antibodies. In my hands expression of IE1x4 using αIE1x4 antibody could not be detected in latently infected KASUMI-3 cells, but expression of IE1 was observed using αIE1/2 (Fig. I.9) similarly to our observations in latently infected T98G cells. Cell lysate from uninfected KASUMI-3 cells was used as a negative control and the viral proteins were not detected in it. Cell lysates from T98G cells transfected with IE and IE1x4 (myc tagged) expressing vectors were used as positive controls to confirm the detection by the antibodies mentioned above. αIE1x4 could detect both IE1 and IE1x4 whereas αIE1/2 could detect only IE1 in transfected T98G cells (Fig. I.9). GAPDH was used as a loading control.

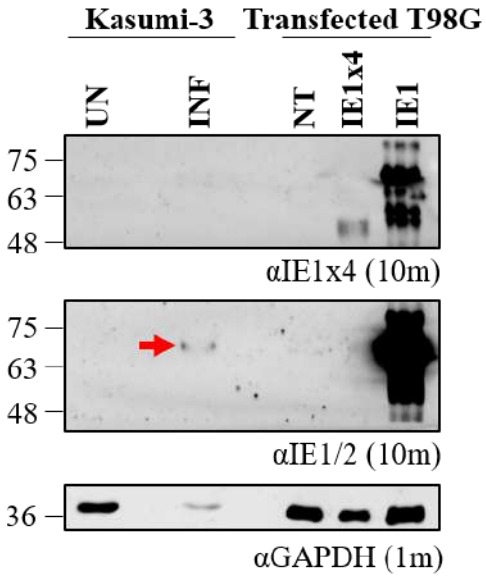

Figure I.9. IE1, but not IE1x4 is expressed in latently infected KASUMI-3 cells. Cell lysate of latently infected KASUMI-3 cells (a kind gift from the laboratory of prof. John Sinclair) was analyzed for the expression of IE1x4 using antibodies anti-IE1x4 and anti-IE1/2. Cell lysate from T98G cells transfected with myc-tagged IE1 and IE1x4 was used as control for antibody detection. Expression of GAPDH was used as loading control.

5.2 CHAPTER II - Significance of unique localization pattern of IE1 on chromosomes

5.2.1 HCMV IE1 forms spots on mitotic chromosomes in transfected cells

It was previously published that IE1 distributes evenly over the mitotic chromosomes in a pattern referred to as "chromosome painting" [137]. I have observed that in T98G cells in addition to this painting pattern, myc-IE1 localizes as paired spots on some mitotic chromosomes (Fig. II.1A). I have also detected this localization pattern with EGFP-IE1 in T98G cells (Fig. II.1B). I will be referring to the localization pattern of IE1 in the form of spots as **chromosome-associated spots** (**CAS**) henceforth. Quantification of the localization patterns showed that in T98G cells transfected with myc-IE1, IE1 localizes in the **painting pattern** in **60%** of the cells and **40%** as **CAS** (Fig. II.1C) whereas in T98G cells transfected with EGFP-IE1, **61%** of the cells showed the **painting pattern** and **39% CAS** (Fig. II.1C). No statistically significant difference was observed upon comparison of IE1 CAS localization patterns with myc-IE1 and EGFP-IE1 constructs ($p=0.1627$). No signal was observed in the secondary antibody control sample (Fig. II.1A). EGFP protein, used as a control, localized in an "off chromosomes" pattern (Fig. II.1B). IE1 is always present as double CAS on a few chromosomes (Fig. II.1A and II.1B). This is in contrast to KSHV LANA, a known genome maintenance protein of a gammaherpesvirus, which in the presence of the KSHV latent ori forms multiple spots on both arms of all chromosomes (Fig. II.2).

5.2.2 HCMV IE1 forms CAS in infected cells

Localization of IE1 in spots was novel, therefore I set out to confirm that what I detected is not an artifact of protein overexpression. First, I infected T98G cells with TB40E strain of HCMV and stained for IE1 protein using two different antibodies: αIE1/2 and αIE1x4. I was able to detect IE1 CAS, in addition to the painting localization pattern, with both αIE1/2 (Fig. II.3A) and αIE1x4 (Fig. II.3B) validating the novel localization in a more natural system. No specific signal was observed in the uninfected control samples (Fig. II.3A and II.3B).

5.2.3 HCMV IE1 CAS can be observed with different fixation methods

Since IE1 CAS was observed for the first time, I also wanted to check if IE1 CAS could be detected following different fixation methods such as methanol and ethanol, in addition to the paraformaldehyde (PFA) fixation that was used for the chromosome spreads. Additionally, to ensure that the IE1 CAS observed are not an artifact of the protocol used to prepare the

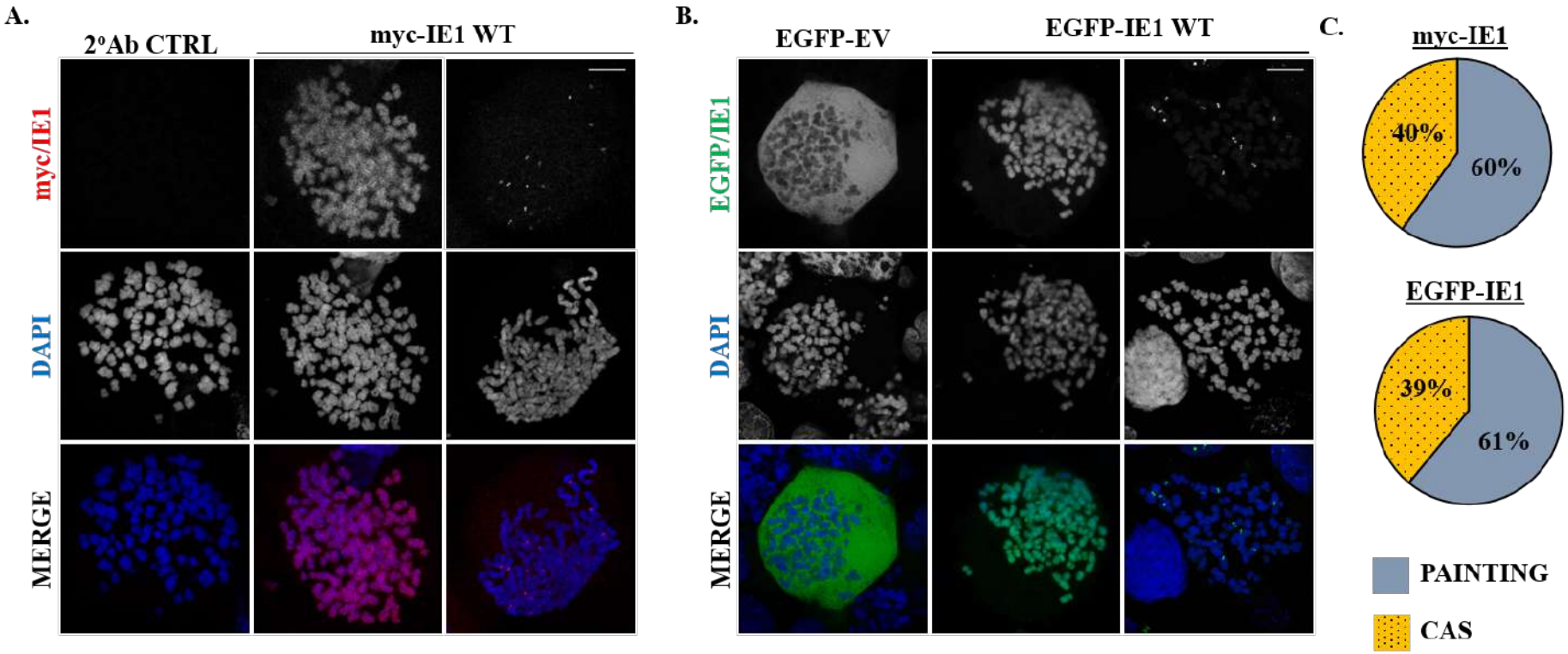

Figure II.1. IE1 forms chromosome associated spots (CAS) in transfected T98G cells. T98G cells transfected with myc/EGFP-tagged IE1 were arrested in metaphase to perform chromosome spreads. The cells were fixed and stained with anti-myc antibody (myc-IE1) and AF594 conjugated secondary antibody (A) or just stained with DAPI (GFP-IE1) (B). Chromosomes were stained with DAPI. The localization of the stained proteins was analyzed using 63x objective of Zeiss LSM800 confocal microscope. The scale bar represents 10µm. Brightness and contrast were increased for better visualization. Quantification of IE1 painting and CAS localization patterns (C). Percentages represent the average from three independant experiments and SEM is indicated in the table in brackets.

	PAINTING	CAS
myc-IE1	60% (+/- 4)	40% (+/- 4)
EGFP-IE1	61% (+/- 2)	39% (+/- 2)

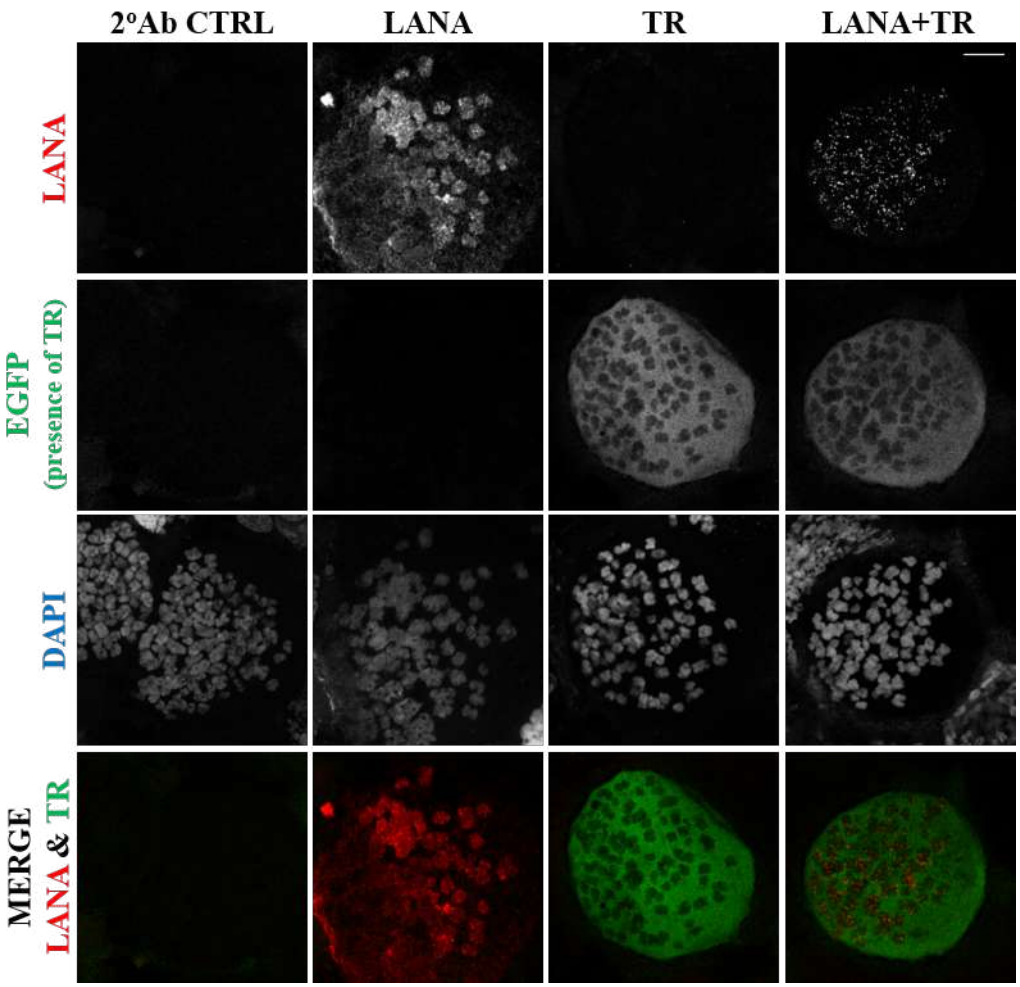

Figure II.2. KASHV LANA forms spots on both arms of the chromosome in the presence of KSHV TR. T98G cells transfected with plasmids encoding KSHV LANA or KSHV LANA+TR was arrested in metaphase to perform chromosome spreads. The cells were fixed and stained with anti-LANA antibody and AF594 conjugated secondary antibody. Chromosomes were stained with DAPI. The localization of the stained proteins was analyzed using 63x objective of Zeiss LSM800 confocal microscope. The scale bar represents 10µm. Brightness and contrast were increased for better visualization.

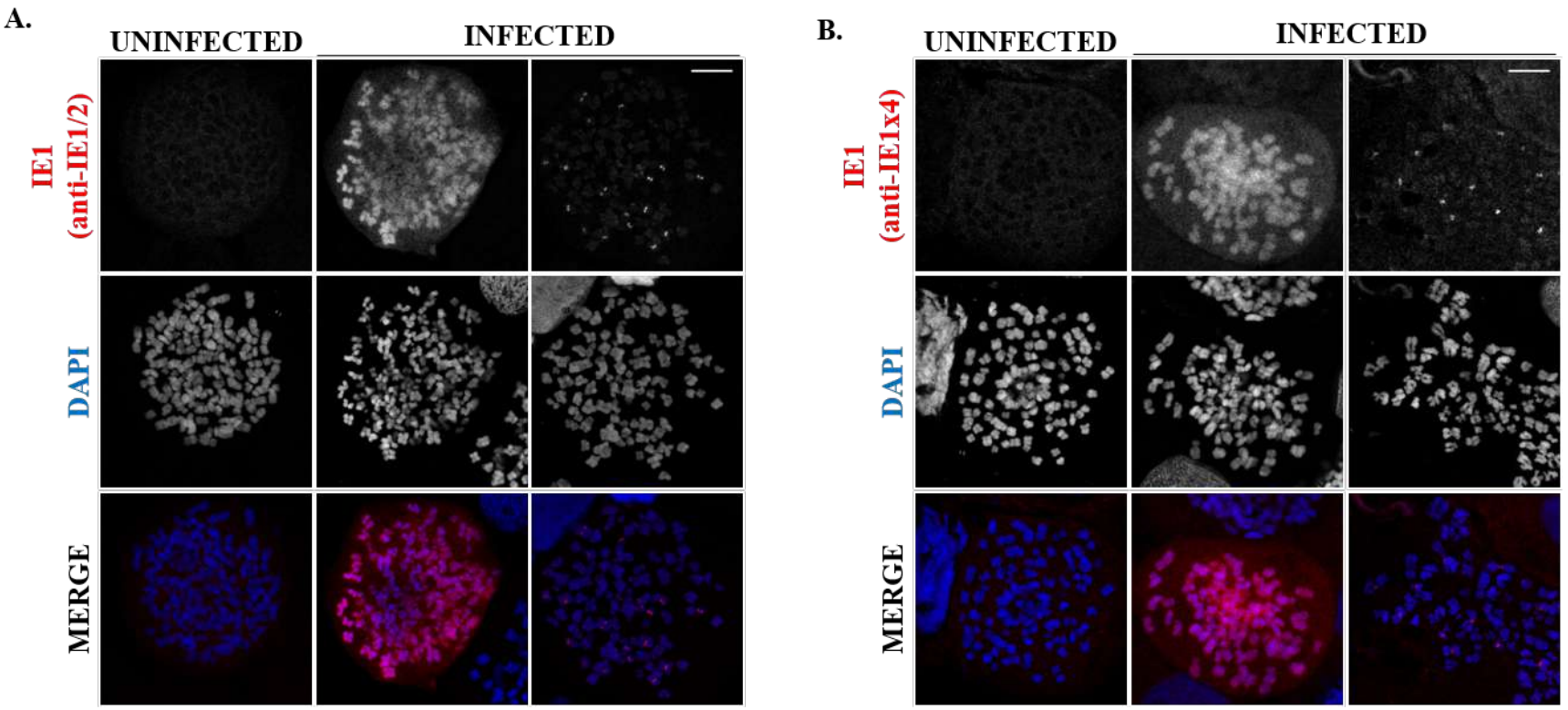

Figure II.3. IE1 CAS are present in HCMV infected T98G cells. Infected or uninfected T98G cells were arrested in metaphase to perform chromosome spreads. The cells were fixed and stained with anti-IE1/2 (A) or anti-IE1x4 (B) antibody and AF594 conjugated secondary antibody. Chromosomes were stained with DAPI. The localization of the stained proteins was analyzed using 63x objective of Zeiss LSM800 confocal microscope. The scale bar represents 10µm. Brightness and contrast were increased for better visualization.

chromosome spreads, immunofluorescence staining was performed on T98G cells transfected with myc-IE1 not treated with colcemid and without the procedure of spreading the chromosomes. I analyzed each sample for the presence of mitotic cells containing spots. I was able to detect IE1 CAS in samples that did not undergo chromosome spreading regardless of the fixation method used (Fig. II.4). This suggests that IE1 CAS is not an artifact of the chromosome spreading protocol or the specific fixation treatment.

5.2.4 HCMV IE1 CAS can be detected in some tumor cells

As IE1 CAS were observed in T98G (Fig. II.1A and II.1B), but not in HeLa cells (Fig. I.5A and I.5B), I wanted to further understand which property of T98G contributes to this specific localization pattern. T98G is a tumor cell line (glioblastoma) of neural origin and HCMV latency can be established in these cells [265]. A panel of cells (Table 10) with features overlapping those of T98G were infected with HCMV TB40E strain and following IE1 staining tested for presence of IE1 CAS. I observed IE1 **CAS** in **U87MG and THP1** cells, but **not** in human placental fibroblasts (**HPF)**, neural stem cells (**NSC**), and **HT-29** cells (Fig. II.5A and II.5B). No specific signal was observed in the respective uninfected control samples (Fig. II.5A and II.5B).These results suggest that IE1 forms CAS in some tumor cells, but not all. The common feature of the cells, in which I observed IE1 CAS is that they allow HCMV latency establishment. However, IE1 CAS was not observed in NSC, which were shown to allow HCMV latent infection, but are not a tumor cell line. Taking into account all of the cell types tested, at the current state of investigation a conclusion can be drawn that the IE1 CAS localization is present only in cells that allow HCMV latency establishment and are at the same time tumor cell lines.

Analysis of the number of chromosomes with IE1 CAS in T98G, U87MG, and THP1 showed that IE1 CAS is present on 8-10% chromosomes per cell (Fig. II.5C). This suggests that IE1 CAS forms only on a subset of chromosomes and not all chromosomes.

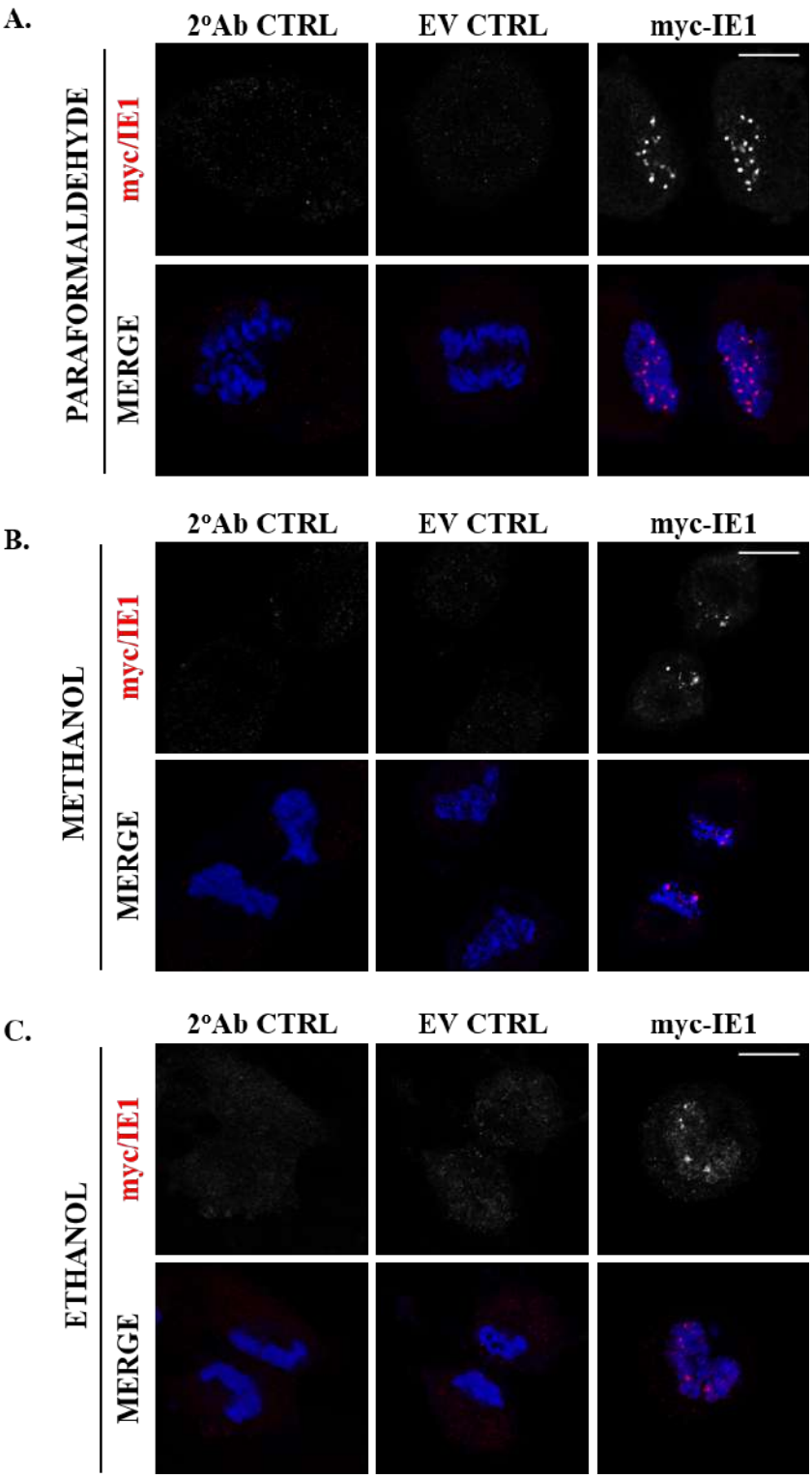

Figure II.4. IE1 CAS can be observed with different fixation methods. T98G cells transfected with myc-IE1 were fixed with 4% paraformaldehyde (A), methanol (B), or ethanol (C). The cells were stained with anti-myc antibody and AF594 conjugated secondary antibody. Nuclei were stained with DAPI. The localization of the stained proteins was analyzed using 63x objective of Zeiss LSM800 confocal microscope. The scale bar represents 10µm. Brightness and contrast were increased for better visualization.

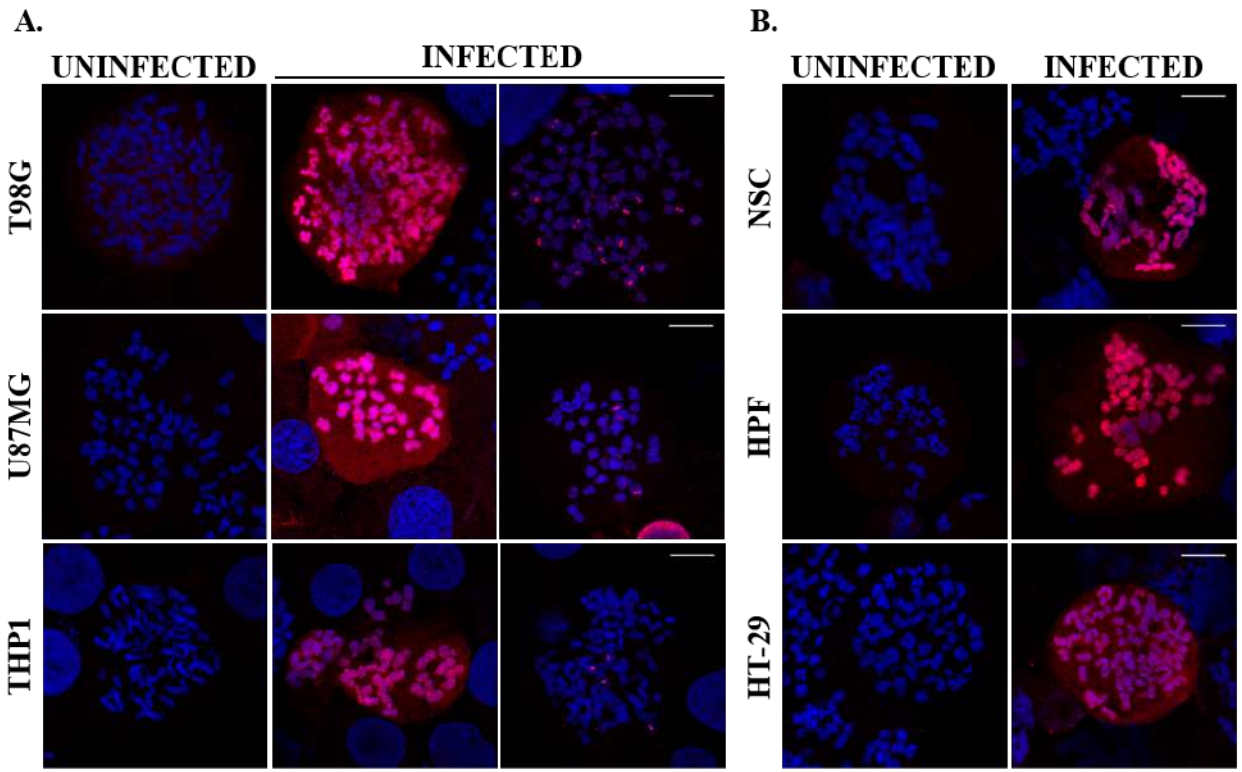

C.

	T98G	U87MG	THP1
Average number of chromosomes with spots per cell	13.16	3.76	4.81
Modal number of chromosomes per cell	130 (128-132)	44	46
Percentage of chromosomes with spots per cell with respect to modal number of chromosomes	10.12%	8.55%	10.93%
n	100	100	50

Figure II.5. IE1 forms CAS only in some tumor cells. Chromosome spreads of HCMV infected cells were stained with anti-IE1 antibody and AF594 conjugated secondary antibody. Cell lines showing IE1 spots in addition to painting pattern: T98G, U87MG, and THP1 (A), cell lines showing only IE1 painting pattern: NSC, HPF, and HT-29 (B). Chromosomes were stained with DAPI. The localization of the stained proteins was analyzed using 63x objective of Zeiss LSM800 confocal microscope. The scale bar represents 10µm. Brightness and contrast were increased for better visualization. Analysis of number of chromosomes with IE1 CAS localization pattern in different cell lines (C).

Table 10. Cell lines tested for IE1 chromosome associated spots (CAS) formation on mitotic chromosomes

Cell type	Cell characteristics	HCMV latency	Neural origin	Tumor	CAS
THP1	CD14+	+	-	+	+
T98G	GBM	+	+	+	+
U87MG	GBM	+	+	+	+
HT-29	colon cancer	?	-	+	-
NSC	primary	+	+	-	-
HPF	primary	-	-	-	-

5.2.5 HCMV IE1 spots localize to the peri-centromeric regions of the chromosomes

The IE1 in form of spots on chromosomes had a very unique positioning, namely double spots in the vicinity of primary constriction. Hence, I wanted to check what was the localization of IE1 CAS in relation to centromeres. It is important to recall at this point that in interphase IE1 in some cells is distributed diffusely in the nucleus and in others forms nuclear spots. I observed that during interphase in T98G cells, IE1 spots were always found juxtaposed to CENP-A, one of the major components of the centromere (Fig. II.6A). During mitosis, IE1 spots also localized adjacent to CENP-A, therefore in the peri-centromeric regions of the chromosomes (Fig. II.6B). No signal was observed in the secondary antibody control samples (Fig. II.6A and II.6B).

5.2.6 PML is recruited to IE1 CAS in the peri-centromeric regions of the chromatin

HCMV IE1 localized in the painting pattern was reported to recruit PML to mitotic chromosomes [126]. I wanted to check if IE1 CAS also have the ability to mediate PML association with mitotic chromosomes. Upon co-staining of PML and CENP-A in T98G cells transfected with EGFP-IE1, I observed that IE1 spots present in the interphase colocalize with PML and are found juxtaposed to CENP-A (Fig. II.7A). In mitosis, I observed that IE1 present in form of CAS recruited PML to the pericentromeric region of chromosome found adjacent to centromeres marked by CENP-A (Fig. II.7B). No signal was observed in the secondary

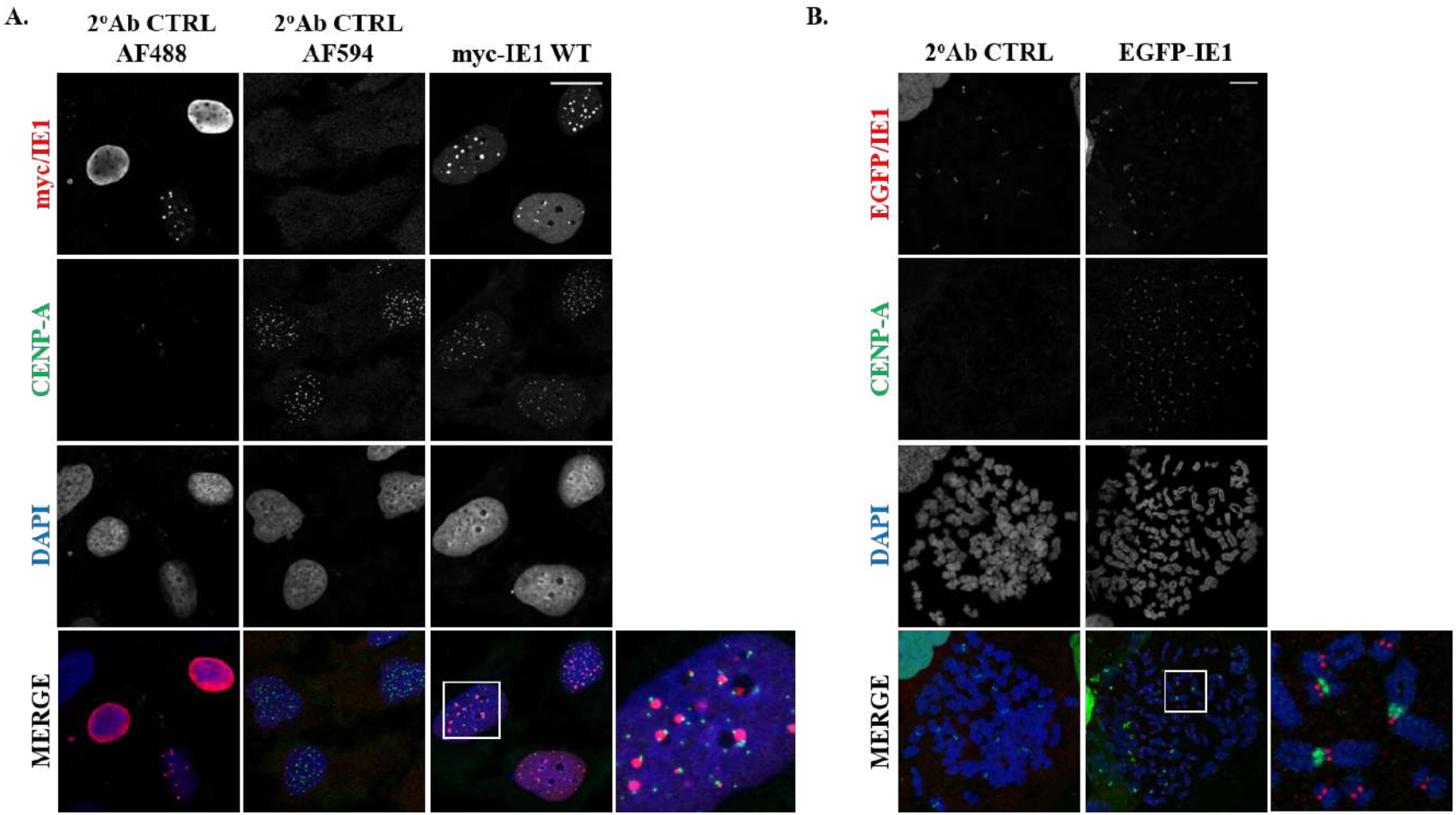

Figure II.6. IE1 CAS localize to the peri-centromeric regions of the chromosome. T98G cells transfected with myc/EGFP-tagged IE1 WT were fixed in interphase (A) or were arrested in metaphase to perform chromosome spreads (B). The cells were fixed and stained with anti-CENP-A antibody and AF594 conjugated secondary antibody (A and B) and myc-IE1 was stained with anti-IE1 antibody and AF488 conjugated secondary antibody (A). Nuclei and chromosomes were stained with DAPI. The localization of the stained proteins was analyzed using 63x objective of Zeiss LSM800 confocal microscope. The scale bar represents 20µm (A) and 10µm (B). Brightness and contrast were increased for better visualization.

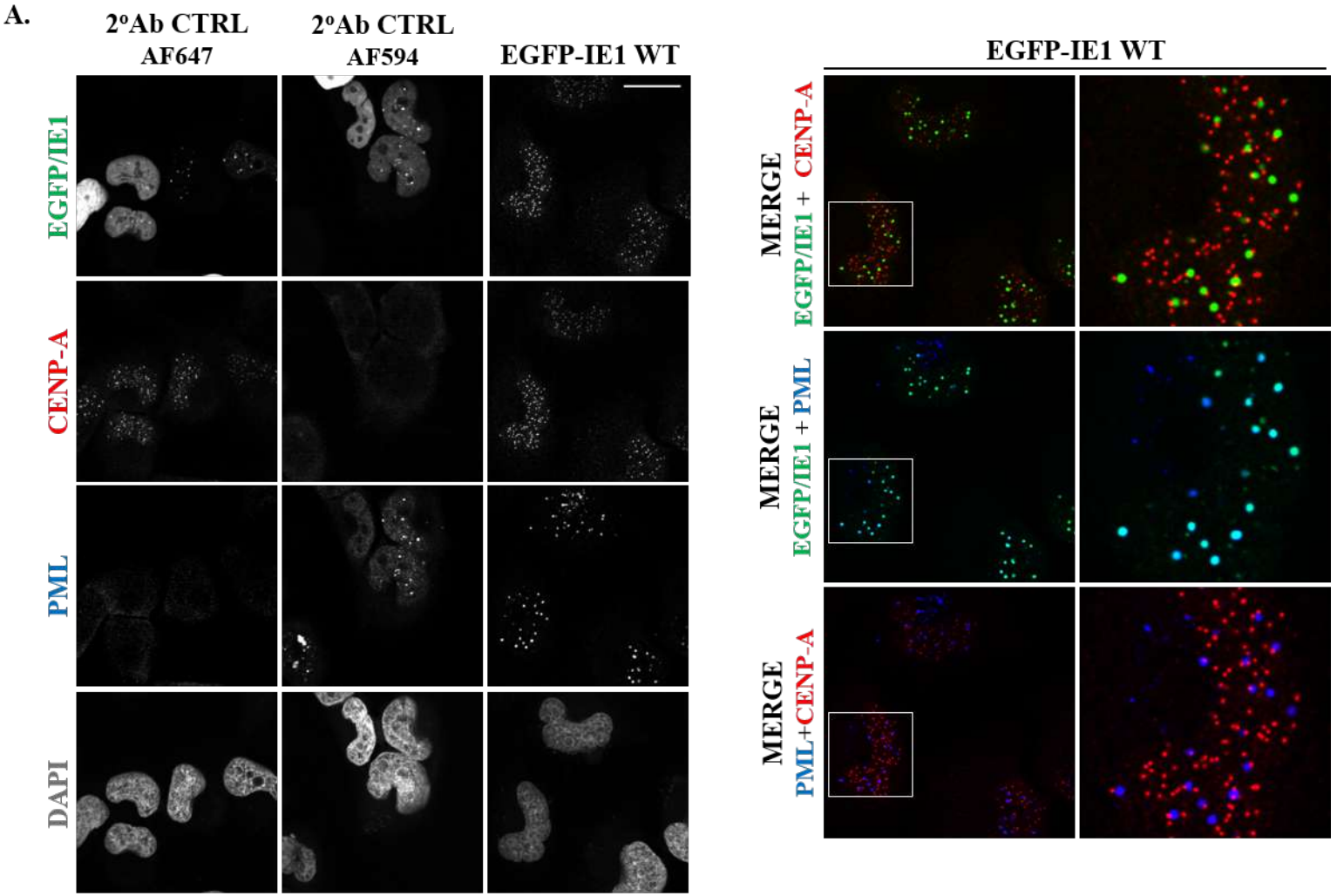
A.
2°Ab CTRL AF647
2°Ab CTRL AF594
EGFP-IE1 WT
EGFP/IE1
CENP-A
PML
DAPI
EGFP-IE1 WT
MERGE EGFP/IE1 + CENP-A
MERGE EGFP/IE1 + PML
MERGE PML+CENP-A

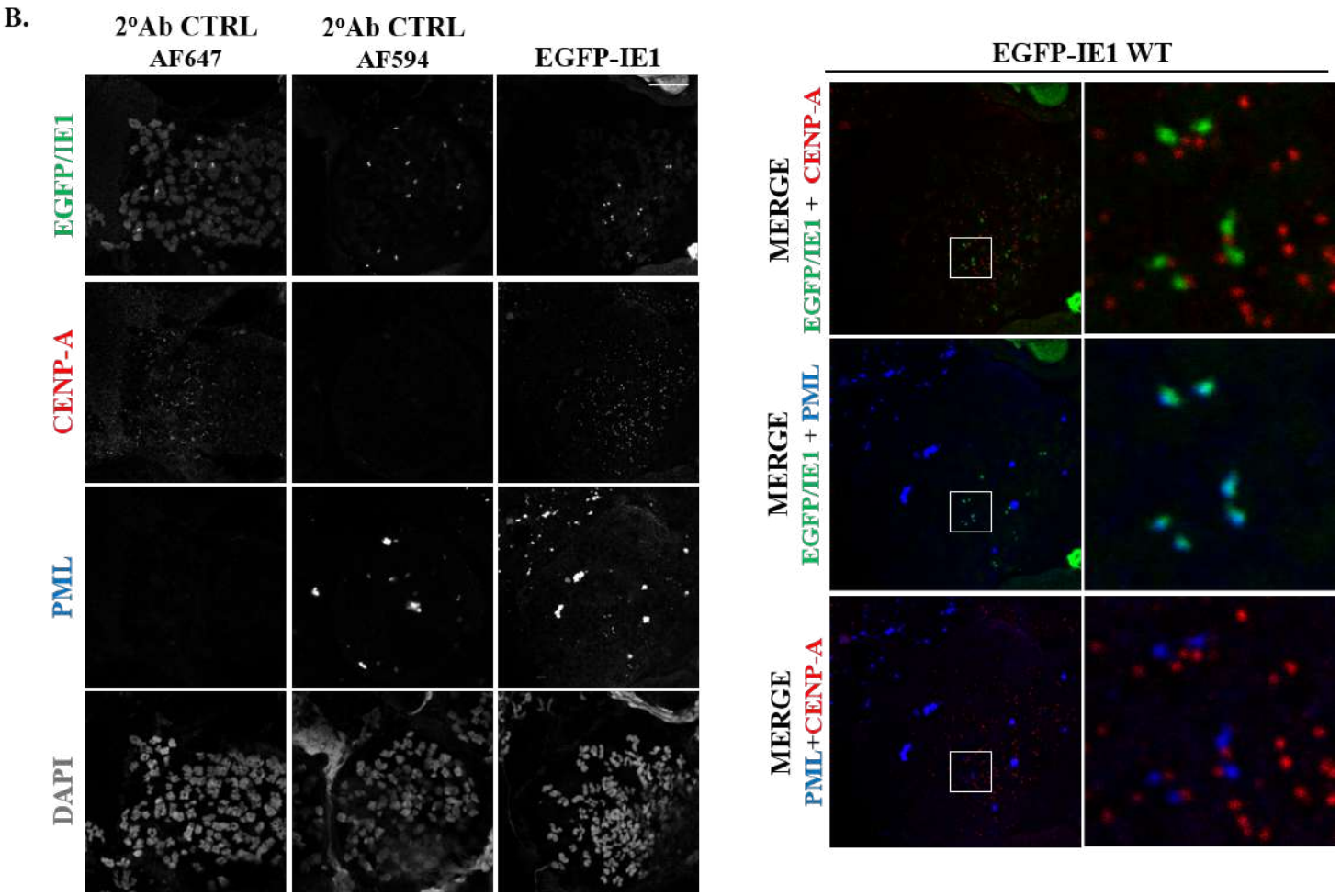

Figure II.7. PML colocalizes with IE1 CAS in the peri-centromeric regions of the chromatin. T98G cells transfected with EGFP-IE1 WT were fixed in interphase (A) or arrested in metaphase to perform chromosome spreads (B). The cells were fixed and stained with anti-CENP-A and anti-PML antibodies and AF594 and AF647 conjugated secondary antibodies respectively. Nuclei and chromosomes were stained with DAPI. The localization of the stained proteins was analyzed using 63x objective of Zeiss LSM800 confocal microscope. The scale bar represents 20µm (A) and 10µm (B). Merged images of EGFP-IE1 WT are presented in the right panel. Brightness and contrast were increased for better visualization.

antibody control samples (Fig. II.7A and II.7B). In conclusion, the IE1 protein co-localizes with PML in interphase and in mitosis and this co-localization is independent of the type of localization pattern represented by IE1 (diffuse vs spotty).

5.2.7 A novel domain independent of CTD is involved in IE1 CAS localization pattern

The IE1 chromatin tethering domain (CTD), and more specifically the nucleosome binding motif (NBM), was reported to be responsible for association of this protein with mitotic chromosomes [137, 138]. To test if the CTD is also involved in mediating the IE1 chromosome-associated spots localization pattern, I generated two IE1 mutants: M483A (one of the critical residues in the NBM) and the full NBM mutation (H481A, M483A, T485A, and R486A) [138]. Analysis of T98G cell lysates transfected with the IE1 M483A and NBM mutants showed that both could be expressed in T98G cells (Fig. II.8A). Expression was not observed in non-transfected (NT) and empty vector (EV) controls (Fig. II.8A). GAPDH was used as loading control.

In transfected T98G cells in the interphase I observed that both the M483A and NBM mutant localized to the nucleus in two localization patterns, diffuse and spotty, same as IE1 WT (Fig. II.8B). During mitosis, the M483A and NBM mutants did not paint chromosomes and localized off the chromosomes, as reported previously [138], in majority of the cells - 86% for M483A and 90% for NBM . However, IE1 CAS could still be observed for both of the mutants - 14% for M483A and 10% for NBM mutant (Fig. II.8C and II.8D). This suggests that a **novel domain independent of CTD is involved in CAS localization pattern**. No signal was observed in the secondary antibody control sample (Fig. II.8B and II.8C). Nuclear diffuse and spotty localization was observed for IE1 WT during interphase (Fig. II.8B), while painting and CAS localization patterns were observed during mitosis (Fig. II.8C).

5.2.8 Identification of a novel chromatin association domain of IE1

To identify the region of IE1 involved in CAS formation a series of c-myc- and EGFP-tagged IE1 constructs were generated including: individual domains i.e. the core domain (CD), acidic domain (AD), and the chromatin tethering domain (CTD), a fusion of AD and CTD (AD+CTD) and IE1 lacking exon 2 and exon 3 regions (IE1_ Δexon2+3) as well as construct lacking the N-terminal domain (IE1_ΔNTD) (Fig. II.9A). Analysis of T98G cell lysates transfected with the above mentioned constructs, showed that among the EGFP-tagged constructs, the CD, AD,

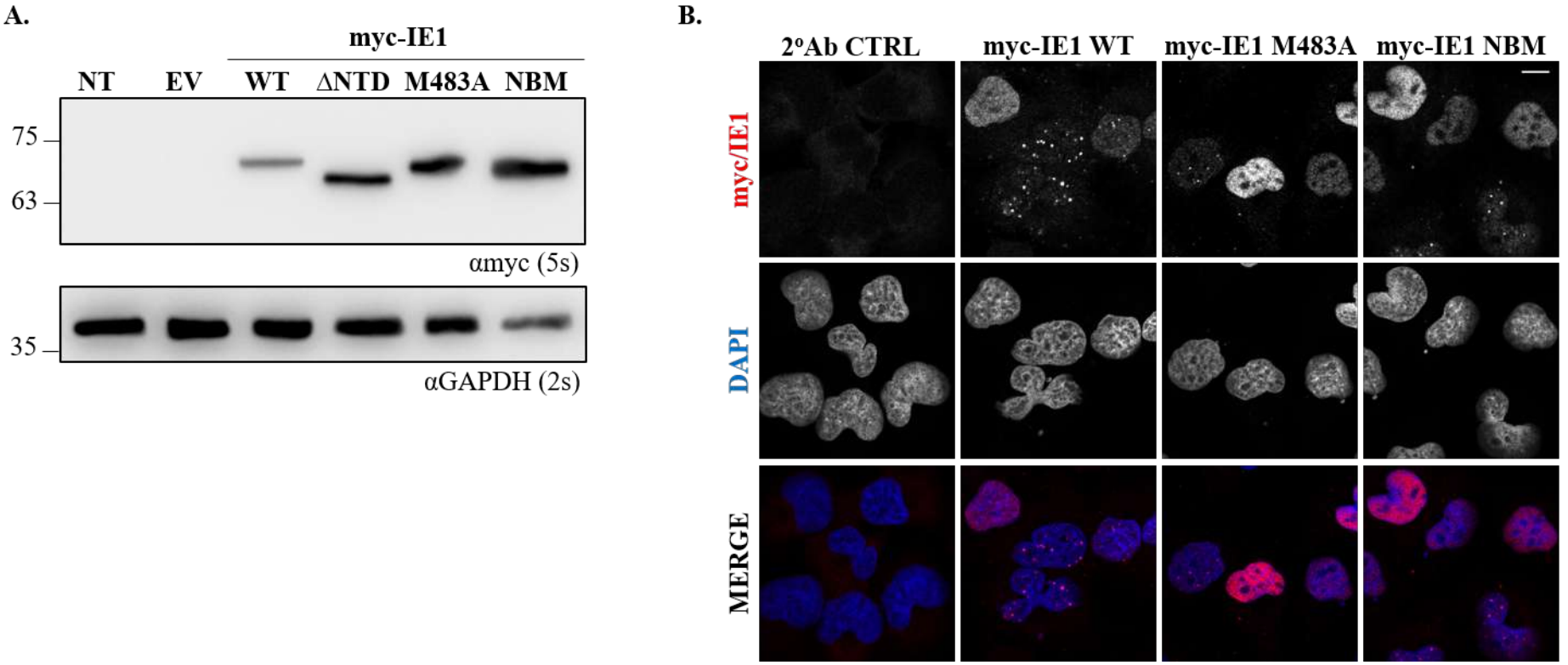
A.
myc-IE1
NT
EV
WT
ΔNTD
M483A
NBM
75
63
αmyc (5s)
35
αGAPDH (2s)
B.
2ºAb CTRL
myc-IE1 WT
myc-IE1 M483A
myc-IE1 NBM
myc/IE1
DAPI
MERGE

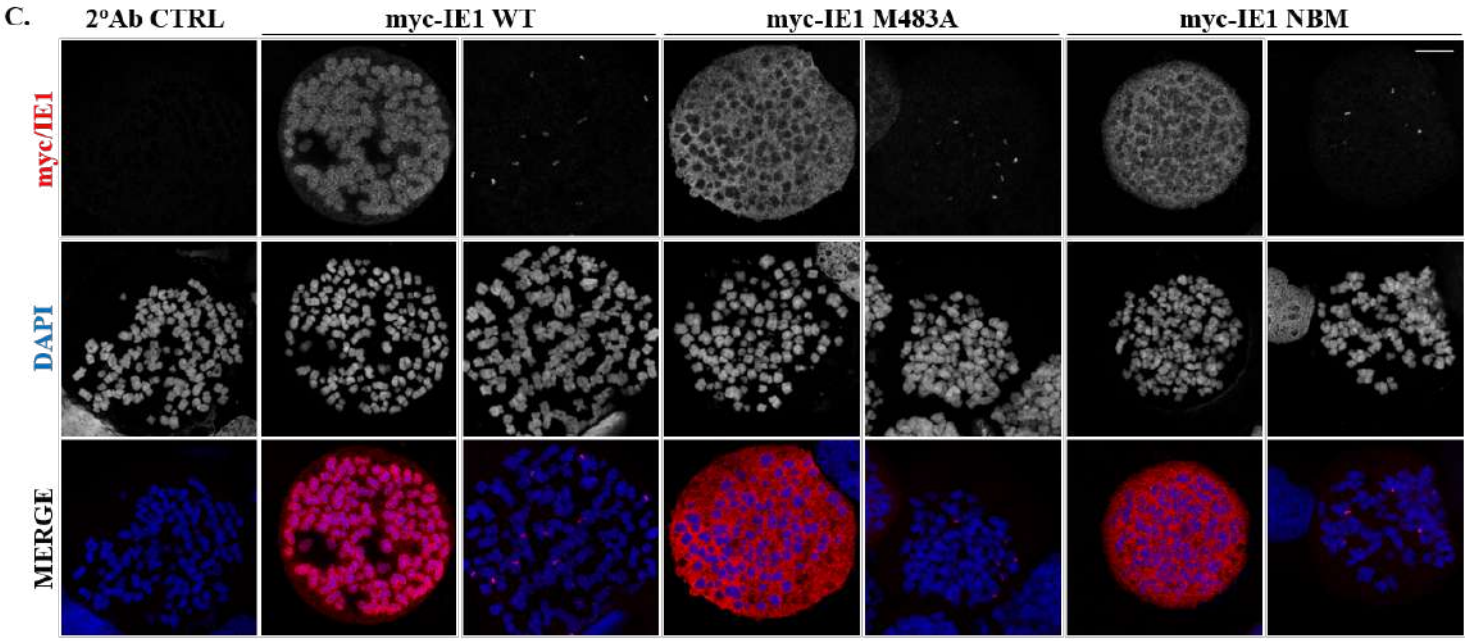

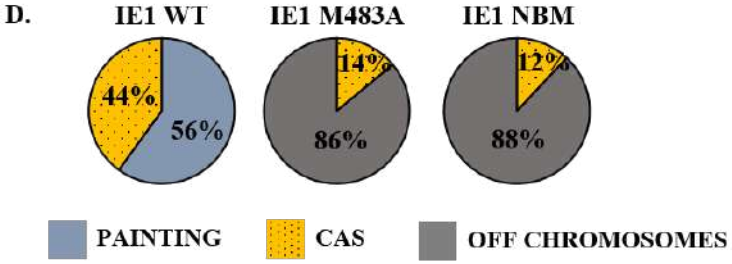

	PAINTING	CAS	OFF CHROMOSOMES
IE1 WT	56% (+/-4)	44% (+/-3)	0% (+/-0)
IE1 M483A	0% (+/-0)	14% (+/-2)	86% (+/-2)
IE1 NBM	0% (+/-0)	12% (+/-2)	88% (+/-2)

Figure II.8. A novel domain independent of CTD is involved in IE1 CAS localization pattern. T98G cells transfected with myc-tagged IE1 WT, M483A or NBM mutants were analyzed for expression by immunoblotting with anti-myc antibody and GAPDH was used as loading control (A). Antibodies used to detect the proteins are indicated below the blot, the exposure time is indicated in the brackets. Localization during interphase (B) and mitosis (C) was analyzed by staining with anti-myc antibody and AF594 conjugated secondary antibody. Chromosomes were stained with DAPI. The localization of the stained proteins was analyzed using 63x objective of Zeiss LSM800 confocal microscope. The scale bar represents 10µm. Brightness and contrast were increased for better visualization. Quantification of IE1 spots and painting phenotype (D). Percentages represent the average from three individual experiments and SEM is indicated in the table in brackets.

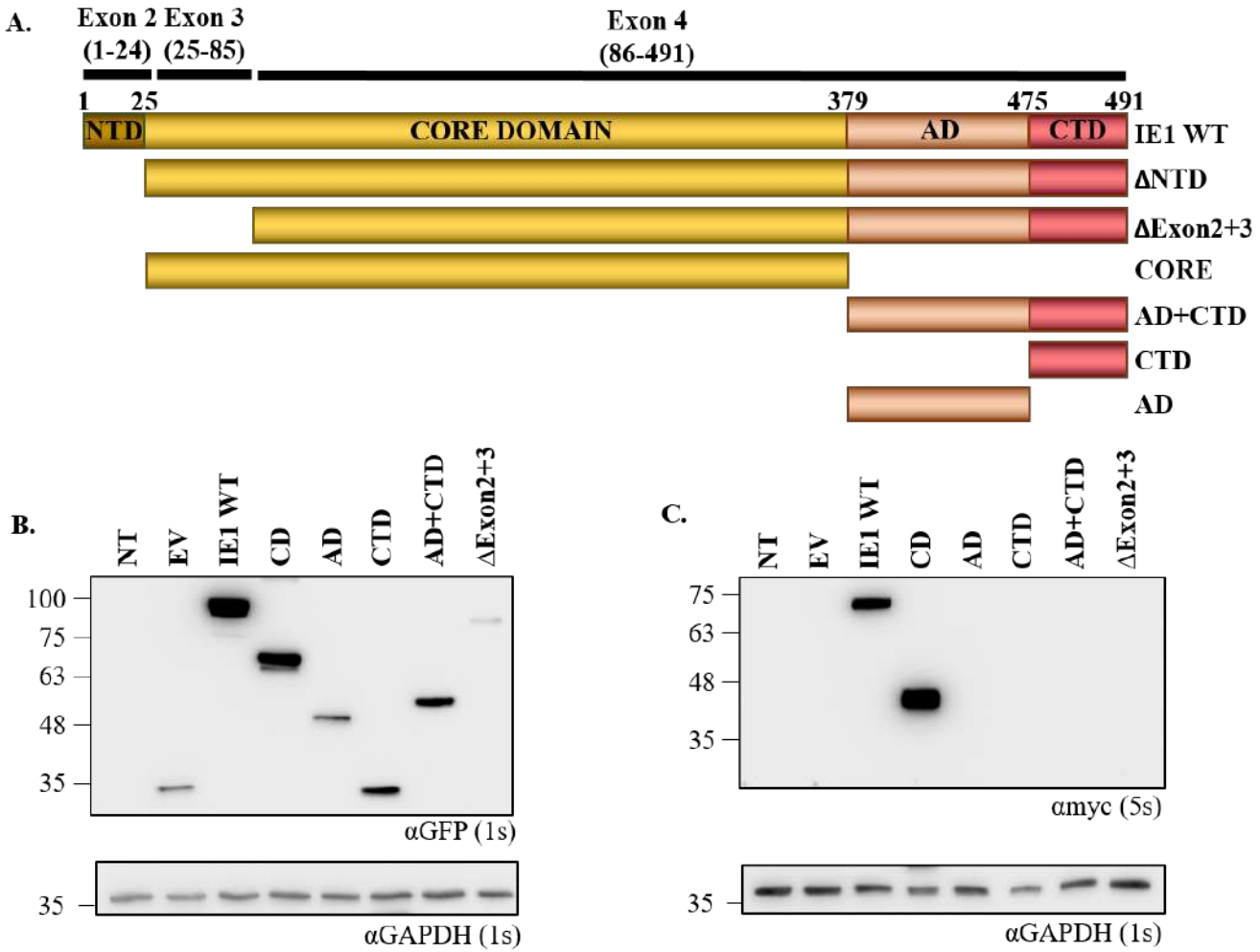

Figure II.9. Deletion mutants of IE1 are expressed in transfected T98G cells. Schematic of HCMV IE1 protein domains and deletion mutants of IE1 cloned (A). T98G cells transfected with myc/EGFP-tagged IE1 were harvested, and expression was analyzed by immunoblotting with anti-GFP antibody (B) and anti-myc antibody (C). GAPDH was used as loading control. Antibodies used to detect the proteins are indicated below the blot, the exposure time is indicated in the brackets. NT – non transfected, EV – empty vector, CD – core domain, AD – acidic domain, CTD – chromatin tethering domain

AD+CTD, and IE1_ Δexon2+3 could be expressed, whereas the CTD could not be detected (Fig. II.9B). In the case of myc-tagged constructs, only the CD could be expressed whereas, the AD, CTD, AD+CTD and IE1_ Δexon2+3 could not be detected (Fig. II.9C). Expression was not observed in non-transfected (NT) and empty vector (EV) controls (Fig. II.9B and II.9C). GAPDH was used as loading control. Although the AD, CTD, AD+CTD, and IE1_ Δexon2+3 myc-tagged constructs were not detected by western blot, a few cells were found to be positive by IFA (II.10B). This is probably due to IFA being a more sensitive method.

Analyzing the distribution of the transfected EGFP-tagged constructs in interphase T98G cells I observed that HCMV IE1 EGFP-tagged constructs of CD localized to the nucleus as spots, AD and AD+CTD localized to the nucleus and cytoplasm, CTD localized to the nucleus in a diffuse manner and IE1_ Δexon2+3 was found exclusively in the cytoplasm as observed with the myc-tagged constructs (Fig. II.10A). Since myc-tagged IE1_ Δexon2+3 was not expressed and high toxicity was observed with EGFP-tagged IE1_ Δexon2+3, these constructs were not used in further experiments. I observed that the localization patterns of the myc-tagged constructs were consistent with the above results of experiments with EGFP-tagged vectors (Fig. II.10B).

During **mitosis**, EGFP-**CD** was found to localize as **spots** on mitotic chromosomes (100%), EGFP-IE1-**AD** localized in an **off-chromosomes** pattern (100%), and EGFP-IE1-**AD+CTD** was found to **paint** the chromosomes (100%) (Fig. II.11A). No signal could be detected with the EGFP-tagged CTD. Myc-IE1_ΔNTD localized in three distinct patterns during mitosis: painting (72%), CAS (22%), and off-chromosomes (6%) (Fig. II.11C, D). Myc-IE1-CD was also found to localize as spots on mitotic chromosomes, confirming the results obtained with EGFP-IE1-CD construct (Fig. II.11C). No signal could be detected with myc-tagged AD, CTD, and AD+CTD constructs. No signal was observed in the secondary antibody control sample (Fig. II.11B and II.11C).

5.2.9 Clustered charge mutations in the core domain of HCMV IE1 do not disrupt IE1 CAS formation

I have identified the core domain of IE1 as responsible and sufficient for IE1 CAS localization pattern (Fig. II.12A and II.12C). To identify specific residues in the core domain that are responsible for IE1 CAS formation, I cloned a set of **clustered charge (cc) mutants** of the core domain that have been previously reported to be stable and not disrupt the structure of IE1 [130]. I observed that all the clustered charge mutants tested localized to mitotic chromosomes

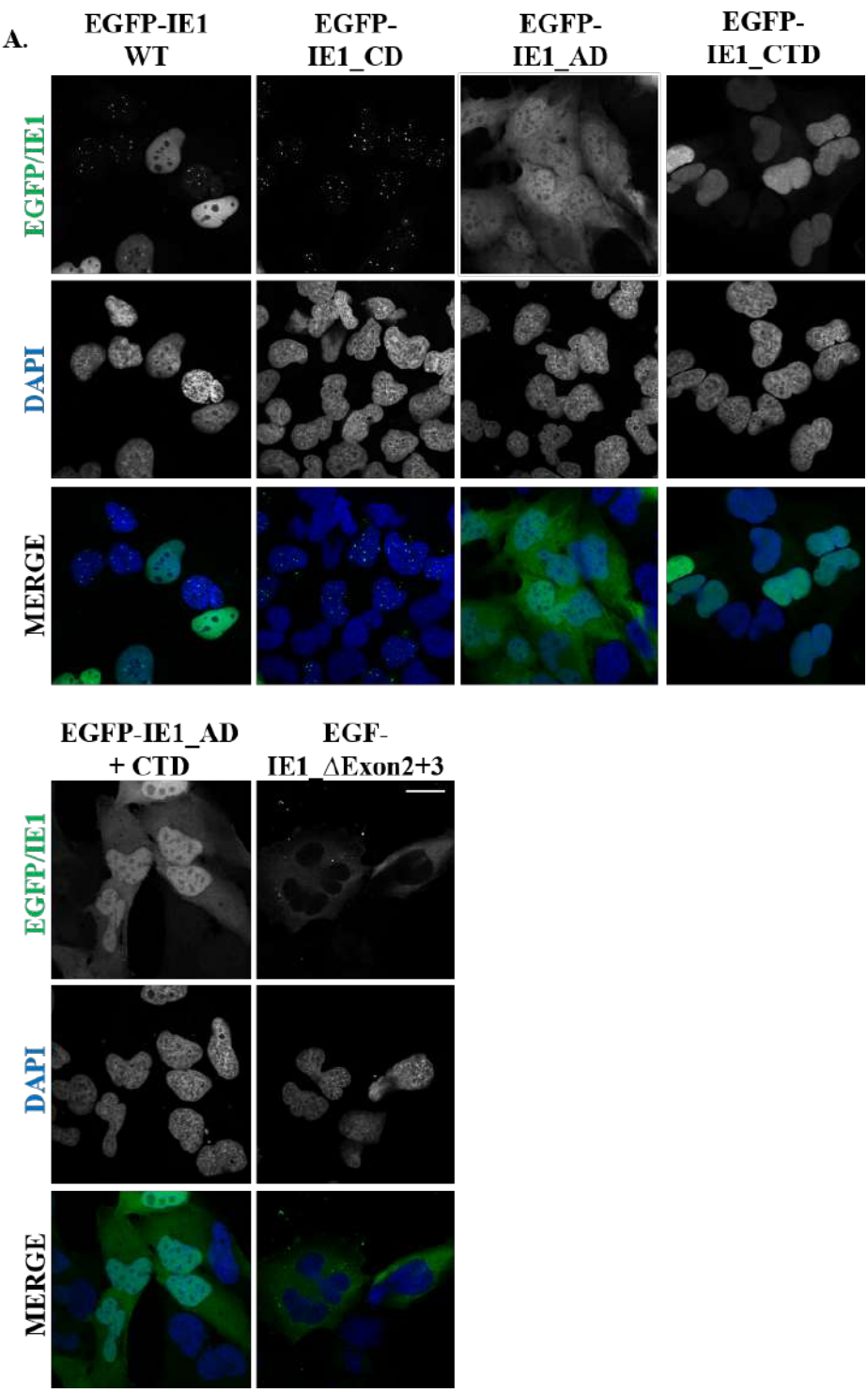
A.
EGFP-IE1 WT
EGFP-IE1_CD
EGFP-IE1_AD
EGFP-IE1_CTD
EGFP/IE1
DAPI
MERGE
EGFP-IE1_AD + CTD
EGF-IE1_ΔExon2+3
EGFP/IE1
DAPI
MERGE

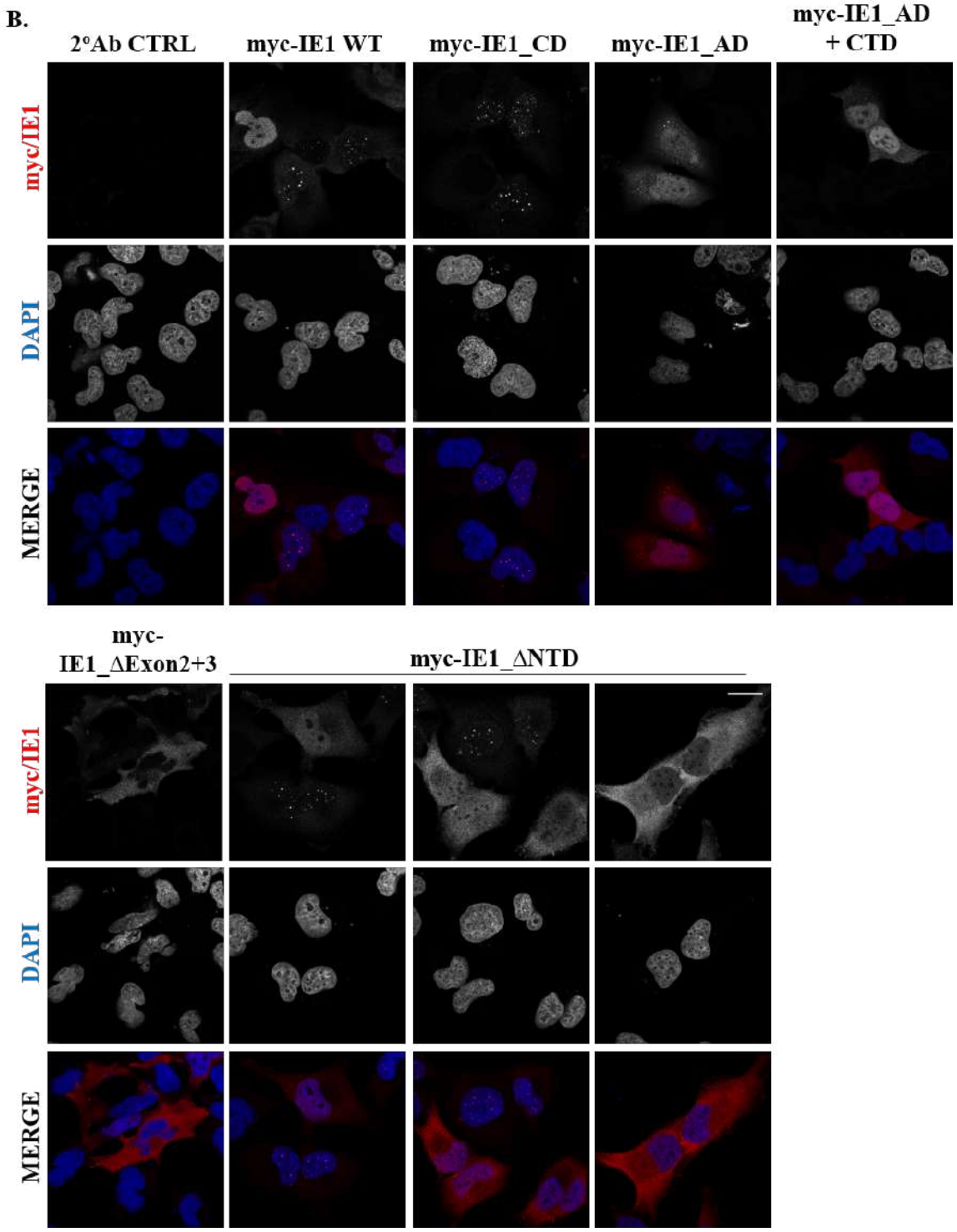

Figure II.10. Localization of deletion mutants of IE1 during interphase in T98G cells. T98G cells transfected with myc/GFP-tagged IE1 WT, core domain (CD), acidic domain (AD), chromatin tethering domain (CTD), a fusion of AD and CTD (AD + CTD), IE1 ΔExon2+3, and IE1_ΔNTD were just stained with DAPI (for EGFP-tagged constructs) (A) or fixed and stained with anti-myc antibody (for myc-tagged constructs) and AF594 secondary antibody (B). The localization of the stained proteins was analyzed using 63x objective of Zeiss LSM800 confocal microscope. The scale bar represents 20µm. Brightness and contrast were increased for better visualization.

A.

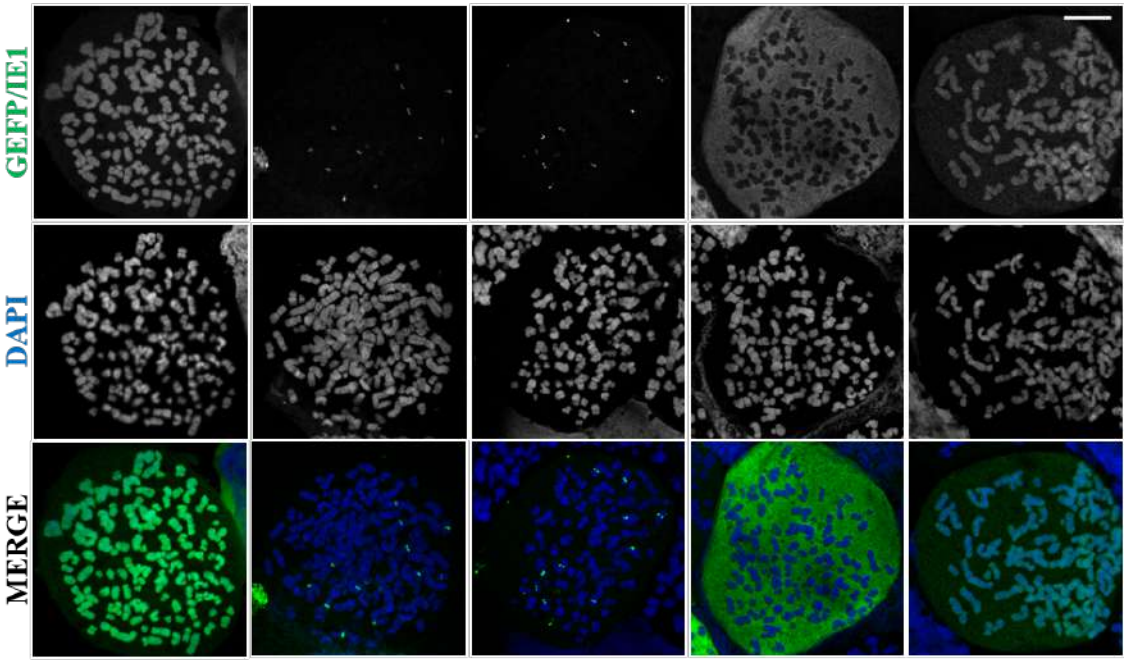

B.

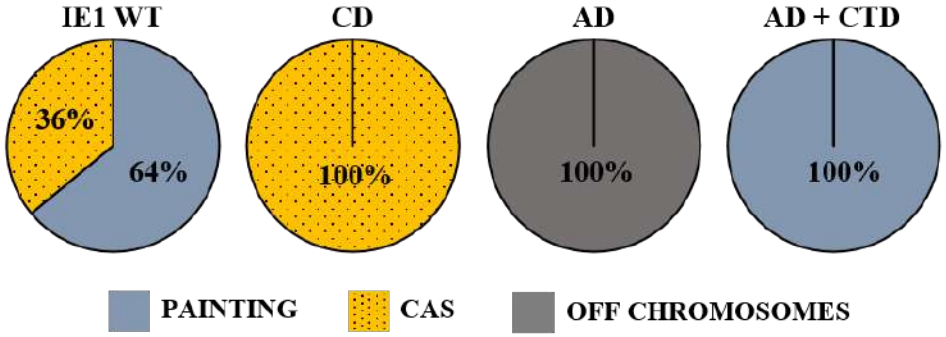

EGFP-IE1	PAINTING	CAS	OFF CHROMOSOMES
WT	61% (+/- 2)	39% (+/- 2)	0% (+/- 0)
CD	0% (+/- 0)	100% (+/- 0)	0% (+/- 0)
AD	0% (+/- 0)	0% (+/- 0)	100% (+/- 0)
AD+CTD	100% (+/- 0)	0% (+/- 0)	0% (+/- 0)

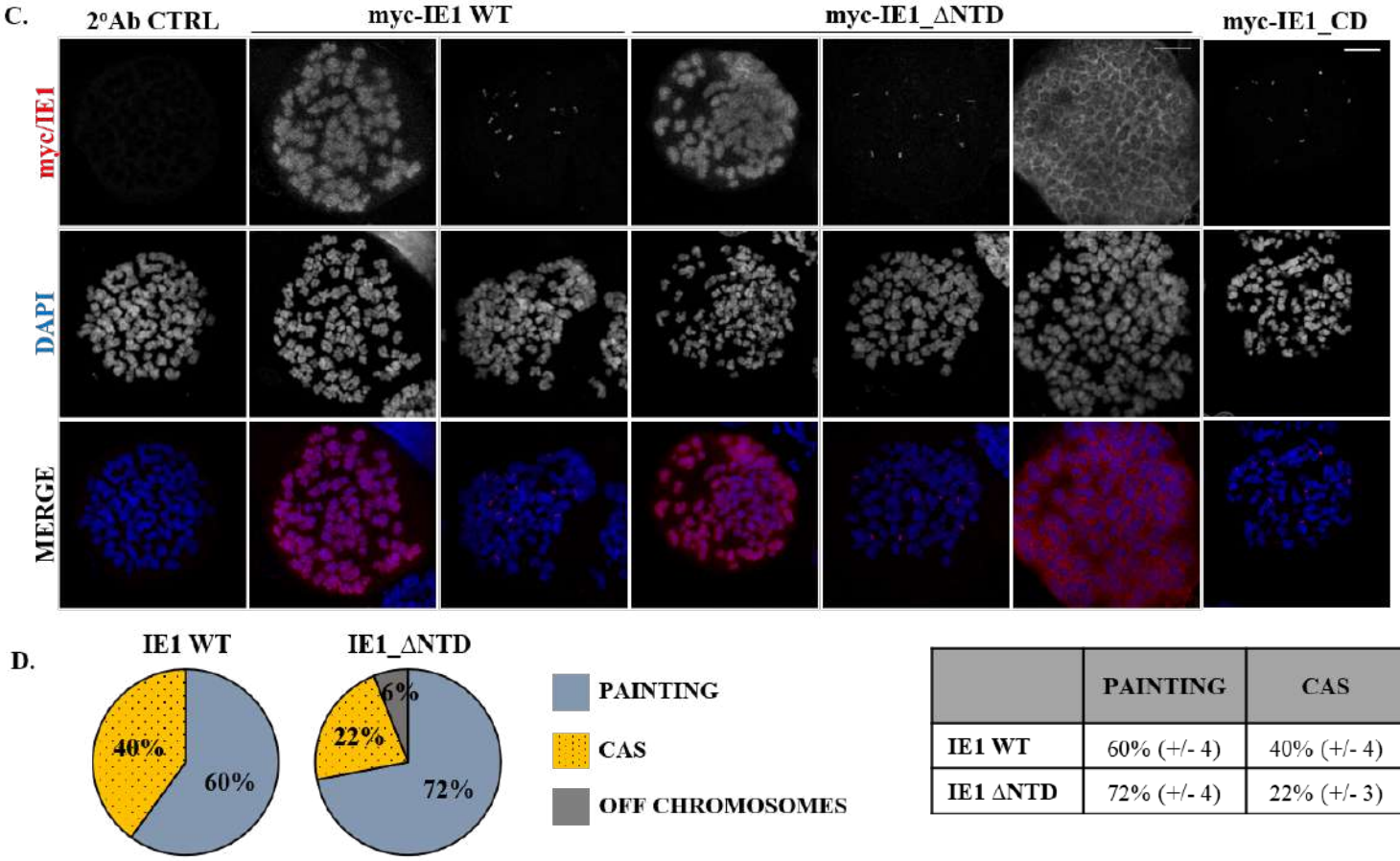

	PAINTING	CAS	OFF CHROMOSOMES
IE1 WT	60% (+/- 4)	40% (+/- 4)	0% (+/- 0)
IE1 ΔNTD	72% (+/- 4)	22% (+/- 3)	6 % (+/- 1)

Figure II.11. Core domain is the novel chromatin association domain of IE1. T98G cells transfected with myc/EGFP-tagged IE1 WT, core domain (CD), acidic domain (AD), chromatin tethering domain (CTD), a fusion of AD and CTD (AD + CTD), and IE1_ΔNTD were arrested in metaphase to perform chromosome spreads. The cells were fixed and stained with DAPI (for EGFP-tagged constructs) (A) or stained with anti-myc antibody (for myc-tagged constructs) and AF594 conjugated secondary antibody (C and E). The localization of the stained proteins was analyzed using 63x objective of Zeiss LSM800 confocal microscope. The scale bar represents 10µm. Brightness and contrast were increased for better visualization. Quantification of spots and painting phenotype for EGFP-tagged constructs (B) and myc-tagged constructs (D). Percentages represent the average from three independent experiments and SEM is indicated in the table in the brackets.

in both painting and CAS patterns (Fig. II.12 – middle and lower panels). Hence, I was unable to identify residues that are responsible for CAS localization pattern. This suggests that residues 41-43, 78-80, 196-199, 210-217, 244-245, 326-328, 332-334, and 359-362 of the core domain are not involved in IE1 CAS formation. No signal was observed in the secondary antibody control sample (Fig. II.12 – upper panel). EGFP protein, used as a control, localized in an off chromosomes pattern (Fig. II.12 – upper panel).

5.2.10 HCMV IE1 protein expression level influences its localization pattern

Since, the painting and CAS localization patterns of IE1 were observed in the same population of cells, in one phase of the cell cycle i.e., metaphase, one of the possible explanations of this phenomenon could be different levels of protein expression in the cells determining the localization. To test this hypothesis, I transfected T98G cells with increasing amounts of myc-IE1 plasmid and quantified the localization patterns in metaphase and correlated it with the IE1 protein expression levels estimated by densitometric analysis of western blot (Fig. II.13A-D). I observed that when IE1 protein level was low, IE1 CAS was the dominant localization pattern (75%) and when IE1 protein level was high, IE1 chromosome painting was the dominant localization pattern (72%) (Fig. II.13A-D). To understand the correlation between with IE1 CAS localization pattern and the level of IE1 expression, I plotted percentage of cells with IE1 CAS localization pattern with the level of IE1 expression determined by densitometric analysis of IE1 western blot signal determined by densitometric analysis of IE1 western blot signal in samples transfected with decreasing concentrations of myc-IE1 plasmid. I observed a negative correlation (Pearson coefficient r = -0.858) between percentage of cells with IE1 CAS localization pattern and the level of IE1 expression. This suggests that the fraction of cells presenting IE1 CAS localization pattern is inversely proportional to IE1 protein expression levels in these cells. I also observed that the biggest change in percentage of cells with IE1 CAS pattern was detected between 1.0 μg (34%) and 0.5 μg (69%) (Fig II.13B). This suggests that in T98G cells there is a threshold for the switch from IE1 chromosome painting pattern to IE1 CAS and it lies between 1.0 μg and 0.5 μg of transfected myc-IE1 plasmid. IE1 was not detected in non-transfected (NT) and empty vector (EV) controls (Fig II.13C). GAPDH was used as loading control. This suggested that IE1 protein level influences its localization pattern.

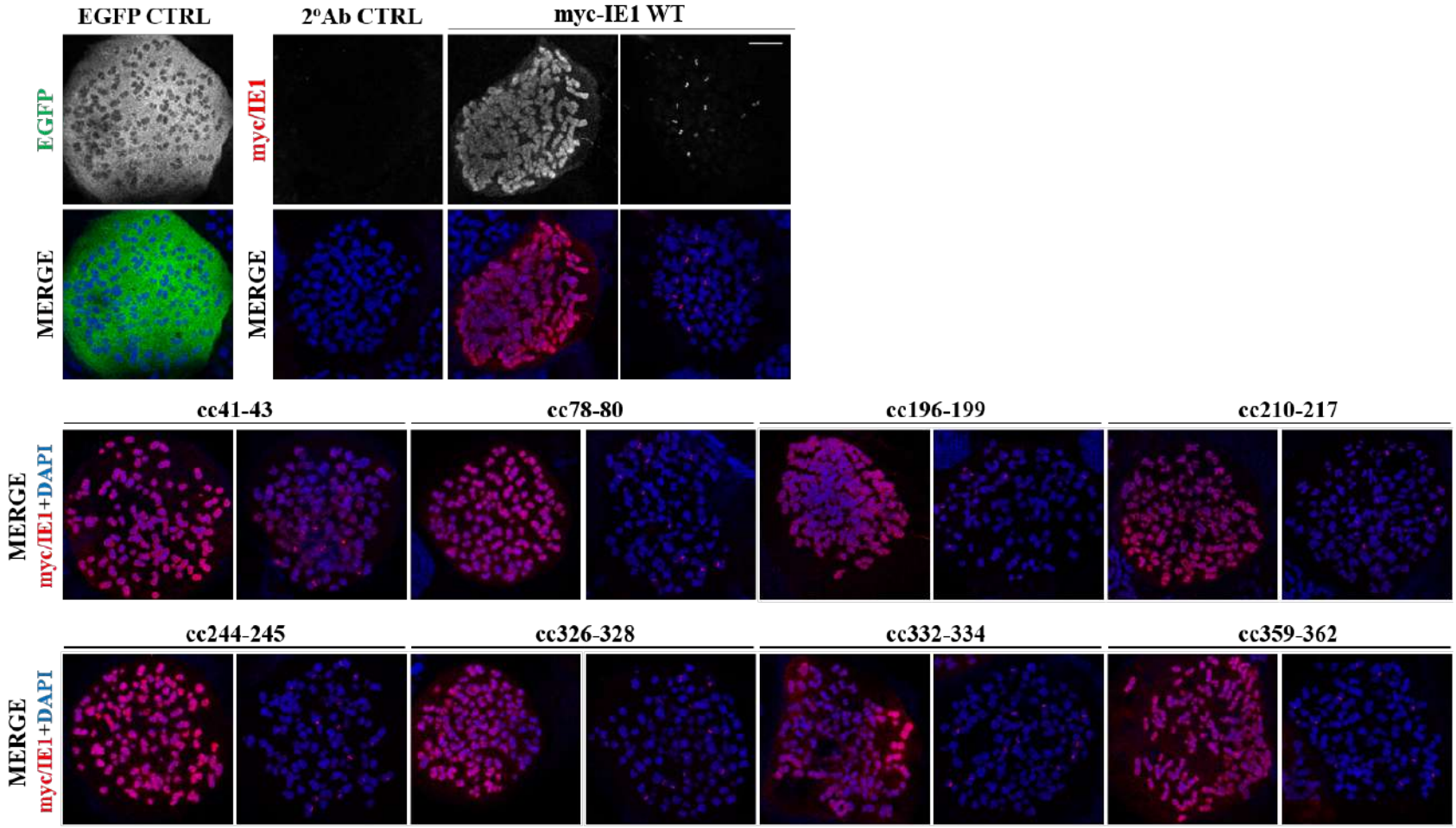

Figure II.12. Clustered charge mutations in the core domain of IE1 do not affect IE1 CAS formation. T98G cells transfected with myc-tagged clustered charge (cc) mutants of IE1 were arrested in metaphase to perform chromosome spreads. The cells were fixed and stained with anti-myc antibody and AF594 conjugated secondary antibody. Chromosomes were stained with DAPI. The localization of the stained proteins was analyzed using 63x objective of Zeiss LSM800 confocal microscope. The scale bar represents 10µm. Localization of myc-IE1 WT (upper panel), cc41-43, cc78-80, cc196-199, and cc210-217 (middle panel), and cc244-245, 326-328, cc332-334, and cc359-362 (bottom panel). Brightness and contrast were increased for better visualization.

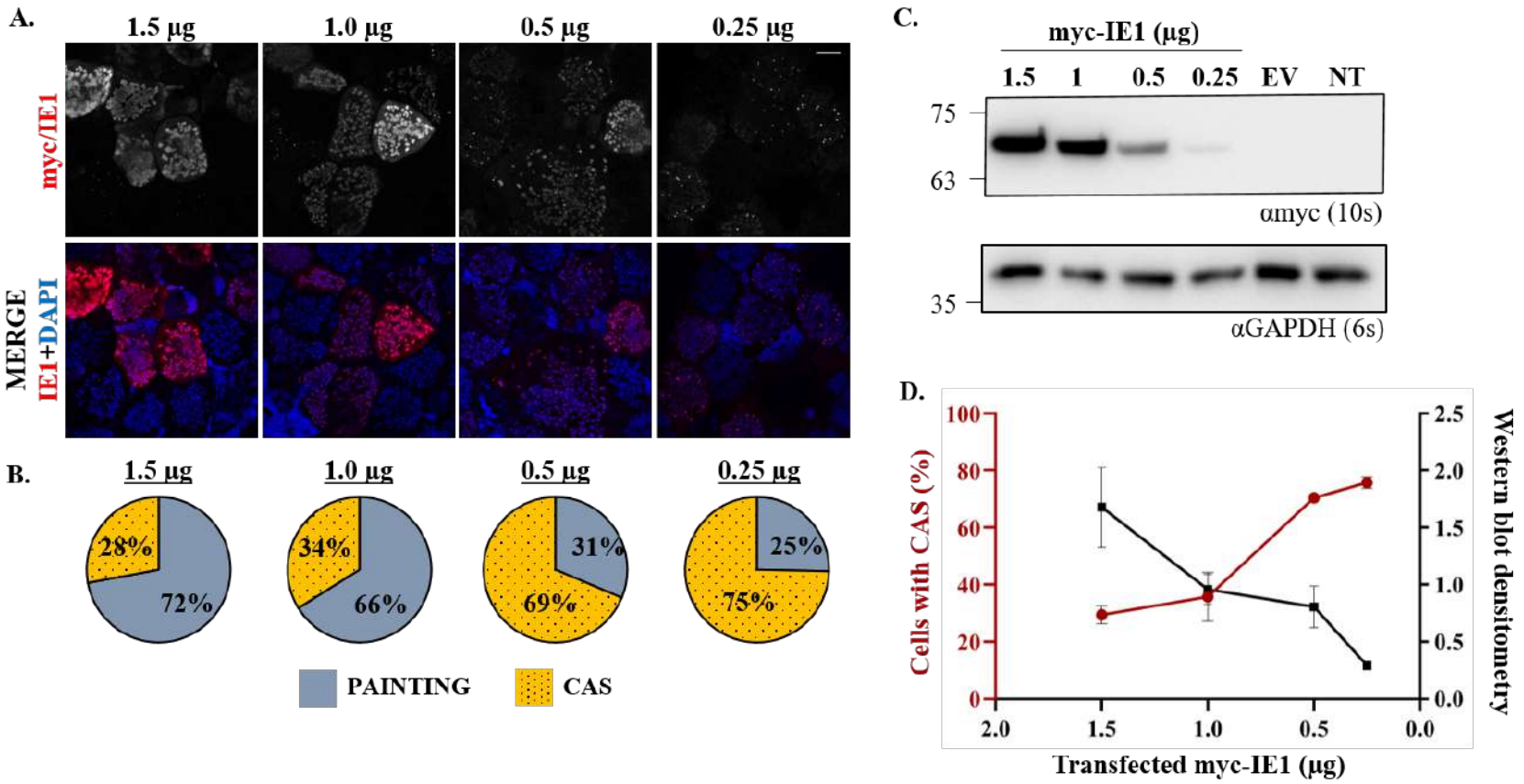

Figure II.13. IE1 protein expression level influences its localization pattern in transfected cells. T98G cells transfected with myc-IE1 WT were arrested in metaphase to perform chromosome spreads or harvested for immunoblotting. The cells were fixed and stained with anti-myc antibody and AF594 conjugated secondary antibody. Chromosomes were stained with DAPI. The localization of the stained proteins was analyzed using 40x objective of Zeiss LSM800 confocal microscope. The scale bar represents 20µm. myc-IE1 WT transfected at decreasing concentrations (A) and quantification of myc-IE1 painting and CAS localization patterns at the respective concentration (B). Percentages represent the average from three independent experiments. Brightness and contrast were increased for better visualization. Expression of myc-IE1 analyzed by immunoblotting (C). GAPDH was used as loading control. Antibodies used to detect the proteins are indicated below the blot, the exposure time is indicated in the brackets. EV- empty vector, NT- non transfected. Plots of myc-IE1 protein levels as analyzed by immunoblotting vs percentage of cells with CAS localization pattern with decreasing concentrations of transfected myc-IE1 (D).

5.2.11 HCMV IE1 localization pattern on mitotic chromosomes changes dynamically upon latency establishment in T98G cells

As the next step I wanted to start addressing the function of the two localization patterns during viral infection. It is well established that IE1 protein expression level is very high in the lytic cycle and that this expression drops significantly upon latency establishment and remains on low level in latency [87, 88, 93, 94, 265, 267]. I have, therefore analyzed the ratio of the IE1 chromosome painting and CAS localization patterns in mitosis as infection progressed from lytic to latent phase in T98G cells. I observed that at 1 dpi, when the IE1 protein level was the highest, the chromosome painting was the dominant localization pattern (89%). On the contrary, at 14 dpi when IE1 protein level was the lowest (undetectable by immunoblotting, but positive cells could be detected by immunofluorescence), IE1 CAS was the dominant localization pattern (84%) (Fig. II.14A-D). No specific signal was observed in the respective uninfected control sample (Fig. II.14C). To understand the correlation between with IE1 CAS localization pattern and the level of IE1 expression, I plotted percentage of cells with IE1 CAS localization pattern with the level of IE1 expression determined by densitometric analysis of IE1 western blot signal determined by densitometric analysis of IE1 western blot signal at different timepoints post infection. I observed a negative correlation (Spearman coefficient r = -1) was observed between percentage of cells with IE1 CAS localization pattern and IE1 expression level.. This suggests that the fraction of cells with IE1 CAS localization pattern in mitosis is inversely proportional to IE1 protein expression levels in these cells at different times post infection, similar to my observations in the transfection setting.

Moreover, I observed that percentage of cells with the IE1 CAS localization pattern increased as the latency establishment was taking place (with the increasing time post infection) (Fig. II.14A and II.14B) and this correlated with decrease in IE1 protein expression levels as infection progressed (Fig. II.14C). The percentage of cells with IE1 CAS localization correlated positively (Spearman coefficient r = -1) with the time post infection. I also observed that the biggest change in percentage of cells with IE1 CAS localization was detected between 4 dpi (24%) and 7 dpi (61%) (Fig II.14B), which taking into account the length of HCMV replication cycle in T98G cells (6-7 days) possibly correlates with the drop in lytic replication and transition to latency. In this situation changing ratio between the two populations of cells with the distinct IE1 localization patterns might suggest that they are important for different parts of viral life cycle (latent vs lytic).

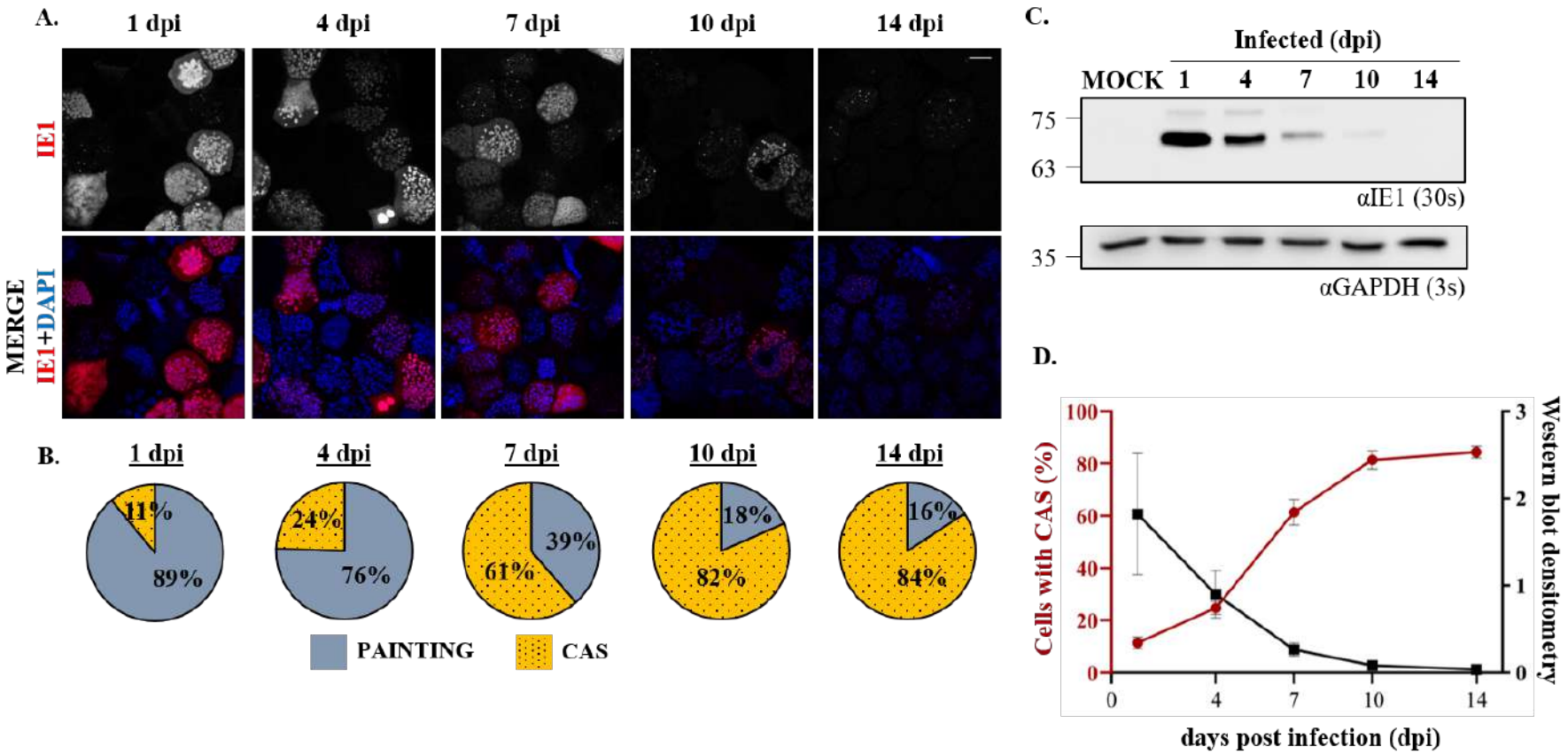

Figure II.14. IE1 localization pattern changes dynamically upon latency establishment. Infected or mock infected T98G cells were arrested in metaphase to perform chromosome spreads or harvested for immunoblotting on 1, 4, 7, 10, and 14 days postinfection (dpi). Chromosome spreads were stained with anti-IE1 and AF594 conjugated secondary antibody. Chromosomes were stained with DAPI. The localization of the stained proteins was analyzed using 40x objective of Zeiss LSM800 confocal microscope. The scale bar represents 20µm. Staining of IE1 WT in infected cells at indicated dpi (A) and quantification of IE1 painting and CAS localization patterns in infected cells at indicated dpi (B). Percentages represent the average from three independent experiments. Brightness and contrast were increased for better visualization. Expression of IE1 analyzed by immunoblotting (C). GAPDH was used as loading control. Antibodies used to detect the proteins are indicated below the blot, the exposure time is indicated in the brackets. EV- empty vector, NT- non transfected. Plots of IE1 protein levels as analyzed by immunoblotting vs percentage of cells with CAS localization pattern at various concentrations (D).

5.2.12 HCMV IE1 CAS localization is maintained during cell division

As we observed the IE1 CAS localization pattern during mitosis, I wanted to understand what happens to these spots during cell division i.e., if the spots would also be present or become diffuse after the cell divides. To test this, I performed time-lapse confocal imaging of T98G cells transfected with EGFP-IE1. I observed that cells that have CAS or painting localization pattern during mitosis appear to maintain the type of localization pattern (spotty or diffuse/painting) as the cell undergoes cell division and the daughter cells enter G0 phase of the cell cycle (Fig. II.15A and II.15B). This suggests that the switch from spotty pattern to painting and vice versa most probably does not occur during mitosis and occurs during interphase.

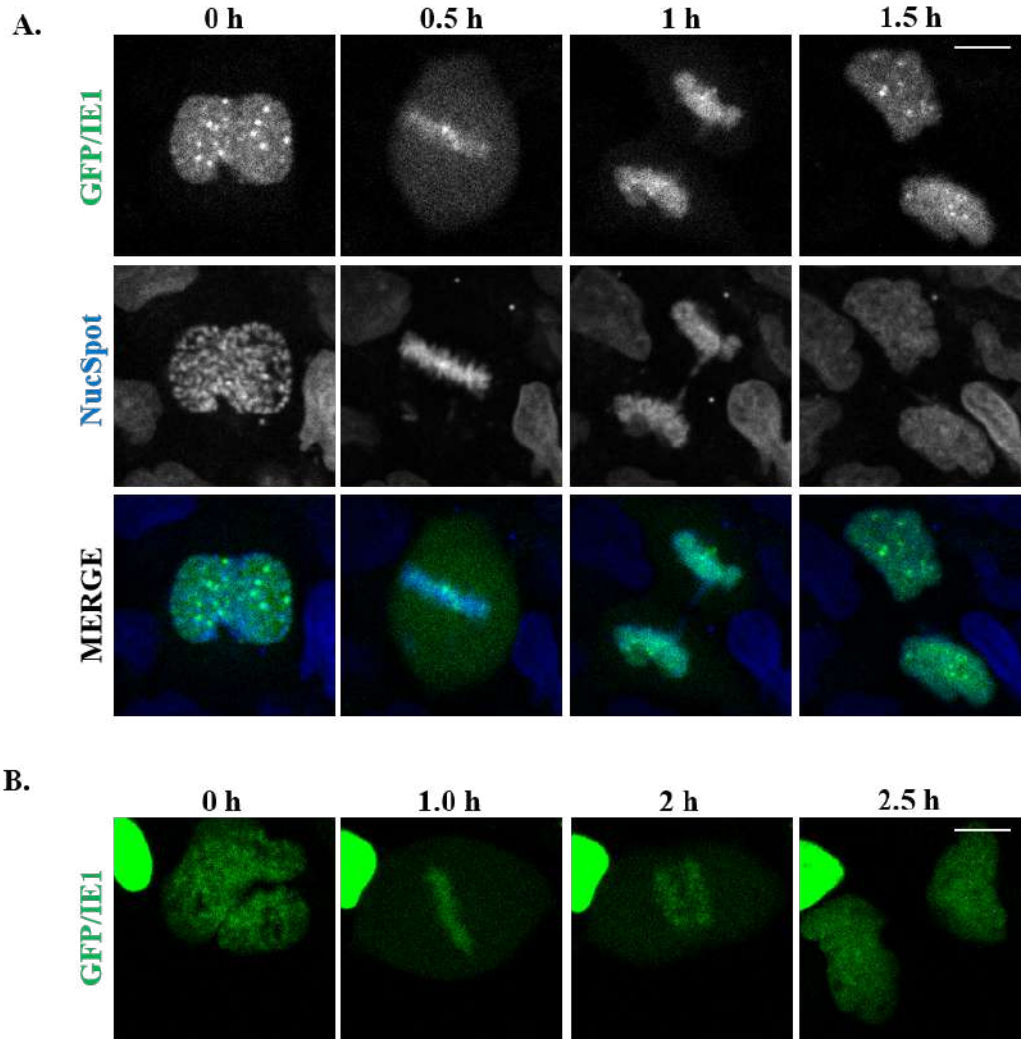

Figure II.15. Localization of IE1 CAS is maintained in the daughter cells after division. T98G cells transfected with EGFP-IE1 and time lapse images of mitotic cells with CAS (A) – treated with live DNA stain and painting (B) localization patterns were acquired every 30 min using 40x objective of Zeiss LSM800 confocal microscope. Some images have not been shown in the cell with painting pattern (B) as there was no change in the cell cycle stage of the cell. The scale bar represents 50µm. Brightness and contrast were increased for better visualization.

6. DISCUSSION

IE1x4, an isoform of HCMV IE1, reported to be expressed exclusively during latency, in the absence of IE1 full length expression, was proposed to be involved in the maintenance of the latent HCMV genome in CD34+ hematopoietic progenitor cells (HPC) [101]. IE1x4 was shown to bind the terminal repeat (TR) region of the HCMV genome, as well as host DNA-binding proteins Sp-1 and topoisomerase IIβ [101]. The authors suggested that IE1x4 may tether the HCMV genome to cellular chromatin in a manner similar to that of KSHV LANA and EBV EBNA1, gamma-herpesviral maintenance proteins [101]. In fact, there are some similarities between IE1x4 and LANA. The chromatin tethering domains (CTDs) of LANA and IE1 were both shown to mediate association of these proteins with histones – H2A and H2B and the CTD of LANA was shown to compete with the CTD of IE1 for binding to histones [138, 142]. Comparison of the structures of LANA and IE1 CTDs bound to nucleosomes showed that they occupy similar regions on the nucleosome [142]. Since IE1x4 isoform contains the CTD, same as IE1, it is possible that it could mediate genome tethering using a mechanism similar to LANA [101]. LANA is known to paint mitotic chromosomes in transfected cells. However, LANA localization pattern changes to spots in transfected cells in the presence of the KSHV latent origin to which it binds. LANA is also present in spots in infected cells, where the viral genome, and within it the latent ori with LANA binding sites, is naturally present [171, 173, 175, 249]. The relocalization from painting chromosomes to spots in the presence of the viral genome can also be observed for EBNA1 of EBV [146, 154-156]. Following from that I hypothesized that if IE1x4 was to mediate genome tethering in a manner analogous to LANA and EBNA1, it would need to localize to chromosomes in mitosis, which has not been shown so far and this localization pattern would be predicted to change in the presence of the HCMV TR region – the presumed latent ori of replication for HCMV.

My results show for the first time that IE1x4 localizes to mitotic chromosomes in both HeLa and T98G cells (Fig. I.3A-C), which would be consistent with its possible role as a maintenance protein of HCMV. A previous study reported that ectopically expressed IE1x4 did not localize to mitotic chromosomes however, an N-terminally tagged IE1x4 was used in this case [208]. I have observed that N-terminally tagged constructs of IE1x4 do not perform reliably in experimental setting – present low expression levels, aberrant localization patterns, and their

expression is toxic to cells (Fig. I.1A, I.1B, and I.3). Additionally, increased expression of IE1x4 was observed upon inhibition of the proteasome, suggesting degradation of the protein, which could be responsible for the low expression level of this construct in the absence of MG132 (Fig. I.1A, I.1B). These observations suggest that N-terminal tagging of IE1x4 might disrupt its structure thereby leading to instability.

In my hands the localization pattern of IE1x4 did not change in the presence of the HCMV TR region in HeLa, MRC-5, and T98G cells during neither interphase nor mitosis (Fig. I.4 to I.7). Since I have tested cells of different permissivity to HCMV infection, including cells allowing latency establishment, I have checked two different fragments of HCMV genome containing TR region (latent ori) and I have examined different ratios of introduced constructs carrying TR and IE1x4 gene, I conclude that **IE1x4 most probably does not mediate genome tethering in a manner analogous to LANA**. I also failed to detect IE1x4 protein expression in latently infected T98G cells (Fig. I.8). Further, analysis of cell lysate from latently infected KASUMI-3 cells, a CD34+ cell line, also failed to detect the IE1x4 protein expression (Fig. I.13). Collectively, these results **do not support the role of IE1x4 as the maintenance protein of HCMV**. However, it is possible that IE1x4 may be involved in HCMV genome tethering only in CD34+ HPCs as reported [101]. I have checked for IE1x4 protein expression in latently infected T98G and CD34+ KASUMI-3 cells, both of which are tumor cell lines and may not be the correct model system for this type of analysis. It is also possible that contrary to what has been published the HCMV TR is not the maintenance element of this viral genome. It is also conceivable that, though it does not affect protein stability, the C-terminal tag added to IE1x4 interferes with some protein interactions required for genome tethering. Finally, it cannot be excluded that in the in vitro system used here i.e., transfecting IE1x4 and TR-containing plasmids we were missing some other, as yet unidentified viral component of the tethering complex. Further studies would be required to clarify more definitely whether IE1x4 plays a role in HCMV genome tethering to cellular chromatin.

Although, I did not observe expression of IE1x4 protein in latent T98G and KASUMI-3 cells, I was able to detect IE1 in both T98G (by IFA and qRT-PCR – Fig. I.8A and I.8D) and KASUMI-3 cells (by immunoblotting – Fig. I.9). Traditionally, IE1 expression, as an immediate early gene, was considered to be completely absent during latency due to repression of the MIEP. However, IE1 transcript was detected in latently infected cells as shown in some

studies [87, 88, 93, 94]. Long-term IE1 expression (up to 41 days) was previously detected in latently infected T98G cells in the absence of UL44 expression and infectious viral particle production [265]. Additionally, IE1 transcript was observed up to 10 dpi (latency established between 5 and 10 dpi) in KASUMI-3 cells [266]. This is in accordance with the observations in my work (Fig. I.8 and I.9). These findings hint towards an additional yet undefined role of IE1 in HCMV latency establishment, whether this includes a role in genome tethering remains to be determined.

The T98G model system was proposed to be appropriate to analyze viral and cellular factors involved in genome maintenance during latency, as these cells can harbor high number of genomes for as long as 41 days [265]. Interestingly, in T98G cells in addition to the chromosome painting pattern reported previously, I also observed that IE1 forms chromosome-associated spots (CAS) (Fig. II.1A-C) [121, 137, 138]. I observed IE1 CAS only in certain cell types i.e., T98G, U87MG, and THP1 (Fig. II.5A and II.5B). T98G and U87MG are both glioblastoma cell lines and THP1 is a CD14+ monocytic leukemia cell line. T98G, U87MG, and THP1 cell lines support HCMV latency establishment and are of tumor origin. At current state of investigation, it seems that **IE1 CAS are formed in cells of tumor origin that can support HCMV latency**, although more cell types need to be tested to confirm this. Viruses such as KSHV, EBV, and HPV for which viral genome maintenance was demonstrated are all oncogenic. HCMV was recently shown to play an oncomodulatory role in glioblastoma multiforme (GBM) progression [218, 223-225]. In addition to this, high risk oncogenic HCMV strains were also shown to have transformation potential [227, 228]. HCMV has been shown to persist in the GBM cells for long periods – both DNA and certain viral proteins such as IE1, pp65, gB and US28 have been detected in these cells. However, the status of HCMV in GBM cells, lytic or latent, is still not clear. The presence of some lytic proteins in addition to long term persistence of HCMV genome in GBM cells suggests that it is neither the latency nor the lytic cycle in a classical sense. High correlation between IE1 positivity and tumor grade in glioma samples was reported, suggesting that IE1 may play a role in progression of this tumor [213, 248]. Based on this information and my results I propose that during latent HCMV infection of tumor cells, IE1 CAS could play a role in tumor progression or mediate genome tethering in T98G cells.

The observed localization of IE1 in CAS was reminiscent of distribution known for other viral maintenance proteins. EBNA1 forms double spots in the pericentromeric regions of all the

chromosomes, occasionally it is also observed as double spots further away from the centromeres [155]. LANA is present in multiple spots per chromosome and is found on all the chromosomes (Fig. II.2). HPV8 and HPV5 E2 spots are specifically localized to the pericentromeric regions of the chromosomes [203-205]. Additionally, HPV8 E2 was found to form these spots only on the short arms of the acrocentric chromosomes – 13, 21, 14, 22, and 15 [204]. In contrast to EBNA1 and LANA, which form spots only in the presence of the viral genome or the latent origin of replication, HPV E2 forms spots even in the absence of the viral DNA [146, 154-156, 171, 173, 175, 249]. I found that **IE1 CAS localize to the pericentromeric regions of the chromosomes** as assessed by co-staining with CENP-A (Fig. II.7B). Reminiscent of what has been observed for HPV8 E2, which forms double spots only on a subset of chromosomes, IE1 forms double spots on 8-10% of chromosomes (~5 chromosomes in cells with normal karyotype) (Fig. II.5C). The pericentromeric region is composed of heterochromatin and is enriched with repressive epigenetic markers [268]. The pericentromeric heterochromatin is essential for preserving the integrity of the genome and promoting correct chromosomal segregation [268-271]. Based on these observations and my results I hypothesize that it would be beneficial for the viral genome to be targeted to the highly repressive environment of the pericentromeric region, which would allow for latency establishment by repressing the HCMV genome. In addition to this, involvement of the pericentromeric region in promoting proper chromosomal segregation, could be taken advantage of by HCMV in order to maintain its genome during latency. Therefore, it is possible that IE1 CAS may be the sites of HCMV genome tethering in T98G cells during latent phase of infection.

IE1 shares several similarities with known viral maintenance proteins i.e., HPV E2, EBV EBNA1, and KSHV LANA. These proteins form dimers, contain a chromatin binding region that tethers the viral genome to cellular chromatin and carry a DNA binding domain that mediates association with the respective viral genome in a sequence specific manner [144, 145]. Similar to these maintenance proteins, **IE1 also dimerizes** and contains a **chromatin binding region** that could potentially mediate association with cellular chromatin [101, 132, 138]. I also postulate that IE1 may mediate genome tethering in a manner analogous to HPV8 E2 rather than LANA or EBNA1. Similar to HPV8 and HPV5 E2, IE1 chromosome-associated spots are present in doublets, localize to the pericentromeric regions of the chromosome, form spots only on a subset of chromosomes, and in the absence of the viral genome. A possible weakness of this hypothesis is that IE1 does not directly bind to DNA as has been shown for

the other maintenance proteins. It was proposed that IE1 binding to the viral genome may occur in a manner similar to its binding to cellular chromatin, i.e. indirectly through chromatin binding proteins, as the viral genome is also chromatinized in the cell [209]. Another possibility is that IE1 may mediate genome tethering in concert with another viral protein that can directly bind to the viral DNA. Nonetheless, these observations warrant further investigation of the possible role of IE1 CAS in HCMV genome tethering.

The nucleosome binding motif (NBM) in the CTD was identified as a mediator of IE1 binding to histones and shown to be responsible for the IE1 chromosome painting pattern [138, 142]. The IE1 NBM mutant fails to associate with mitotic chromosomes as previously reported, however in T98G cells I have observed that it can still form CAS (Fig. II.9C) [138]. This suggested that there is a second chromatin association region distinct from the CTD in IE1. I analyzed the localization pattern of individual domains of IE1 during mitosis and discovered that the core domain is responsible and sufficient for IE1 CAS formation (Fig. II.11A). This identifies **the core domain as the second chromatin binding region of IE1**. Since the core domain is rather long (353 amino acids), identification of the specific amino acid residue(s) is challenging, which is further complicated by the fact that mutations in the core domain lead to structural instability and apparent problems with expression [130]. I generated clustered charge mutants previously shown to be stable, to identify the residues involved in CAS formation [130]. I did not observe loss of IE1 CAS phenotype with any of these mutants (Fig. II.12). This suggests that the residue/s involved in CAS formation are most probably not charged, but rather hydrophobic. This hypothesis requires further mutational studies. It would be very important to identify the residue/s involved in CAS formation, as this would give us a strong tool to dissect the roles of individual chromatin binding domains of IE1 in the context of HCMV infection.

HCMV IE1 present in a chromosome painting pattern was shown to recruit PML to mitotic chromosomes [126, 130, 140]. The functional relevance of this recruitment is not completely understood. My results show that IE1 present in form of CAS also recruits PML to the pericentromeric regions of mitotic chromosomes (Fig. II.7B). During mitosis, PML forms aggregates known as mitotic accumulations of PML protein (MAPPs), 20% of which show association with mitotic chromosomes [272]. It was proposed that the chromosome associated

MAPPs contribute towards reformation of PML nuclear bodies during G1 phase [272]. What role this plays during HCMV infection will require further studies.

Results from my study show that IE1 protein expression levels influence the localization pattern of IE1 during mitosis in both transfected and infected T98G cells (Fig. II.13 and II.14). In T98G cells transfected with different concentrations of the myc-IE1 plasmid, the fraction of cells with IE1 CAS localization pattern increased with decreasing concentration of the plasmid (Fig. II.13A, II.13B, and II.13D). The highest percentage of mitotic cells (75%) with IE1 CAS localization pattern was observed with 0.25 μg of transfected myc-IE1 and the biggest change in percentage of cells with IE1 CAS pattern was detected between 1.0 μg (34%) and 0.5 μg (69%) (Fig II.13B). This suggests that there is a threshold for the switch from IE1 chromosome painting pattern to IE1 CAS and it lies between 1.0 μg and 0.5 μg of transfected myc-IE1 plasmid. Tukey's multiple comparison test showed that the most significant change in percentage of cells with the IE1 CAS localization pattern is observed between 1.0 μg and 0.5 μg of transfected myc-IE1 plasmid. whereas no significant change is observed between other concentration of transfected myc-IE1 (table 11). This can be observed in the graph (Fig II.13D).

Table 11. Tukey's multiple comparison for change in percentage of cells with IE1 CAS localization pattern with decreasing concentrations of transfected myc-IE1 plasmid

μg of myc-IE1	P value	Significance
1.5 vs 1	0.4187	ns
1 vs 0.5	<0.0001	****
0.5 vs 0.25	0.5508	ns

In infected T98G cells, the fraction of mitotic cells with the IE1 chromosome-associated spots localization pattern changes dynamically as infection progresses from the lytic phase to latency as demonstrated by quantification on days 1, 4, 7, 10, and 14 post infection (Fig. II.14B and II.14D). High percentage of mitotic cells (89%) with the IE1 chromosome painting pattern can be observed at 1 dpi, whereas this dramatically switches at 14 dpi (latency), when majority of mitotic cells (84%) display IE1 CAS localization pattern (Fig. II.14A and II.14B). This correlated well with the decrease in IE1 protein levels as infection progressed from day 1 to day 14 (Fig. II.14D). Tukey's multiple comparison test showed that the most significant change in percentage of cells with the IE1 CAS localization pattern is observed between days 4 and 7

post infection, whereas no significant change is observed between days 10 and 14 (table 12). This is visible in Fig. II.14D, where line representing percentage of cells with IE1 CAS localization pattern shows a dramatic rise between day 4 and 7, whereas it reaches a plateau between day 10 and 14 post infection. This suggests that the major switch from IE1 chromosome painting to chromosome-associated spots pattern happens between day 4 and 7 post infection following which IE1 CAS become the dominant localization form from day 10 up to day 14. It is probable that between day 4 and 7, the lytic cycle shuts down, as evidenced by drop in IE1 protein expression (Fig. II.14. D) and from day 7 to 14, the transition to latent phase occurs as observed by the increase in the percentage of cells with IE1 CAS localization pattern. As I have observed that during latency in T98G cells, a small percentage of cells remain positive for IE1 up to 35 dpi (Fig I.8A), it would be interesting to see if these IE1 positive cells (at later timepoints i.e., after 14 dpi) would also have a dominant CAS localization pattern. If that is the case, it would point to IE1 playing a role in HCMV latency in T98G cells.

Table 12. Tukey's multiple comparison for change in percentage of cells with IE1 CAS localization pattern at different times post infection

days post infection	P value	Significance
1 vs 4	0.0039	**
4 vs 7	<0.0001	****
7 vs 10	0.0002	***
10 vs 14	0.7923	ns

The dynamic change in IE1 CAS localization in transfection and infection settings, suggests that the switch from painting to CAS localization pattern should take place at some point during the cell cycle. Results from live imaging show that the switch from painting to CAS localization pattern does not occur during mitosis in the cells that I have observed (Fig. II.15). This suggests that the switch in localization pattern occurs in another phase of the cell cycle. Further live imaging needs to be carried out to identify at which stage of the cell cycle the switch occurs.

In conclusion, my study shows that IE1x4 may not be the maintenance protein of HCMV in T98G and KASUMI-3 cells and that IE1x4 does not behave like LANA in the presence of the HCMV latent origin of replication. However, this needs to be confirmed in CD34+ cells. I have discovered that IE1 forms CAS in T98G, U87MG, and THP1 cells. IE1 CAS can only be

observed on ~5 chromosomes in cells with normal karyotype. CAS formation is mediated by a novel chromatin binding region in IE1 – the core domain. IE1 CAS localize to peri-centromeric regions and also recruit PML to this location. The percentage of cells with CAS localization pattern increases in infected T98G cells, as the infection progresses from lytic to the latent phase, suggesting a role for IE1 CAS in latency or latency establishment. The IE1 CAS are reminiscent of the localization pattern of HPV8 and HPV5 E2 proteins and I propose that IE1 CAS could mediate HCMV genome tethering in T98G cells.

7. REFERENCES

1. Pellett, P.E. and B. Roizman, Herpesviridae, in Fields Virology, D.M. Knipe and P.M. Howley, Editors. 2013, Lippincott Williams & Wilkins: Philadelphia, PA, USA.
2. Spear, P.G. and R. Longnecker, Herpesvirus entry: an update. J Virol, 2003. **77**(19): p. 10179-85.
3. Whitley, R.J., Herpesviruses, in Medical Microbiology, B. S, Editor. 1996, University of Texas Medical Branch at Galveston: Galveston (TX).
4. Mocarski, E.S., T. Shenk, and R.F. Pass, Cytomegalovirus, in Fields Virology, D.M. Knipe and P.M. Howley, Editors. 2013, Lippincott Williams & Wilkins: Philadelphia, PA, USA.
5. Davison, A.J., Herpesviruses: General Features. Reference Module in Biomedical Sciences, 2014.
6. Hahn, G., R. Jores, and E.S. Mocarski, Cytomegalovirus remains latent in a common precursor of dendritic and myeloid cells. Proc Natl Acad Sci U S A, 1998. **95**(7): p. 3937-42.
7. Luppi, M., et al., Human herpesvirus 6 latently infects early bone marrow progenitors in vivo. J Virol, 1999. **73**(1): p. 754-9.
8. Means, R.E., S.M. Lang, and J.U. Jung, Human gammaherpesvirus immune evasion strategies, in Human Herpesviruses: Biology, Therapy, and Immunoprophylaxis, A. Arvin, et al., Editors. 2007, Cambridge University Press: Cambridge.
9. Zuhair, M., et al., Estimation of the worldwide seroprevalence of cytomegalovirus: A systematic review and meta-analysis. Rev Med Virol, 2019. **29**(3): p. e2034.
10. Fowler, K., et al., A systematic literature review of the global seroprevalence of cytomegalovirus: possible implications for treatment, screening, and vaccine development. BMC Public Health, 2022. **22**(1): p. 1659.
11. Siennicka, J., et al., High Seroprevalence of CMV Among Women of Childbearing Age Implicates High Burden of Congenital Cytomegalovirus Infection in Poland. Pol J Microbiol, 2017. **65**(4): p. 425-432.
12. Kanecki, K., et al., Congenital cytomegalovirus infections in Poland - a national hospital register-based study. Ann Agric Environ Med, 2020. **27**(4): p. 574-578.
13. Griffiths, P., I. Baraniak, and M. Reeves, The pathogenesis of human cytomegalovirus. J Pathol, 2015. **235**(2): p. 288-97.
14. Britt, W., Manifestations of human cytomegalovirus infection: proposed mechanisms of acute and chronic disease. Curr Top Microbiol Immunol, 2008. **325**: p. 417-70.
15. Lang, D.J. and J.F. Kummer, Cytomegalovirus in semen: observations in selected populations. J Infect Dis, 1975. **132**(4): p. 472-3.
16. Stagno, S., et al., Breast milk and the risk of cytomegalovirus infection. N Engl J Med, 1980. **302**(19): p. 1073-6.
17. Gandhi, M.K. and R. Khanna, Human cytomegalovirus: clinical aspects, immune regulation, and emerging treatments. Lancet Infect Dis, 2004. **4**(12): p. 725-38.
18. Azevedo, L.S., et al., Cytomegalovirus infection in transplant recipients. Clinics (Sao Paulo), 2015. **70**(7): p. 515-23.
19. Humar, A., M. Michaels, and A.I.W.G.o.I.D. Monitoring, American Society of Transplantation recommendations for screening, monitoring and reporting of infectious complications in immunosuppression trials in recipients of organ transplantation. Am J Transplant, 2006. **6**(2): p. 262-74.

20. Ljungman, P., P. Griffiths, and C. Paya, Definitions of cytomegalovirus infection and disease in transplant recipients. Clin Infect Dis, 2002. **34**(8): p. 1094-7.
21. Britt, W.J., Maternal Immunity and the Natural History of Congenital Human Cytomegalovirus Infection. Viruses, 2018. **10**(8).
22. Leruez-Ville, M., et al., Cytomegalovirus infection during pregnancy: state of the science. Am J Obstet Gynecol, 2020. **223**(3): p. 330-349.
23. Orlikowski, D., et al., Guillain-Barré syndrome following primary cytomegalovirus infection: a prospective cohort study. Clin Infect Dis, 2011. **52**(7): p. 837-44.
24. Ranganathan, P., et al., Significant association of multiple human cytomegalovirus genomic Loci with glioblastoma multiforme samples. J Virol, 2012. **86**(2): p. 854-64.
25. Savva, G.M., et al., Cytomegalovirus infection is associated with increased mortality in the older population. Aging Cell, 2013. **12**(3): p. 381-7.
26. Simanek, A.M., et al., Seropositivity to cytomegalovirus, inflammation, all-cause and cardiovascular disease-related mortality in the United States. PLoS One, 2011. **6**(2): p. e16103.
27. Peredo-Harvey, I., A. Rahbar, and C. Söderberg-Nauclér, Presence of the Human Cytomegalovirus in Glioblastomas-A Systematic Review. Cancers (Basel), 2021. **13**(20).
28. Gibson, W., Structure and formation of the cytomegalovirus virion. Curr Top Microbiol Immunol, 2008. **325**: p. 187-204.
29. Terhune, S.S., J. Schröer, and T. Shenk, RNAs are packaged into human cytomegalovirus virions in proportion to their intracellular concentration. J Virol, 2004. **78**(19): p. 10390-8.
30. Bresnahan, W.A. and T. Shenk, A subset of viral transcripts packaged within human cytomegalovirus particles. Science, 2000. **288**(5475): p. 2373-6.
31. Nguyen, C.C. and J.P. Kamil, Pathogen at the Gates: Human Cytomegalovirus Entry and Cell Tropism. Viruses, 2018. **10**(12).
32. Belzile, J.P., et al., Human cytomegalovirus infection of human embryonic stem cell-derived primitive neural stem cells is restricted at several steps but leads to the persistence of viral DNA. J Virol, 2014. **88**(8): p. 4021-39.
33. Larsson, S., et al., Cytomegalovirus DNA can be detected in peripheral blood mononuclear cells from all seropositive and most seronegative healthy blood donors over time. Transfusion, 1998. **38**(3): p. 271-8.
34. Mendelson, M., et al., Detection of endogenous human cytomegalovirus in CD34+ bone marrow progenitors. J Gen Virol, 1996. **77 (Pt 12)**: p. 3099-102.
35. Sinclair, J. and P. Sissons, Latency and reactivation of human cytomegalovirus. J Gen Virol, 2006. **87**(Pt 7): p. 1763-79.
36. Taylor-Wiedeman, J., et al., Monocytes are a major site of persistence of human cytomegalovirus in peripheral blood mononuclear cells. J Gen Virol, 1991. **72 (Pt 9)**: p. 2059-64.
37. Fish, K.N., et al., Human cytomegalovirus persistently infects aortic endothelial cells. J Virol, 1998. **72**(7): p. 5661-8.
38. Compton, T., D.M. Nowlin, and N.R. Cooper, Initiation of human cytomegalovirus infection requires initial interaction with cell surface heparan sulfate. Virology, 1993. **193**(2): p. 834-41.
39. Kari, B. and R. Gehrz, A human cytomegalovirus glycoprotein complex designated gC-II is a major heparin-binding component of the envelope. J Virol, 1992. **66**(3): p. 1761-4.

40. Kari, B. and R. Gehrz, Structure, composition and heparin binding properties of a human cytomegalovirus glycoprotein complex designated gC-II. J Gen Virol, 1993. **74 (Pt 2)**: p. 255-64.
41. Feire, A.L., H. Koss, and T. Compton, Cellular integrins function as entry receptors for human cytomegalovirus via a highly conserved disintegrin-like domain. Proc Natl Acad Sci U S A, 2004. **101**(43): p. 15470-5.
42. Wang, X., et al., Integrin alphavbeta3 is a coreceptor for human cytomegalovirus. Nat Med, 2005. **11**(5): p. 515-21.
43. Wang, X., et al., Epidermal growth factor receptor is a cellular receptor for human cytomegalovirus. Nature, 2003. **424**(6947): p. 456-61.
44. Isaacson, M.K. and T. Compton, Human cytomegalovirus glycoprotein B is required for virus entry and cell-to-cell spread but not for virion attachment, assembly, or egress. J Virol, 2009. **83**(8): p. 3891-903.
45. Isaacson, M.K., L.K. Juckem, and T. Compton, Virus entry and innate immune activation. Curr Top Microbiol Immunol, 2008. **325**: p. 85-100.
46. Ryckman, B.J., et al., Human cytomegalovirus entry into epithelial and endothelial cells depends on genes UL128 to UL150 and occurs by endocytosis and low-pH fusion. J Virol, 2006. **80**(2): p. 710-22.
47. Ryckman, B.J., M.C. Chase, and D.C. Johnson, HCMV gH/gL/UL128-131 interferes with virus entry into epithelial cells: evidence for cell type-specific receptors. Proc Natl Acad Sci U S A, 2008. **105**(37): p. 14118-23.
48. Vanarsdall, A.L., et al., Human Cytomegalovirus gH/gL Forms a Stable Complex with the Fusion Protein gB in Virions. PLoS Pathog, 2016. **12**(4): p. e1005564.
49. Vanarsdall, A.L., M.C. Chase, and D.C. Johnson, Human cytomegalovirus glycoprotein gO complexes with gH/gL, promoting interference with viral entry into human fibroblasts but not entry into epithelial cells. J Virol, 2011. **85**(22): p. 11638-45.
50. Wille, P.T., et al., A human cytomegalovirus gO-null mutant fails to incorporate gH/gL into the virion envelope and is unable to enter fibroblasts and epithelial and endothelial cells. J Virol, 2010. **84**(5): p. 2585-96.
51. Wu, Y., et al., Human cytomegalovirus glycoprotein complex gH/gL/gO uses PDGFR-α as a key for entry. PLoS Pathog, 2017. **13**(4): p. e1006281.
52. Wang, J., et al., High-molecular-weight protein (pUL48) of human cytomegalovirus is a competent deubiquitinating protease: mutant viruses altered in its active-site cysteine or histidine are viable. J Virol, 2006. **80**(12): p. 6003-12.
53. Kalejta, R.F., Functions of human cytomegalovirus tegument proteins prior to immediate early gene expression. Curr Top Microbiol Immunol, 2008. **325**: p. 101-15.
54. Feng, X., et al., Human cytomegalovirus pUS24 is a virion protein that functions very early in the replication cycle. J Virol, 2006. **80**(17): p. 8371-8.
55. Bechtel, J.T. and T. Shenk, Human cytomegalovirus UL47 tegument protein functions after entry and before immediate-early gene expression. J Virol, 2002. **76**(3): p. 1043-50.
56. McVoy, M.A. and S.P. Adler, Human cytomegalovirus DNA replicates after early circularization by concatemer formation, and inversion occurs within the concatemer. J Virol, 1994. **68**(2): p. 1040-51.
57. Pari, G.S., Nuts and bolts of human cytomegalovirus lytic DNA replication. Curr Top Microbiol Immunol, 2008. **325**: p. 153-66.
58. Prichard, M.N., et al., Identification of persistent RNA-DNA hybrid structures within the origin of replication of human cytomegalovirus. J Virol, 1998. **72**(9): p. 6997-7004.

59. Colletti, K.S., et al., Human cytomegalovirus UL84 interacts with an RNA stem-loop sequence found within the RNA/DNA hybrid region of oriLyt. J Virol, 2007. **81**(13): p. 7077-85.
60. Zhu, Y., L. Huang, and D.G. Anders, Human cytomegalovirus oriLyt sequence requirements. J Virol, 1998. **72**(6): p. 4989-96.
61. Anders, D.G., et al., Boundaries and structure of human cytomegalovirus oriLyt, a complex origin for lytic-phase DNA replication. J Virol, 1992. **66**(6): p. 3373-84.
62. Kagele, D., et al., Analysis of the interactions of viral and cellular factors with human cytomegalovirus lytic origin of replication, oriLyt. Virology, 2012. **424**(2): p. 106-14.
63. Pari, G.S. and D.G. Anders, Eleven loci encoding trans-acting factors are required for transient complementation of human cytomegalovirus oriLyt-dependent DNA replication. J Virol, 1993. **67**(12): p. 6979-88.
64. Kim, Y.E. and J.H. Ahn, Role of the specific interaction of UL112-113 p84 with UL44 DNA polymerase processivity factor in promoting DNA replication of human cytomegalovirus. J Virol, 2010. **84**(17): p. 8409-21.
65. Ahn, J.H., W.J. Jang, and G.S. Hayward, The human cytomegalovirus IE2 and UL112-113 proteins accumulate in viral DNA replication compartments that initiate from the periphery of promyelocytic leukemia protein-associated nuclear bodies (PODs or ND10). J Virol, 1999. **73**(12): p. 10458-71.
66. Park, M.Y., et al., Interactions among four proteins encoded by the human cytomegalovirus UL112-113 region regulate their intranuclear targeting and the recruitment of UL44 to prereplication foci. J Virol, 2006. **80**(6): p. 2718-27.
67. Sarisky, R.T. and G.S. Hayward, Evidence that the UL84 gene product of human cytomegalovirus is essential for promoting oriLyt-dependent DNA replication and formation of replication compartments in cotransfection assays. J Virol, 1996. **70**(11): p. 7398-413.
68. Ertl, P.F. and K.L. Powell, Physical and functional interaction of human cytomegalovirus DNA polymerase and its accessory protein (ICP36) expressed in insect cells. J Virol, 1992. **66**(7): p. 4126-33.
69. Ertl, P.F., M.S. Thomas, and K.L. Powell, High level expression of DNA polymerases from herpesviruses. J Gen Virol, 1991. **72 (Pt 7)**: p. 1729-34.
70. Smith, J.A. and G.S. Pari, Human cytomegalovirus UL102 gene. J Virol, 1995. **69**(3): p. 1734-40.
71. Smith, J.A., et al., Characterization of the human cytomegalovirus UL105 gene and identification of the putative helicase protein. Virology, 1996. **220**(1): p. 251-5.
72. Mettenleiter, T.C., Herpesvirus assembly and egress. J Virol, 2002. **76**(4): p. 1537-47.
73. Varnum, S.M., et al., Identification of proteins in human cytomegalovirus (HCMV) particles: the HCMV proteome. J Virol, 2004. **78**(20): p. 10960-6.
74. Roller, R.J., et al., Herpes simplex virus type 1 U(L)34 gene product is required for viral envelopment. J Virol, 2000. **74**(1): p. 117-29.
75. Reynolds, A.E., et al., U(L)31 and U(L)34 proteins of herpes simplex virus type 1 form a complex that accumulates at the nuclear rim and is required for envelopment of nucleocapsids. J Virol, 2001. **75**(18): p. 8803-17.
76. Reynolds, A.E., et al., Ultrastructural localization of the herpes simplex virus type 1 UL31, UL34, and US3 proteins suggests specific roles in primary envelopment and egress of nucleocapsids. J Virol, 2002. **76**(17): p. 8939-52.
77. Fuchs, W., et al., The UL48 tegument protein of pseudorabies virus is critical for intracytoplasmic assembly of infectious virions. J Virol, 2002. **76**(13): p. 6729-42.

78. Scholl, B.C., et al., Prokaryotic expression of immunogenic polypeptides of the large phosphoprotein (pp150) of human cytomegalovirus. J Gen Virol, 1988. **69 (Pt 6)**: p. 1195-204.
79. Sanchez, V., et al., Accumulation of virion tegument and envelope proteins in a stable cytoplasmic compartment during human cytomegalovirus replication: characterization of a potential site of virus assembly. J Virol, 2000. **74**(2): p. 975-86.
80. Sanchez, V., E. Sztul, and W.J. Britt, Human cytomegalovirus pp28 (UL99) localizes to a cytoplasmic compartment which overlaps the endoplasmic reticulum-golgi-intermediate compartment. J Virol, 2000. **74**(8): p. 3842-51.
81. Silva, M.C., et al., Human cytomegalovirus UL99-encoded pp28 is required for the cytoplasmic envelopment of tegument-associated capsids. J Virol, 2003. **77**(19): p. 10594-605.
82. Chambers, J., et al., DNA microarrays of the complex human cytomegalovirus genome: profiling kinetic class with drug sensitivity of viral gene expression. J Virol, 1999. **73**(7): p. 5757-66.
83. Weekes, M.P., et al., Quantitative temporal viromics: an approach to investigate host-pathogen interaction. Cell, 2014. **157**(6): p. 1460-1472.
84. Rozman, B., et al., Temporal dynamics of HCMV gene expression in lytic and latent infections. Cell Rep, 2022. **39**(2): p. 110653.
85. Slobedman, B., et al., Human cytomegalovirus latent infection and associated viral gene expression. Future Microbiol, 2010. **5**(6): p. 883-900.
86. Goodrum, F., Human Cytomegalovirus Latency: Approaching the Gordian Knot. Annu Rev Virol, 2016. **3**(1): p. 333-357.
87. Goodrum, F.D., et al., Human cytomegalovirus gene expression during infection of primary hematopoietic progenitor cells: a model for latency. Proc Natl Acad Sci U S A, 2002. **99**(25): p. 16255-60.
88. Cheung, A.K., et al., Viral gene expression during the establishment of human cytomegalovirus latent infection in myeloid progenitor cells. Blood, 2006. **108**(12): p. 3691-9.
89. Nitzsche, A., C. Paulus, and M. Nevels, Temporal dynamics of cytomegalovirus chromatin assembly in productively infected human cells. J Virol, 2008. **82**(22): p. 11167-80.
90. Reeves, M.B., et al., Latency, chromatin remodeling, and reactivation of human cytomegalovirus in the dendritic cells of healthy carriers. Proc Natl Acad Sci U S A, 2005. **102**(11): p. 4140-5.
91. Reeves, M.B., et al., An in vitro model for the regulation of human cytomegalovirus latency and reactivation in dendritic cells by chromatin remodelling. J Gen Virol, 2005. **86**(Pt 11): p. 2949-2954.
92. Murphy, J.C., et al., Control of cytomegalovirus lytic gene expression by histone acetylation. EMBO J, 2002. **21**(5): p. 1112-20.
93. Rossetto, C.C., M. Tarrant-Elorza, and G.S. Pari, Cis and trans acting factors involved in human cytomegalovirus experimental and natural latent infection of CD14 (+) monocytes and CD34 (+) cells. PLoS Pathog, 2013. **9**(5): p. e1003366.
94. Goodrum, F., et al., Differential outcomes of human cytomegalovirus infection in primitive hematopoietic cell subpopulations. Blood, 2004. **104**(3): p. 687-95.
95. Kondo, K., J. Xu, and E.S. Mocarski, Human cytomegalovirus latent gene expression in granulocyte-macrophage progenitors in culture and in seropositive individuals. Proc Natl Acad Sci U S A, 1996. **93**(20): p. 11137-42.

96. Shnayder, M., et al., Defining the Transcriptional Landscape during Cytomegalovirus Latency with Single-Cell RNA Sequencing. MBio, 2018. **9**(2).
97. Cheng, S., et al., Transcriptome-wide characterization of human cytomegalovirus in natural infection and experimental latency. Proc Natl Acad Sci U S A, 2017. **114**(49): p. E10586-E10595.
98. Kim, J.H., et al., Human Cytomegalovirus Requires Epidermal Growth Factor Receptor Signaling To Enter and Initiate the Early Steps in the Establishment of Latency in CD34. J Virol, 2017. **91**(5).
99. Buehler, J., et al., Host signaling and EGR1 transcriptional control of human cytomegalovirus replication and latency. PLoS Pathog, 2019. **15**(11): p. e1008037.
100. Krishna, B.A., et al., Human cytomegalovirus G protein-coupled receptor US28 promotes latency by attenuating c-fos. Proc Natl Acad Sci U S A, 2019. **116**(5): p. 1755-1764.
101. Tarrant-Elorza, M., C.C. Rossetto, and G.S. Pari, Maintenance and replication of the human cytomegalovirus genome during latency. Cell Host Microbe, 2014. **16**(1): p. 43-54.
102. Petrucelli, A., et al., Characterization of a novel Golgi apparatus-localized latency determinant encoded by human cytomegalovirus. J Virol, 2009. **83**(11): p. 5615-29.
103. Bego, M., et al., Characterization of an antisense transcript spanning the UL81-82 locus of human cytomegalovirus. J Virol, 2005. **79**(17): p. 11022-34.
104. Keyes, L.R., et al., HCMV protein LUNA is required for viral reactivation from latently infected primary $CD14^{+}$ cells. PLoS One, 2012. **7**(12): p. e52827.
105. Reeves, M.B. and J.H. Sinclair, Analysis of latent viral gene expression in natural and experimental latency models of human cytomegalovirus and its correlation with histone modifications at a latent promoter. J Gen Virol, 2010. **91**(Pt 3): p. 599-604.
106. Beisser, P.S., et al., Human cytomegalovirus chemokine receptor gene US28 is transcribed in latently infected THP-1 monocytes. J Virol, 2001. **75**(13): p. 5949-57.
107. Vomaske, J., J.A. Nelson, and D.N. Streblow, Human Cytomegalovirus US28: a functionally selective chemokine binding receptor. Infect Disord Drug Targets, 2009. **9**(5): p. 548-56.
108. Jenkins, C., A. Abendroth, and B. Slobedman, A novel viral transcript with homology to human interleukin-10 is expressed during latent human cytomegalovirus infection. J Virol, 2004. **78**(3): p. 1440-7.
109. Lau, B., et al., The Expression of Human Cytomegalovirus MicroRNA MiR-UL148D during Latent Infection in Primary Myeloid Cells Inhibits Activin A-triggered Secretion of IL-6. Sci Rep, 2016. **6**: p. 31205.
110. Stenberg, R.M., D.R. Thomsen, and M.F. Stinski, Structural analysis of the major immediate early gene of human cytomegalovirus. J Virol, 1984. **49**(1): p. 190-9.
111. Stenberg, R.M., P.R. Witte, and M.F. Stinski, Multiple spliced and unspliced transcripts from human cytomegalovirus immediate-early region 2 and evidence for a common initiation site within immediate-early region 1. J Virol, 1985. **56**(3): p. 665-75.
112. Stenberg, R.M., et al., Regulated expression of early and late RNAs and proteins from the human cytomegalovirus immediate-early gene region. J Virol, 1989. **63**(6): p. 2699-708.
113. Puchtler, E. and T. Stamminger, An inducible promoter mediates abundant expression from the immediate-early 2 gene region of human cytomegalovirus at late times after infection. J Virol, 1991. **65**(11): p. 6301-6.
114. Meier, J.L. and M.F. Stinski, Regulation of human cytomegalovirus immediate-early gene expression. Intervirology, 1996. **39**(5-6): p. 331-42.

115. Awasthi, S., J.A. Isler, and J.C. Alwine, Analysis of splice variants of the immediate-early 1 region of human cytomegalovirus. J Virol, 2004. **78**(15): p. 8191-200.
116. Greaves, R.F. and E.S. Mocarski, Defective growth correlates with reduced accumulation of a viral DNA replication protein after low-multiplicity infection by a human cytomegalovirus ie1 mutant. J Virol, 1998. **72**(1): p. 366-79.
117. Mocarski, E.S., et al., A deletion mutant in the human cytomegalovirus gene encoding IE1(491aa) is replication defective due to a failure in autoregulation. Proc Natl Acad Sci U S A, 1996. **93**(21): p. 11321-6.
118. Zalckvar, E., et al., Nucleosome maps of the human cytomegalovirus genome reveal a temporal switch in chromatin organization linked to a major IE protein. Proc Natl Acad Sci U S A, 2013. **110**(32): p. 13126-31.
119. Wilkinson, G.W., et al., Disruption of PML-associated nuclear bodies mediated by the human cytomegalovirus major immediate early gene product. J Gen Virol, 1998. **79 (Pt 5)**: p. 1233-45.
120. Xu, Y., et al., Proteasome-independent disruption of PML oncogenic domains (PODs), but not covalent modification by SUMO-1, is required for human cytomegalovirus immediate-early protein IE1 to inhibit PML-mediated transcriptional repression. J Virol, 2001. **75**(22): p. 10683-95.
121. Reinhardt, J., et al., The carboxyl-terminal region of human cytomegalovirus IE1491aa contains an acidic domain that plays a regulatory role and a chromatin-tethering domain that is dispensable during viral replication. J Virol, 2005. **79**(1): p. 225-33.
122. Lee, H.R., et al., N-terminal determinants of human cytomegalovirus IE1 protein in nuclear targeting and disrupting PML-associated subnuclear structures. Biochem Biophys Res Commun, 2007. **356**(2): p. 499-504.
123. Stenberg, R.M., et al., Promoter-specific trans activation and repression by human cytomegalovirus immediate-early proteins involves common and unique protein domains. J Virol, 1990. **64**(4): p. 1556-65.
124. Hayhurst, G.P., et al., CCAAT box-dependent activation of the TATA-less human DNA polymerase alpha promoter by the human cytomegalovirus 72-kilodalton major immediate-early protein. J Virol, 1995. **69**(1): p. 182-8.
125. Lee, H.R., et al., Ability of the human cytomegalovirus IE1 protein to modulate sumoylation of PML correlates with its functional activities in transcriptional regulation and infectivity in cultured fibroblast cells. J Virol, 2004. **78**(12): p. 6527-42.
126. Ahn, J.H., E.J. Brignole, and G.S. Hayward, Disruption of PML subnuclear domains by the acidic IE1 protein of human cytomegalovirus is mediated through interaction with PML and may modulate a RING finger-dependent cryptic transactivator function of PML. Mol Cell Biol, 1998. **18**(8): p. 4899-913.
127. Poma, E.E., et al., The human cytomegalovirus IE1-72 protein interacts with the cellular p107 protein and relieves p107-mediated transcriptional repression of an E2F-responsive promoter. J Virol, 1996. **70**(11): p. 7867-77.
128. Zhang, Z., et al., Interactions between human cytomegalovirus IE1-72 and cellular p107: functional domains and mechanisms of up-regulation of cyclin E/cdk2 kinase activity. J Virol, 2003. **77**(23): p. 12660-70.
129. Johnson, R.A., et al., Domain mapping of the human cytomegalovirus IE1-72 and cellular p107 protein-protein interaction and the possible functional consequences. J Gen Virol, 1999. **80 (Pt 5)**: p. 1293-1303.
130. Paulus, C., et al., Revisiting promyelocytic leukemia protein targeting by human cytomegalovirus immediate-early protein 1. PLoS Pathog, 2020. **16**(5): p. e1008537.

131. Scherer, M., et al., Crystal structure of cytomegalovirus IE1 protein reveals targeting of TRIM family member PML via coiled-coil interactions. PLoS Pathog, 2014. **10**(11): p. e1004512.
132. Schweininger, J., et al., Cytomegalovirus immediate-early 1 proteins form a structurally distinct protein class with adaptations determining cross-species barriers. PLoS Pathog, 2021. **17**(8): p. e1009863.
133. Delmas, S., et al., Optimization of CD4+ T lymphocyte response to human cytomegalovirus nuclear IE1 protein through modifications of both size and cellular localization. J Immunol, 2005. **175**(10): p. 6812-9.
134. Paulus, C., S. Krauss, and M. Nevels, A human cytomegalovirus antagonist of type I IFN-dependent signal transducer and activator of transcription signaling. Proc Natl Acad Sci U S A, 2006. **103**(10): p. 3840-5.
135. Harwardt, T., et al., Human Cytomegalovirus Immediate-Early 1 Protein Rewires Upstream STAT3 to Downstream STAT1 Signaling Switching an IL6-Type to an IFNγ-Like Response. PLoS Pathog, 2016. **12**(7): p. e1005748.
136. Huh, Y.H., et al., Binding STAT2 by the acidic domain of human cytomegalovirus IE1 promotes viral growth and is negatively regulated by SUMO. J Virol, 2008. **82**(21): p. 10444-54.
137. Lafemina, R.L., et al., Expression of the acidic nuclear immediate-early protein (IE1) of human cytomegalovirus in stable cell lines and its preferential association with metaphase chromosomes. Virology, 1989. **172**(2): p. 584-600.
138. Mücke, K., et al., Human cytomegalovirus major immediate early 1 protein targets host chromosomes by docking to the acidic pocket on the nucleosome surface. J Virol, 2014. **88**(2): p. 1228-48.
139. Krauss, S., et al., Physical requirements and functional consequences of complex formation between the cytomegalovirus IE1 protein and human STAT2. J Virol, 2009. **83**(24): p. 12854-70.
140. Shin, H.J., et al., The chromatin-tethering domain of human cytomegalovirus immediate-early (IE) 1 mediates associations of IE1, PML and STAT2 with mitotic chromosomes, but is not essential for viral replication. J Gen Virol, 2012. **93**(Pt 4): p. 716-721.
141. Dimitropoulou, P., et al., Differential relocation and stability of PML-body components during productive human cytomegalovirus infection: detailed characterization by live-cell imaging. Eur J Cell Biol, 2010. **89**(10): p. 757-68.
142. Fang, Q., et al., Human cytomegalovirus IE1 protein alters the higher-order chromatin structure by targeting the acidic patch of the nucleosome. Elife, 2016. **5**.
143. Al-Qahtani, A.A., et al., Efficient proliferation and mitosis of glioblastoma cells infected with human cytomegalovirus is mediated by RhoA GTPase. Mol Med Rep, 2020. **22**(4): p. 3066-3072.
144. Coursey, T.L. and A.A. McBride, Hitchhiking of Viral Genomes on Cellular Chromosomes. Annu Rev Virol, 2019. **6**(1): p. 275-296.
145. Aydin, I. and M. Schelhaas, Viral Genome Tethering to Host Cell Chromatin: Cause and Consequences. Traffic, 2016. **17**(4): p. 327-40.
146. Marechal, V., et al., Mapping EBNA-1 domains involved in binding to metaphase chromosomes. J Virol, 1999. **73**(5): p. 4385-92.
147. Aras, S., et al., Zinc coordination is required for and regulates transcription activation by Epstein-Barr nuclear antigen 1. PLoS Pathog, 2009. **5**(6): p. e1000469.
148. Hussain, M., D. Gatherer, and J.B. Wilson, Modelling the structure of full-length Epstein-Barr virus nuclear antigen 1. Virus Genes, 2014. **49**(3): p. 358-72.

149. Ambinder, R.F., et al., Functional domains of Epstein-Barr virus nuclear antigen EBNA-1. J Virol, 1991. **65**(3): p. 1466-78.
150. Nakada, R., H. Hirano, and Y. Matsuura, Structural basis for the regulation of nuclear import of Epstein-Barr virus nuclear antigen 1 (EBNA1) by phosphorylation of the nuclear localization signal. Biochem Biophys Res Commun, 2017. **484**(1): p. 113-117.
151. Shire, K., et al., EBP2, a human protein that interacts with sequences of the Epstein-Barr virus nuclear antigen 1 important for plasmid maintenance. J Virol, 1999. **73**(4): p. 2587-95.
152. Bochkarev, A., et al., Crystal structure of the DNA-binding domain of the Epstein-Barr virus origin-binding protein EBNA 1. Cell, 1995. **83**(1): p. 39-46.
153. Bochkarev, A., et al., Crystal structure of the DNA-binding domain of the Epstein-Barr virus origin-binding protein, EBNA1, bound to DNA. Cell, 1996. **84**(5): p. 791-800.
154. Sears, J., et al., The amino terminus of Epstein-Barr Virus (EBV) nuclear antigen 1 contains AT hooks that facilitate the replication and partitioning of latent EBV genomes by tethering them to cellular chromosomes. J Virol, 2004. **78**(21): p. 11487-505.
155. Kanda, T., et al., Symmetrical localization of extrachromosomally replicating viral genomes on sister chromatids. J Cell Sci, 2007. **120**(Pt 9): p. 1529-39.
156. Nayyar, V.K., K. Shire, and L. Frappier, Mitotic chromosome interactions of Epstein-Barr nuclear antigen 1 (EBNA1) and human EBNA1-binding protein 2 (EBP2). J Cell Sci, 2009. **122**(Pt 23): p. 4341-50.
157. Reisman, D., J. Yates, and B. Sugden, A putative origin of replication of plasmids derived from Epstein-Barr virus is composed of two cis-acting components. Mol Cell Biol, 1985. **5**(8): p. 1822-32.
158. Rawlins, D.R., et al., Sequence-specific DNA binding of the Epstein-Barr virus nuclear antigen (EBNA-1) to clustered sites in the plasmid maintenance region. Cell, 1985. **42**(3): p. 859-68.
159. Gahn, T.A. and C.L. Schildkraut, The Epstein-Barr virus origin of plasmid replication, oriP, contains both the initiation and termination sites of DNA replication. Cell, 1989. **58**(3): p. 527-35.
160. Middleton, T. and B. Sugden, EBNA1 can link the enhancer element to the initiator element of the Epstein-Barr virus plasmid origin of DNA replication. J Virol, 1992. **66**(1): p. 489-95.
161. Yates, J.L., S.M. Camiolo, and J.M. Bashaw, The minimal replicator of Epstein-Barr virus oriP. J Virol, 2000. **74**(10): p. 4512-22.
162. Chaudhuri, B., et al., Human DNA replication initiation factors, ORC and MCM, associate with oriP of Epstein-Barr virus. Proc Natl Acad Sci U S A, 2001. **98**(18): p. 10085-9.
163. Ritzi, M., et al., Complex protein-DNA dynamics at the latent origin of DNA replication of Epstein-Barr virus. J Cell Sci, 2003. **116**(Pt 19): p. 3971-84.
164. Dhar, S.K., et al., Replication from oriP of Epstein-Barr virus requires human ORC and is inhibited by geminin. Cell, 2001. **106**(3): p. 287-96.
165. Ceccarelli, D.F. and L. Frappier, Functional analyses of the EBNA1 origin DNA binding protein of Epstein-Barr virus. J Virol, 2000. **74**(11): p. 4939-48.
166. Wu, H., P. Kapoor, and L. Frappier, Separation of the DNA replication, segregation, and transcriptional activation functions of Epstein-Barr nuclear antigen 1. J Virol, 2002. **76**(5): p. 2480-90.
167. Lin, A., et al., The EBNA1 protein of Epstein-Barr virus functionally interacts with Brd4. J Virol, 2008. **82**(24): p. 12009-19.

168. Kapoor, P., B.D. Lavoie, and L. Frappier, EBP2 plays a key role in Epstein-Barr virus mitotic segregation and is regulated by aurora family kinases. Mol Cell Biol, 2005. **25**(12): p. 4934-45.
169. Chakravorty, A. and B. Sugden, The AT-hook DNA binding ability of the Epstein Barr virus EBNA1 protein is necessary for the maintenance of viral genomes in latently infected cells. Virology, 2015. **484**: p. 251-258.
170. Deschamps, T., et al., Epstein-Barr virus nuclear antigen 1 interacts with regulator of chromosome condensation 1 dynamically throughout the cell cycle. J Gen Virol, 2017. **98**(2): p. 251-265.
171. Piolot, T., et al., Close but distinct regions of human herpesvirus 8 latency-associated nuclear antigen 1 are responsible for nuclear targeting and binding to human mitotic chromosomes. J Virol, 2001. **75**(8): p. 3948-59.
172. Wong, L.Y., G.A. Matchett, and A.C. Wilson, Transcriptional activation by the Kaposi's sarcoma-associated herpesvirus latency-associated nuclear antigen is facilitated by an N-terminal chromatin-binding motif. J Virol, 2004. **78**(18): p. 10074-85.
173. Szekely, L., et al., Human herpesvirus-8-encoded LNA-1 accumulates in heterochromatin- associated nuclear bodies. J Gen Virol, 1999. **80 (Pt 11)**: p. 2889-2900.
174. Cotter, M.A., C. Subramanian, and E.S. Robertson, The Kaposi's sarcoma-associated herpesvirus latency-associated nuclear antigen binds to specific sequences at the left end of the viral genome through its carboxy-terminus. Virology, 2001. **291**(2): p. 241-59.
175. Cotter, M.A. and E.S. Robertson, The latency-associated nuclear antigen tethers the Kaposi's sarcoma-associated herpesvirus genome to host chromosomes in body cavity-based lymphoma cells. Virology, 1999. **264**(2): p. 254-64.
176. Hellert, J., et al., The 3D structure of Kaposi sarcoma herpesvirus LANA C-terminal domain bound to DNA. Proc Natl Acad Sci U S A, 2015. **112**(21): p. 6694-9.
177. Garber, A.C., J. Hu, and R. Renne, Latency-associated nuclear antigen (LANA) cooperatively binds to two sites within the terminal repeat, and both sites contribute to the ability of LANA to suppress transcription and to facilitate DNA replication. J Biol Chem, 2002. **277**(30): p. 27401-11.
178. Correia, B., et al., Crystal structure of the gamma-2 herpesvirus LANA DNA binding domain identifies charged surface residues which impact viral latency. PLoS Pathog, 2013. **9**(10): p. e1003673.
179. Domsic, J.F., et al., Molecular basis for oligomeric-DNA binding and episome maintenance by KSHV LANA. PLoS Pathog, 2013. **9**(10): p. e1003672.
180. Komatsu, T., et al., KSHV LANA1 binds DNA as an oligomer and residues N-terminal to the oligomerization domain are essential for DNA binding, replication, and episome persistence. Virology, 2004. **319**(2): p. 225-36.
181. Hu, J. and R. Renne, Characterization of the minimal replicator of Kaposi's sarcoma-associated herpesvirus latent origin. J Virol, 2005. **79**(4): p. 2637-42.
182. Barbera, A.J., et al., The nucleosomal surface as a docking station for Kaposi's sarcoma herpesvirus LANA. Science, 2006. **311**(5762): p. 856-61.
183. Barbera, A.J., M.E. Ballestas, and K.M. Kaye, The Kaposi's sarcoma-associated herpesvirus latency-associated nuclear antigen 1 N terminus is essential for chromosome association, DNA replication, and episome persistence. J Virol, 2004. **78**(1): p. 294-301.

184. Krithivas, A., et al., Protein interactions targeting the latency-associated nuclear antigen of Kaposi's sarcoma-associated herpesvirus to cell chromosomes. J Virol, 2002. **76**(22): p. 11596-604.
185. Kelley-Clarke, B., et al., Kaposi's sarcoma herpesvirus C-terminal LANA concentrates at pericentromeric and peri-telomeric regions of a subset of mitotic chromosomes. Virology, 2007. **357**(2): p. 149-57.
186. Si, H., et al., Kaposi's sarcoma-associated herpesvirus-encoded LANA can interact with the nuclear mitotic apparatus protein to regulate genome maintenance and segregation. J Virol, 2008. **82**(13): p. 6734-46.
187. Xiao, B., et al., Bub1 and CENP-F can contribute to Kaposi's sarcoma-associated herpesvirus genome persistence by targeting LANA to kinetochores. J Virol, 2010. **84**(19): p. 9718-32.
188. Lim, C., et al., Functional dissection of latency-associated nuclear antigen 1 of Kaposi's sarcoma-associated herpesvirus involved in latent DNA replication and transcription of terminal repeats of the viral genome. J Virol, 2002. **76**(20): p. 10320-31.
189. Matsumura, S., et al., The latency-associated nuclear antigen interacts with MeCP2 and nucleosomes through separate domains. J Virol, 2010. **84**(5): p. 2318-30.
190. You, J., et al., Kaposi's sarcoma-associated herpesvirus latency-associated nuclear antigen interacts with bromodomain protein Brd4 on host mitotic chromosomes. J Virol, 2006. **80**(18): p. 8909-19.
191. Platt, G.M., et al., Latent nuclear antigen of Kaposi's sarcoma-associated herpesvirus interacts with RING3, a homolog of the Drosophila female sterile homeotic (fsh) gene. J Virol, 1999. **73**(12): p. 9789-95.
192. Viejo-Borbolla, A., et al., Brd2/RING3 interacts with a chromatin-binding domain in the Kaposi's Sarcoma-associated herpesvirus latency-associated nuclear antigen 1 (LANA-1) that is required for multiple functions of LANA-1. J Virol, 2005. **79**(21): p. 13618-29.
193. Giri, I. and M. Yaniv, Structural and mutational analysis of E2 trans-activating proteins of papillomaviruses reveals three distinct functional domains. EMBO J, 1988. **7**(9): p. 2823-9.
194. McBride, A.A., R. Schlegel, and P.M. Howley, The carboxy-terminal domain shared by the bovine papillomavirus E2 transactivator and repressor proteins contains a specific DNA binding activity. EMBO J, 1988. **7**(2): p. 533-9.
195. McBride, A.A., J.C. Byrne, and P.M. Howley, E2 polypeptides encoded by bovine papillomavirus type 1 form dimers through the common carboxyl-terminal domain: transactivation is mediated by the conserved amino-terminal domain. Proc Natl Acad Sci U S A, 1989. **86**(2): p. 510-4.
196. McBride, A.A., The papillomavirus E2 proteins. Virology, 2013. **445**(1-2): p. 57-79.
197. Hegde, R.S., et al., Crystal structure at 1.7 A of the bovine papillomavirus-1 E2 DNA-binding domain bound to its DNA target. Nature, 1992. **359**(6395): p. 505-12.
198. Baxter, M.K., et al., The mitotic chromosome binding activity of the papillomavirus E2 protein correlates with interaction with the cellular chromosomal protein, Brd4. J Virol, 2005. **79**(8): p. 4806-18.
199. Ilves, I., S. Kivi, and M. Ustav, Long-term episomal maintenance of bovine papillomavirus type 1 plasmids is determined by attachment to host chromosomes, which Is mediated by the viral E2 protein and its binding sites. J Virol, 1999. **73**(5): p. 4404-12.

200. Lehman, C.W. and M.R. Botchan, Segregation of viral plasmids depends on tethering to chromosomes and is regulated by phosphorylation. Proc Natl Acad Sci U S A, 1998. **95**(8): p. 4338-43.
201. Skiadopoulos, M.H. and A.A. McBride, Bovine papillomavirus type 1 genomes and the E2 transactivator protein are closely associated with mitotic chromatin. J Virol, 1998. **72**(3): p. 2079-88.
202. You, J., et al., Interaction of the bovine papillomavirus E2 protein with Brd4 tethers the viral DNA to host mitotic chromosomes. Cell, 2004. **117**(3): p. 349-60.
203. Oliveira, J.G., L.A. Colf, and A.A. McBride, Variations in the association of papillomavirus E2 proteins with mitotic chromosomes. Proc Natl Acad Sci U S A, 2006. **103**(4): p. 1047-52.
204. Poddar, A., et al., The human papillomavirus type 8 E2 tethering protein targets the ribosomal DNA loci of host mitotic chromosomes. J Virol, 2009. **83**(2): p. 640-50.
205. Sekhar, V., S.C. Reed, and A.A. McBride, Interaction of the betapapillomavirus E2 tethering protein with mitotic chromosomes. J Virol, 2010. **84**(1): p. 543-57.
206. Bastien, N. and A.A. McBride, Interaction of the papillomavirus E2 protein with mitotic chromosomes. Virology, 2000. **270**(1): p. 124-34.
207. Bolovan-Fritts, C.A., E.S. Mocarski, and J.A. Wiedeman, Peripheral blood CD14(+) cells from healthy subjects carry a circular conformation of latent cytomegalovirus genome. Blood, 1999. **93**(1): p. 394-8.
208. Lyon, S.M., et al., Human Cytomegalovirus Genomes Survive Mitosis via the IE19 Chromatin-Tethering Domain. mBio, 2020. **11**(5).
209. Mauch-Mücke, K., et al., Evidence for Tethering of Human Cytomegalovirus Genomes to Host Chromosomes. Front Cell Infect Microbiol, 2020. **10**: p. 577428.
210. Louis, D.N., et al., The 2016 World Health Organization Classification of Tumors of the Central Nervous System: a summary. Acta Neuropathol, 2016. **131**(6): p. 803-20.
211. Omuro, A. and L.M. DeAngelis, Glioblastoma and other malignant gliomas: a clinical review. JAMA, 2013. **310**(17): p. 1842-50.
212. Poon, M.T.C., et al., Longer-term (≥ 2 years) survival in patients with glioblastoma in population-based studies pre- and post-2005: a systematic review and meta-analysis. Sci Rep, 2020. **10**(1): p. 11622.
213. Cobbs, C.S., et al., Human cytomegalovirus infection and expression in human malignant glioma. Cancer Res, 2002. **62**(12): p. 3347-50.
214. Cobbs, C., Response to "Human cytomegalovirus infection in tumor cells of the nervous system is not detectable with standardized pathologico-virological diagnostics". Neuro Oncol, 2014. **16**(11): p. 1435-6.
215. Baumgarten, P., et al., Human cytomegalovirus infection in tumor cells of the nervous system is not detectable with standardized pathologico-virological diagnostics. Neuro Oncol, 2014. **16**(11): p. 1469-77.
216. Cobbs, C., Reply to: Towards an unbiased, collaborative effort to reach evidence about the presence of human cytomegalovirus in glioblastoma (and other tumors). Neuro Oncol, 2015. **17**(7): p. 1040.
217. Michaelis, M., M. Mittelbronn, and J. Cinatl, Towards an unbiased, collaborative effort to reach evidence about the presence of human cytomegalovirus in glioblastoma (and other tumors). Neuro Oncol, 2015. **17**(7): p. 1039.
218. Dziurzynski, K., et al., Consensus on the role of human cytomegalovirus in glioblastoma. Neuro Oncol, 2012. **14**(3): p. 246-55.
219. Söderberg-Nauclér, C., A. Rahbar, and G. Stragliotto, Survival in patients with glioblastoma receiving valganciclovir. N Engl J Med, 2013. **369**(10): p. 985-6.

220. Stragliotto, G., et al., Effects of valganciclovir as an add-on therapy in patients with cytomegalovirus-positive glioblastoma: a randomized, double-blind, hypothesis-generating study. Int J Cancer, 2013. **133**(5): p. 1204-13.
221. Peng, C., et al., Valganciclovir and bevacizumab for recurrent glioblastoma: A single-institution experience. Mol Clin Oncol, 2016. **4**(2): p. 154-158.
222. Stragliotto, G., et al., Valganciclovir as Add-on to Standard Therapy in Glioblastoma Patients. Clin Cancer Res, 2020. **26**(15): p. 4031-4039.
223. Cinatl, J., et al., Molecular mechanisms of the modulatory effects of HCMV infection in tumor cell biology. Trends Mol Med, 2004. **10**(1): p. 19-23.
224. Barami, K., Oncomodulatory mechanisms of human cytomegalovirus in gliomas. J Clin Neurosci, 2010. **17**(7): p. 819-23.
225. Cobbs, C.S., Evolving evidence implicates cytomegalovirus as a promoter of malignant glioma pathogenesis. Herpesviridae, 2011. **2**(1): p. 10.
226. Geder, K.M., et al., Oncogenic transformation of human embryo lung cells by human cytomegalovirus. Science, 1976. **192**(4244): p. 1134-7.
227. Kumar, A., et al., The Human Cytomegalovirus Strain DB Activates Oncogenic Pathways in Mammary Epithelial Cells. EBioMedicine, 2018. **30**: p. 167-183.
228. El Baba, R., et al., EZH2-Myc driven glioblastoma elicited by cytomegalovirus infection of human astrocytes. Oncogene, 2023. **42**(24): p. 2031-2045.
229. Cobbs, C.S., et al., Modulation of oncogenic phenotype in human glioma cells by cytomegalovirus IE1-mediated mitogenicity. Cancer Res, 2008. **68**(3): p. 724-30.
230. Cobbs, C., et al., HCMV glycoprotein B is expressed in primary glioblastomas and enhances growth and invasiveness via PDGFR-alpha activation. Oncotarget, 2014. **5**(4): p. 1091-100.
231. Lee, K., et al., Downregulation of GFAP, TSP-1, and p53 in human glioblastoma cell line, U373MG, by IE1 protein from human cytomegalovirus. Glia, 2005. **51**(1): p. 1-12.
232. Soroceanu, L., A. Akhavan, and C.S. Cobbs, Platelet-derived growth factor-alpha receptor activation is required for human cytomegalovirus infection. Nature, 2008. **455**(7211): p. 391-5.
233. Soroceanu, L., et al., Human cytomegalovirus US28 found in glioblastoma promotes an invasive and angiogenic phenotype. Cancer Res, 2011. **71**(21): p. 6643-53.
234. Xing, Y., et al., Human cytomegalovirus infection contributes to glioma disease progression via upregulating endocan expression. Transl Res, 2016. **177**: p. 113-126.
235. Stråat, K., et al., Activation of telomerase by human cytomegalovirus. J Natl Cancer Inst, 2009. **101**(7): p. 488-97.
236. Fiallos, E., et al., Human cytomegalovirus gene expression in long-term infected glioma stem cells. PLoS One, 2014. **9**(12): p. e116178.
237. Zhu, X., et al., Human cytomegalovirus infection enhances invasiveness and migration of glioblastoma cells by epithelial-to-mesenchymal transition. Int J Clin Exp Pathol, 2020. **13**(10): p. 2637-2647.
238. Tseliou, M., et al., The Role of RhoA, RhoB and RhoC GTPases in Cell Morphology, Proliferation and Migration in Human Cytomegalovirus (HCMV) Infected Glioblastoma Cells. Cell Physiol Biochem, 2016. **38**(1): p. 94-109.
239. Fornara, O., et al., Cytomegalovirus infection induces a stem cell phenotype in human primary glioblastoma cells: prognostic significance and biological impact. Cell Death Differ, 2016. **23**(2): p. 261-9.
240. Liu, C., et al., Human Cytomegalovirus-Infected Glioblastoma Cells Display Stem Cell-Like Phenotypes. mSphere, 2017. **2**(3).

241. Harrison, M.A.A., et al., Metabolic Reprogramming of Glioblastoma Cells during HCMV Infection Induces Secretome-Mediated Paracrine Effects in the Microenvironment. Viruses, 2022. **14**(1).
242. Merchut-Maya, J.M., et al., Human cytomegalovirus hijacks host stress response fueling replication stress and genome instability. Cell Death Differ, 2022. **29**(8): p. 1639-1653.
243. Matlaf, L.A., et al., Cytomegalovirus pp71 protein is expressed in human glioblastoma and promotes pro-angiogenic signaling by activation of stem cell factor. PLoS One, 2013. **8**(7): p. e68176.
244. Slinger, E., et al., HCMV-encoded chemokine receptor US28 mediates proliferative signaling through the IL-6-STAT3 axis. Sci Signal, 2010. **3**(133): p. ra58.
245. de Wit, R.H., et al., Human cytomegalovirus encoded chemokine receptor US28 activates the HIF-1α/PKM2 axis in glioblastoma cells. Oncotarget, 2016. **7**(42): p. 67966-67985.
246. Scheurer, M.E., et al., Detection of human cytomegalovirus in different histological types of gliomas. Acta Neuropathol, 2008. **116**(1): p. 79-86.
247. Soroceanu, L., et al., Cytomegalovirus Immediate-Early Proteins Promote Stemness Properties in Glioblastoma. Cancer Res, 2015. **75**(15): p. 3065-76.
248. Wen, L., et al., Human cytomegalovirus DNA and immediate early protein 1/2 are highly associated with glioma and prognosis. Protein Cell, 2020. **11**(7): p. 525-533.
249. Ballestas, M.E., P.A. Chatis, and K.M. Kaye, Efficient persistence of extrachromosomal KSHV DNA mediated by latency-associated nuclear antigen. Science, 1999. **284**(5414): p. 641-4.
250. Edelheit, O., A. Hanukoglu, and I. Hanukoglu, Simple and efficient site-directed mutagenesis using two single-primer reactions in parallel to generate mutants for protein structure-function studies. BMC Biotechnol, 2009. **9**: p. 61.
251. Ilic, D., M. Kapidzic, and O. Genbacev, Isolation of human placental fibroblasts. Curr Protoc Stem Cell Biol, 2008. **Chapter 1**: p. Unit 1C.6.
252. Hammer, Q., et al., Peptide-specific recognition of human cytomegalovirus strains controls adaptive natural killer cells. Nat Immunol, 2018. **19**(5): p. 453-463.
253. Tischer, B.K., G.A. Smith, and N. Osterrieder, En passant mutagenesis: a two step markerless red recombination system. Methods Mol Biol, 2010. **634**: p. 421-30.
254. Borst, E.M., et al., The Essential Human Cytomegalovirus Proteins pUL77 and pUL93 Are Structural Components Necessary for Viral Genome Encapsidation. J Virol, 2016. **90**(13): p. 5860-5875.
255. Marquardt, A., et al., Single cell detection of latent cytomegalovirus reactivation in host tissue. J Gen Virol, 2011. **92**(Pt 6): p. 1279-1291.
256. Fortunato, E.A., Using Diploid Human Fibroblasts as a Model System to Culture, Grow, and Study Human Cytomegalovirus Infection. Methods Mol Biol, 2021. **2244**: p. 39-50.
257. Cheng, S., et al., iTRAQ-Based Proteomics Analysis of Human Cytomegalovirus Latency and Reactivation in T98G Cells. J Virol, 2022. **96**(2): p. e0147621.
258. Schindelin, J., et al., Fiji: an open-source platform for biological-image analysis. Nat Methods, 2012. **9**(7): p. 676-82.
259. Livak, K.J. and T.D. Schmittgen, Analysis of relative gene expression data using real-time quantitative PCR and the 2(-Delta Delta C(T)) Method. Methods, 2001. **25**(4): p. 402-8.

260. Jackson, S.E., et al., Latent Cytomegalovirus (CMV) Infection Does Not Detrimentally Alter T Cell Responses in the Healthy Old, But Increased Latent CMV Carriage Is Related to Expanded CMV-Specific T Cells. Front Immunol, 2017. **8**: p. 733.
261. Panina, Y., et al., Validation of Common Housekeeping Genes as Reference for qPCR Gene Expression Analysis During iPS Reprogramming Process. Sci Rep, 2018. **8**(1): p. 8716.
262. Spengler, M.L., et al., SUMO-1 modification of human cytomegalovirus IE1/IE72. J Virol, 2002. **76**(6): p. 2990-6.
263. Child, S.J., et al., Evasion of cellular antiviral responses by human cytomegalovirus TRS1 and IRS1. J Virol, 2004. **78**(1): p. 197-205.
264. Luo, M.H. and E.A. Fortunato, Long-term infection and shedding of human cytomegalovirus in T98G glioblastoma cells. J Virol, 2007. **81**(19): p. 10424-36.
265. Duan, Y.L., et al., Maintenance of large numbers of virus genomes in human cytomegalovirus-infected T98G glioblastoma cells. J Virol, 2014. **88**(7): p. 3861-73.
266. O'Connor, C.M. and E.A. Murphy, A myeloid progenitor cell line capable of supporting human cytomegalovirus latency and reactivation, resulting in infectious progeny. J Virol, 2012. **86**(18): p. 9854-65.
267. Maciejewski, J.P. and S.C. St Jeor, Human cytomegalovirus infection of human hematopoietic progenitor cells. Leuk Lymphoma, 1999. **33**(1-2): p. 1-13.
268. Saksouk, N., E. Simboeck, and J. Déjardin, Constitutive heterochromatin formation and transcription in mammals. Epigenetics Chromatin, 2015. **8**: p. 3.
269. Peters, A.H., et al., Loss of the Suv39h histone methyltransferases impairs mammalian heterochromatin and genome stability. Cell, 2001. **107**(3): p. 323-37.
270. Brown, S.W., Heterochromatin. Science, 1966. **151**(3709): p. 417-25.
271. Fioriniello, S., et al., Epigenetic Factors That Control Pericentric Heterochromatin Organization in Mammals. Genes (Basel), 2020. **11**(6).
272. Dellaire, G., et al., Mitotic accumulations of PML protein contribute to the re-establishment of PML nuclear bodies in G1. J Cell Sci, 2006. **119**(Pt 6): p. 1034-42.